Order Number 9117935

Phase separation in submarine hydrothermal systems: Evidence from the Juan de Fuca Ridge

Butterfield, David Allen, Ph.D.

University of Washington, 1990

U·M·I
300 N. Zeeb Rd.
Ann Arbor, MI 48106

Phase Separation in Submarine Hydrothermal Systems:

Evidence from the Juan de Fuca Ridge

by

David Allen Butterfield

A dissertation submitted in partial fulfillment
of the requirements for the degree of

Doctor of Philosophy

University of Washington

1990

Approved by Russell E Mumpton
(Chairperson of Supervisory Committee)

Program Authorized
to Offer Degree OCEANOGRAPHY

Date 12/18/90

In presenting this dissertation in partial fulfillment of the requirements for the Doctoral degree at the University of Washington, I agree that the Library shall make its copies freely available for inspection. I further agree that extensive copying of this dissertation is allowable only for scholarly purposes, consistent with "fair use" as prescribed in the U.S. Copyright Law. Requests for copying or reproduction of this dissertation may be referred to University Microfilms, 300 North Zeeb Road, Ann Arbor, Michigan 48106, to whom the author has granted "the right to reproduce and sell (a) copies of the manuscript in microform and/or (b) printed copies of the manuscript made from microform."

Signature David Bubbo

Date 12/20/90

University of Washington

Abstract

Phase Separation in Submarine Hydrothermal Systems:
Evidence from the Juan de Fuca Ridge

by David Allen Butterfield

Chairperson of the Supervisory Committee: Associate Professor Russell E. McDuff
School of Oceanography

In order to understand processes affecting the composition of hydrothermal fluids, a detailed study was made of the chemical variability within two vent fields along the Juan de Fuca Ridge. Results indicate that phase separation is the cause of compositional gradients at both sites. Hydrothermal fluids collected from the ASHES vent field in 1986, 1987, and 1988 exhibit a very wide range of chemical composition over a small area (~60 m in diameter). Compositions range from a 300°C, gas-enriched (285 mmol/kg CO_2), low-chlorinity (~33% of seawater) fluid to a 328°C, relatively gas-depleted (50 mmol/kg CO_2), high-chlorinity (~116% of seawater) fluid. The range of compositions at ASHES is best explained by a single hydrothermal fluid undergoing phase separation while rising through the ocean crust, followed by partial segregation of the vapor and brine phases. There is good agreement between the measured fluid compositions and compositions generated by a simple model of phase separation, in which gases are partitioned according to Henry's law and all salt remains in the liquid phase. Significant enrichments in silica, lithium and boron in the low-chlorinity fluids over levels predicted by the model are attributed to fluid-rock interaction in the upflow zone. Iron and calcium have been removed by iron-sulfide and anhydrite precipitation at some time in the history of the low-chlorinity fluids. The shallow depth to the seafloor (1540 m) and the observed chemistry at ASHES are consistent with sub-critical phase separation.

Hydrothermal fluids collected at the Endeavour site in 1984, 1987 and 1988 also display major ion trends indicative of phase separation. The low chloride level of all fluids collected, the lack of strong correlation of chloride and gas content, and the repeated measurements of temperatures >400°C are consistent with phase separation in the supercritical region (>407°C), resulting in removal of a gas-depleted brine.

TABLE OF CONTENTS

Chapter 1: Introduction 1

Chapter 2: Axial Seamount: Phase Separation and Subsequent Fluid-Rock Interaction 6

Introduction 6

Geologic Setting 7

Methods 9

Results 10

Summary 10

Gases 13

Anions 18

Cations 21

Other Constituents 23

Comparison to Other Vent Fields 30

Discussion 32

Properties of the H_2O-NaCl System 32

Phase Separation in Hydrothermal Systems 34

Vapor-Liquid-Seawater Mixing Model 38

Fluid-Rock Interaction in the Upflow Zone 57

Mineral Precipitation and Mixing 68

Geographic Distribution of Venting 70

Conclusions 73

Chapter 3: Endeavour Vent Field: Supercritcal Phase Separation 75

Geologic setting. 75

Navigation within the vent field. 75

Results of chemical analysis. 79

Anions 81

Cations 88

Other constituents 98

Time-series sampling results. 107

Time series for a single chimney. 109

Short-term fluctuations in temperature and composition. 109

Intra-field chemical variability. 122
Geographic trend of compositional variability. 122
Correlation of major ions with chlorinity. 123
Hypotheses for generating chlorinity variations at Endeavour. 123
Input of low-chlorinity magmatic fluid. 130
Precipitation of chloride-bearing mineral. 131
Phase separation, loss of brine phase. 132
Phase separation, double diffusive convection. 143
Summary and conclusions. 145
Chapter 4 Conclusions 147
Bibliography 155
Appendix A: Sampling and Analytical Methods 164
Appendix B: Vent Fluid Chemical Data 174

LIST OF FIGURES

Number		*Page*
2.1	ASHES Vent Field Map	8
2.2	Volatile Components versus Magnesium	14
2.3	Anions versus Magnesium	19
2.4	Cations versus Magnesium	22
2.5	Other Properties versus Magnesium	24
2.6	pH versus Total CO_2	28
2.7	Two-phase Curve for Seawater	33
2.8	Effect of CO_2 on Pressure	35
2.9	ASHES Endmember Concentration versus Chloride	41
2.10	Dissolution of Volatiles During Boiling	48
2.11	Evolution of Cl and CO_2 with Boiling	49
2.12	Comparison of CO_2-Cl Model Output with Experimental Data	53
2.13	Comparison of Major Ion Data with Experimental Data	54
2.14	Calculation of Minimum Temperature Range for Boiling	56
2.15	Endmember Li/K Ratio versus Endmember Cl	66
2.16	Cutaway View Schematic of Axial Seamount Caldera	72
3.1	Maps of Endeavour Vent Field	76
3.2	Chloride versus Magnesium	82
3.3	Chloride versus Magnesium by Structure	85
3.4	Bromide and Br/Cl Ratio	87
3.5	Sulfate versus Magnesium	89
3.6	Lithium versus Magnesium	90
3.7	Sodium versus Magnesium	91
3.8	Potassium versus Magnesium	92
3.9	Calcium versus Magnesium	93
3.10	Strontium versus Magnesium	95
3.11	Manganese versus Magnesium	96
3.12	Iron and Fe/Mn Ratio versus Magnesium	97
3.13	Hydrogen Sulfide versus Magnesium	100
3.14	Ammonia versus Magnesium	101

3.15 Silica versus Magnesium 102
3.16 Alkalinity versus Magnesium 104
3.17 pH versus Magnesium 105
3.18 Total Helium versus Magnesium 106
3.19 Carbon Dioxide versus Magnesium 108
3.20 Vent 16 Calcium and Chloride Time Series 110
3.21 Copper versus Magnesium 114
3.22 Extrapolated Lithium and Chloride Endmembers 117
3.23 Conductive Heat Loss in Chimneys 120
3.24 Endeavour Endmember Element versus Chloride 124
3.25 Comparison of Element versus Chloride Data from the Field with Phase Separation Experiments 135
3.26 Comparison of Elemental Partitioning in Experiments with Field Data 136
3.27 Relationship Between Gas Content and Ridge-Crest Depth 142
4.1 Global Trends in Hydrothermal Fluid Composition 152

LIST OF TABLES

Number		*Page*
2.1	Analytical Methods and Associated Uncertainties	11
2.2	Endmember Composition of ASHES Vents	12
2.3	Comparison of Gas Concentration From Several Hydrothermal Systems	16
2.4	Chemical Comparison of ASHES with Other Mid-ocean Ridge Hydrothermal Systems	31
2.5	Comparison of Calculated and Measured Fluid Composition of Virgin Mound	59
2.6	Comparison of Experimental and Predicted Partitioning of Silica Between Liquid and Vapor	60
3.1	Endeavour Endmembers by Structure	80
3.2	Comparison of Hydrothermal Gas Concentrations	141
A.1	Sample Collection Information	165
B.1	Endeavour Anions, Gases, and Silica	175
B.2	Endeavour Cations	177
B.3	Gas-tight Sample Data	179
B.4	ASHES Anions, Gases, and Silica	180
B.5	ASHES Cations	181

ACKNOWLEDGEMENTS

I would like to thank my advisor and friend Russ McDuff for his patience, optimism and good humour. Russ's way of turning complications into discoveries helped me on many occasions. Thanks to John Delaney for sharing his enthusiasm and ideas about phase separation and about science in general. Marv Lilley was invaluable on many occasions at sea and has shared his ideas generously. I would also like to express my appreciation to Gary Massoth, Dick Feely, Bob Embley and Steve Hammond of NOAA/PMEL for including me in the NOAA VENTS research program at Axial Seamount. James Day, Melinda Dudley, and Dean Lambourn were a great help in the lab. I appreciate very much the many other people at U.W. who have provided help, interesting conversation and comraderie, including Brian Laflamme, Geoff Wheat, Janet Pariso, Jim Wells, Mark Ghiorso, Jeff Walters, Eric Olson, Marie DeAngelis, John Barross, and many others. I thank my friends and family for their support. Saving the best for last, I want to thank my wife, Janice, for her love and encouragement, and our daughter, Natalie, for her smile.

Chapter 1
INTRODUCTION

Since the initial discovery of hydrothermal venting at the Galapagos spreading center [Edmond *et al.*, 1979] and the subsequent finding that ~350°C fluids exited the seafloor in the form of black smoker chimneys [Von Damm *et al.*, 1983], many high-temperature hydrothermal systems have been found in a variety of geological settings in the Pacific and Atlantic oceans. The general success of extrapolating the composition of the Galapagos fluids to predict the temperature and composition of the first black smokers led to initial speculation that chemical variability among high-temperature vents would be minimal. However, as more venting sites have been found, it has become increasingly clear that the chemical composition of vent fluids varies dramatically between sites, and that this variation includes very large enrichments and depletions of chlorinity, which is an approximate measure of the total dissolved material in the fluids. As exploration continues, one can assume that more hydrothermal systems will be found with an expanding diversity in the physical form of venting and the chemical composition of the fluids.

It was recognized immediately [Edmond *et al.*, 1979] that hydrothermal circulation had important consequences for elemental fluxes to and from the oceans. For many elements hydrothermal circulation represents a source or sink of the same magnitude as the other known sources and sinks (e.g., rivers and sediments), so it is important to be able to accurately estimate hydrothermal fluxes in order to understand how the chemical balance of seawater is maintained. Balancing the chemical budget of the oceans remains as one of the fundamental problems in chemical oceanography.

Global hydrothermal fluxes for particular elements have been calculated by multiplying the estimated global hydrothermal heat flux by the ratio of the average excess of the element to heat in hydrothermal fluids. There are many uncertainties in this calculation. First of all, the estimation of the global heat flux is uncertain, since

it is usually based on the ratio of ^{3}He to heat in hydrothermal fluids, which can vary significantly between vent fields [Welhan and Craig, 1983], as can the ^{3}He/element ratios [Lupton, 1990]. Geophysical estimates of the global high-temperature hydrothermal heat flux are equally uncertain, due in part to the unknown contribution of off-axis hydrothermal circulation. Secondly, choosing an average element to heat ratio for hydrothermal fluids is problematic since vent fluid concentrations vary over an order of magnitude for many elements.

There may eventually be enough data on hydrothermal systems around the globe to either integrate all of the fluxes from the known hydrothermal sites or to paramaterize the composition and quantity of hydrothermal fluids with known geological variables such as ridge-crest depth, depth to the magma chamber, spreading rate, basalt composition, etc. For now, however, the data are much too scarce, and before we can fully understand the causes of compositional variability in hydrothermal fluids from different vent fields in different oceans, we must first understand what gives rise to variability within a single vent field and along a single section of ocean ridge.

If we confine our view to the chemical variations within a single vent field, we can eliminate nearly all of the major geological variables (e.g. spreading rate, age, and depth) as causes of local variations and focus on what may happen to a hydrothermal fluid as it ascends through the crust. Fluids exiting the seafloor within a few tens or hundreds of meters of each other must share a common history, including a common recharge path and high-temperature reaction zone. Chemical differences within a vent field must be acquired during the last stages of hydrothermal circulation. Just as petrologists must understand the effects of low pressure differentiation of basaltic magmas before they can study the compositional trends in the mantle, it is necessary to understand the processes that can affect the composition of a hydrothermal fluid during ascent to the seafloor in order to understand both local and global trends in composition.

The composition of the essential ingredients to make hydrothermal fluids, seawater and basalt, are very well known, and provide fertile ground for initial attempts to generate experimental analogs of hydrothermal fluids in high temperature, high pressure reaction cells. These studies provide a good deal of insight into the sequence of chemical changes undergone by seawater during hydrothermal circulation [Seyfried, 1987]. General conclusions of these studies [Rosenbauer and Bischoff, 1983] are that 1) experiments can generate fluids with very nearly the same composition as the fluids from 21°N, East Pacific Rise (with the exception of zinc, which is always low in the experiments), provided the temperature is greater than 375°C and 2) the experiments produce mineral assemblages different from those commonly seen in hydrothermally altered rocks. Basalt-seawater experiments do not produce the large variations in chlorinity seen in ridge-crest hydrothermal fluids, though some depletions in chlorinity have been seen [Berndt *et al.*, 1986].

Bowers *et al.* [1988] showed that the calculated mineral affinities (defined as $A = -RTln\left(\frac{Q}{K}\right)$, where R is the gas constant, T is temperature, Q is the ion activity product and K is the equilibrium constant for mineral formation) for hydrothermal fluids with a fairly wide range in composition were generally within a few kilocalories of zero, which is the value expected for equilibrium. This strongly suggests that the composition of the hydrothermal fluids studied, which vary from 62% to 140% of seawater chlorinity, is controlled by equilibrium with some alteration mineral assemblage, although uncertainties in the chemical analyses and in the thermodynamic data make it impossible to specify exactly what minerals are involved. This is an important result, demonstrating that the major ion composition of a wide range of fluids may be controlled by equilibrium with a similar set of minerals, but it does not explain how the wide range in chlorinity was generated.

Furthermore, chemical reaction/equilibrium speciation models such as EQ3/EQ6 have very little value in predicting hydrothermal chemistry because of the inaccuracies of the thermodynamic data used.

Von Damm [1988] proposed that the entire range of observed fluid compositions could be generated by combining primary hydrothermal fluid with high-chlorinity brine and low-chlorinity vapor produced by phase separation. The mixtures could then re-equilibrate with their surrounding minerals before exiting the seafloor. This model and others like it [Cowan and Cann, 1988; Bischoff and Rosenbauer, 1988] can explain the chlorinity variations in seafloor hydrothermal systems, but the models require field data supporting phase separation.

Arguments against phase separation of hydrothermal fluids [Bowers *et al.*, 1988, Campbell *et al.*, 1988] are based on the propositions that 1) fluid temperatures and compositions at the point of sampling (vent orifice) have not changed since leaving a high-temperature reaction zone at depth, except by adiabatic cooling, and 2) phase separation necessarily leads to a significant negative correlation between chlorinity and gas content. Though these two ideas seem to be widely held, the first is highly questionable and the second is incorrect.

This study presents compelling evidence that phase separation does indeed occur in active hydrothermal systems. It will examine in detail the chemical changes which take place in a boiling system when vapor and liquid become physically segregated and exit the seafloor at low- and high-chlorinity vents. The data are interpreted with a mixing model incorporating data on the partitioning of gases between vapor and liquid. Important differences between compositions predicted by the boiling model and the actual measured fluid compositions are interpreted to be a result of continued fluid-rock interaction in the upflow zone. Studying and modeling a reasonably uncomplicated system (the ASHES vent field) undergoing subcritical phase separation (boiling) provides a necessary first step toward understanding variations of composition in systems where sub-seafloor temperature and pressure

are beyond the critical point for seawater. The evidence is steadily mounting that phase separation is the primary cause of chlorinity variations and therefore plays a fundamental role in controlling the chemistry of hydrothermal fluids from the Juan de Fuca Ridge and along the global mid-ocean ridge system.

Chapter 2
AXIAL SEAMOUNT: PHASE SEPARATION AND SUBSEQUENT FLUID-ROCK INTERACTION

Introduction

One of the major challenges in hydrothermal chemistry is to create a model of the fluid history during hydrothermal circulation that can account for the observed differences in composition of hydrothermal fluids. Models developed to date generally divide the hydrothermal circulation system into the three zones of recharge, high-temperature reaction and discharge [*Bowers et al.*, 1988], though little is known about the residence time of hydrothermal fluids in any of these zones. Based on radioisotopic measurements, *Turekian and Cochran* [1986] and *Grasty et al.* [1988] estimate the residence time of hydrothermal fluids in the high-temperature reaction zone to be near 20 years, while *Kadko and Moore* [1988] place the residence time at no more than 3 years. Based on fluid exit velocities, it is assumed that fluids acquire their characteristic chemical signature by the end of the high-temperature reaction phase and ascend rapidly (in a matter of minutes to hours) to the seafloor, but there may be significant gradients of vertical velocity and permeability.

Processes occurring in the upflow zone may alter the chemical signature acquired at depth. Minerals may precipitate or dissolve, fluids may lose heat to the surrounding rock, cold ambient seawater may be mixed into the rising fluid, or the fluid may undergo phase separation. Changes in *p*H, redox state, temperature, and chlorinity, which occur as a direct result of phase separation, can drastically affect mineral solubility and metal transport [*Drummond*, 1981; *Delaney and Cosens*, 1982; *Drummond and Ohmoto*, 1985]. Phase separation is therefore a process of fundamental importance in the study of hydrothermal chemistry and the formation of

sulfide mineral deposits. Processes occurring in the upflow zone must be recognized if one is to use the composition of sampled hydrothermal fluids to infer fluid-mineral reaction at depth.

We have sampled hydrothermal fluids of diverse chemistry within the Axial Seamount Hydrothermal Emissions Study (ASHES) vent field in the caldera of Axial Seamount, where active, high-temperature venting occurs in a roughly circular area of ~60 m in diameter. Compositions of the fluids can be explained by a model involving a single original hydrothermal fluid rising adiabatically through the crust and undergoing phase separation as a result of decompression. Compositional variations of coevally sampled liquid and vapor phases represents the clearest evidence to date of phase separation at an active submarine hydrothermal vent field. Geochemical studies of these fluids provide a unique opportunity to assess the effects of boiling in a submarine hydrothermal system, to compare the results with the predictions of models of boiling hydrothermal systems [*Drummond,* 1981], and to study subseafloor processes of mixing and reaction.

Geologic Setting

High temperature venting was discovered in the southwest corner of the caldera of Axial Seamount in July, 1984 [*Malahoff et al.*, 1984], and the site was revisited in July/August 1986 [*ASHES Expedition,* 1986], September 1987, and August 1988. The vent field is located approximately 100 m east of the western caldera wall and covers an area roughly 60 m in diameter (Figure 2.1*b* and 2.1*c*). Vent structures sit on unsedimented lobate and sheet flow basalts. There are four large (3-10 m^3) sulfide mounds (Inferno, Hell, Hillock, and Mushroom), each with multiple high-temperature orifices venting 136-328°C fluids. In addition to the sulfide structures there are several locations (Virgin Mound and Crack vents) where fluids up to 299°C exit through bare basalt and precipitate nearly pure anhydrite

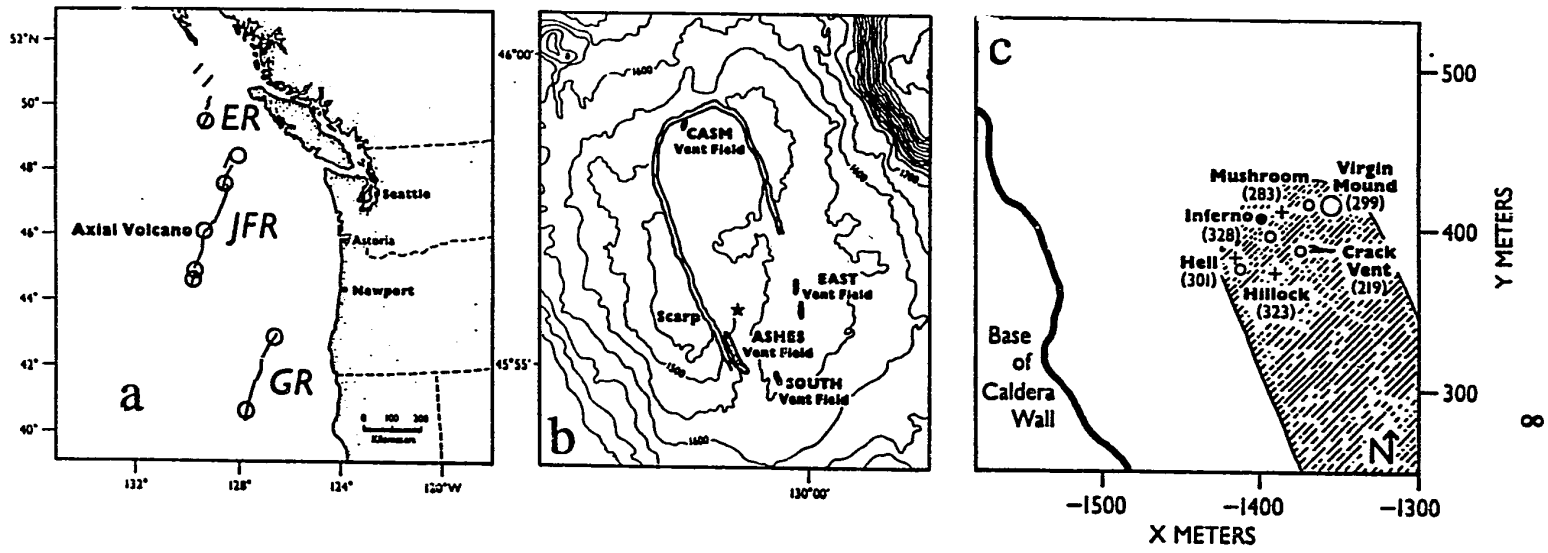

Figure 2.1. (*a*) Regional map of Northeast Pacific showing location of Axial Seamount on the Juan de Fuca Ridge (JFR). Circles mark known venting sites. (*b*) Location of ASHES vent field in the southwest corner of the caldera of Axial Volcano. High-temperature venting is confined to the northern end of the ASHES vent field. Contour interval of bathymetry, 50 m. (*c*) Detail map of high-temperature venting domain within ASHES vent field sampled in 1986, 1987, and 1988. High-temperature vents: plusses and dots, 1- to 4-m-high sulfide edifices with multiple orifices; large open circle and "crack" symbol, <0.7-m-high anhydrite chimney and several meters long, 7- to 10-cm-wide anhydrite-filled cracks. Maximum observed venting temperatures, °C, given in parentheses. [(After *Massoth et al.*, 1989*b*).]

[*Harvey-Kelly et al.*, 1988]. There are also many low-temperature vents exhibiting diffuse flow through worm-covered mounds (e.g., ISCA vent, where the In Situ Chemical Analyzer was deployed, located ~2 m southwest of Hell vent) or low-velocity flow from cracks in sheet flows.

Methods

Samples were collected in 755-mL titanium syringes (major samplers) [*Von Damm et al.*, 1985], and 150-mL titanium gas-tight bottles (all metal, vacuum-tight to 350 bars) deployed singly or in pairs and actuated by the mechanical arm of the Canadian submersible *Pisces IV* in 1986 and by DSV Alvin in 1987 and 1988. In the latter two years we also used a submersible-coupled in situ sensing and sampling system (SIS^3), a flow-through manifold sampling device which allows in-line temperature measurements at the point of sampling and near the intake to the titanium samplers [Massoth *et al.*, 1989a].

Samples were processed as quickly as possible after submersible recovery. A clean piece of Tygon tubing, fitted with a three-way Teflon valve, was slipped over the outlet to the major samplers and rinsed with approximately 20-30 mL of the sample. Aliquots for shipboard gas analysis were drawn into a gas-tight syringe through a piece of surgical tubing attached to the three-way valve and clamped at one end. Aliquots for alkalinity, *p*H, and total sulfide were drawn in the same manner and measured within 8 hours of arrival at the surface, except in 1986, when aliquots for sulfide were sealed in glass with zinc acetate and analyzed colorimetrically on shore. Samples for trace metals and major ions were expressed directly into acid-cleaned polyethylene bottles. Trace metal samples were acidified to *p*H <1.8 with ultrapure HCl. In 1988, aliquots for silica determination were immediately diluted 100- to 200-fold and analyzed shipboard by flow injection

analysis (FIA) colorimetry. Some subsamples were filtered, while others were purged with nitrogen to remove H_2S. Gas-tight samples were transferred shipboard to evacuated glass flasks containing solid mercuric chloride to stop bacterial action.

Shore-based determinations of the major ions (methods described in Appendix A) were carried out at the University of Washington, with the exception of iron and manganese, which were determined at NOAA/PMEL. Shore-based gas analysis was carried out at UCSB. ICP analysis was done in the laboratory of A. Irving, Department of Geology, University of Washington. Table 2.1 summarizes the methods used.

Results

The results of the vent fluid analysis are given in Table 2.2. Endmember [*Edmond et al.*, 1982] values are based on extrapolation to an assumed value of zero magnesium, since magnesium has been shown to be totally removed from solution during experimental high-temperature basalt-seawater interaction [*Bischoff and Dickson,* 1975; *Mottl and Seyfried,* 1980]. Magnesium therefore serves as a measure of the degree of dilution of hydrothermal fluid with local ambient seawater during sampling. Our least diluted samples are 90-95% hydrothermal fluid. The data are shown plotted versus magnesium in Figures 2.2, 2.3, 2.4 and 2.5.

Summary

The extremes in composition in the ASHES vent field are found at the Inferno vent, a large sulfide mound with multiple high-temperature orifices, and at Virgin Mound vent, a single spire of nearly pure anhydrite surrounded by an anhydrite apron of approximately 1.5 m diameter. In general, the Inferno vent has the highest concentrations of nonvolatile elements (Cl, Na, K, Ca, Fe, Mn, etc.) and the lowest concentration of dissolved gasses, while Virgin Mound shows the highest levels of

TABLE 2.1. Analytical Methods and Associated Uncertainties

Analyte	Technique	Precision, % 1σ
*p*H	Potentiometric	0.3
Alkalinity	Potentiometric titration	0.2
Cl	Potentiometric titration with $AgNO_3$	0.2
Br	Colorimetry with phenol red	5
Mg, Ca	EDTA-EGTA titration	0.5
K	Flame Atomic Emission (FAE)	2
Li	Flame Atomic Absorption (FAA)	2
Si	Flow Injection Analysis (FIA), or Inductively Coupled Plasma Atomic Emission Spectrometry (ICPAES)	1 2
SO_4	Polarography by measurement of excess lead	2
H_2S	FIA, methylene blue	4
Fe	FAA	7
Mn, Zn	FAA	2
Fe, Mn, Zn	Graphite Furnace A.A. (at low concentrations)	5
Cu	Graphite Furnace A.A.	2
CO_2	Manometric (gas-tight samples) or shipboard gas chromatography	3 or 5
He	Mass spectrometry	3
B	ICPAES	5
Ba	ICPAES	8
Sr	ICPAES	0.5

TABLE 2.2. Endmember Composition of ASHES Vents.

	Inferno	Hell	Mushroom	Hillock	Crack	ISCA	Virgin Mound	Seawater
Temp, °C	328	301	283	323	217	27.8	299	2.42
pH	3.5	3.5					4.4	7.47
Alk, meq/L	-0.48	-0.51	-0.35	-0.56	+0.40		+0.66	2.354
Cl	624	550	520	482	258	230	176	539
Br	0.956	0.856	0.787	0.723	0.401	0.522	0.250	0.838
Na	501	446	417	391	209		148	462
Ca	46.8	38.85	39.4	34.5	18.9	22.5	10.2	10.25
K	26.8	24.6	22.5	20.6	11.5	9.8	6.98	9.8
Li	0.636	0.578	0.540	0.492	0.286	0.270	0.184	0.028
Sr	0.192			0.145	0.081		0.0464	0.087
Si	15.1						13.5	0.178
Fe, µmol/kg	1065	868	1050	873	13.3	31	12	0.0034
Mn, µmol/kg	1150	1136	1104	866	287	140	142	0.0023
Fe/Mn	0.93	0.76	0.95	1.0	0.046	0.22	0.085	
Cu, µmol/kg	9.9	1	9.6	10.2	0.1		0.4	0.004
Zn, µmol/kg	111	134	122	106	2.6		2.2	0.012
Ba, µmol/kg	26						6	
H_2S	7.1						(18)	0
CO_2	50	(90)		(115)	179		288	2.4
He, µmol/kg	2.45				8.44		11..2	0.045
B	0.587						0.425	0.416

Endmembers calculated by extrapolation of data for individual vents to zero magnesium. Concentrations in mmol/kg except where noted otherwise. Values in parentheses indicate estimates.

dissolved gasses and the lowest levels of nonvolatile elements. The remaining vents have nonvolatile compositions lying between these two extremes. The low-chlorinity fluids are highly depleted in iron, consistent with subsurface precipitation of iron sulfide minerals.

Gases

The reported endmembers for CO_2 and He are based on analysis of samples collected in gas-tight samplers (UCSB). Total condensable gas was measured manometrically after quantitative precipitation of H_2S as mercuric sulfide in the glass flasks in which the samples were stored. SO_2 is thermodynamically unstable in these hydrothermal fluids [*Drummond,* 1981] and can be considered negligible, so CO_2 should constitute >99% of the condensable gas after removal of H_2S.

Shipboard gas chomatographic analysis of CO_2, CH_4, and H_2 on samples taken from the titanium major samplers was carried out in 1987. The shipboard gas data show very high scatter, which can be attributed to degassing of the samples prior to analysis. It is not possible to say whether the data points are minimum or maximum values, since it is possible to have negative errors due to loss of gas and positive errors due to injection of an exsolved gas bubble into the gas chromatograph. The problems are most severe for CH_4 and H_2, which have very low solubilities under measurement conditions.

CO_2. Endmember concentrations for Inferno estimated from the shipboard CO_2 data (47.5 mmol/kg) match the Inferno endmember for total condensable gas (50 mmol/kg as CO_2) determined on samples taken with the gas-tight samplers (Figures 2.2*a* and *b*). This agreement indicates that degassing was not as severe in samples from Inferno, the most gas-depleted of the ASHES vents, and that the condensable gas measurement can be equated to CO_2.

Figure 2.2. Plot of volatile components versus magnesium. Symbols used in this, and all subsequent figures: solid circle, seawater; open circle, Virgin Mound; cross, Crack and ISCA; plus, Hillock; square, Hell; triangle, Mushroom; inverted triangle, Inferno. (*a*) Shipboard CO_2 measurements for Inferno samples only, showing duplicate sample runs. Dashed line is regression of all but the lowest-magnesium sample, and yields an end-member CO_2 concentration of 47.5 mmol/kg. (*b*) Total condensable gas measured manometrically after removal of H_2S. Data point in parentheses was measured from a subsample transferred directly from a titanium major sampler to an evacuated glass flask and has likely been affected by degassing. All other data points are from gas-tight samples. The condensable gas data yield CO_2 end-members of 50 mmol/kg for Inferno and 285 mmol/kg for Virgin Mound, assuming CO_2 is the only important condensable gas after removal of H_2S. Shipboard CO_2 analysis agrees with manometric measurement of condensable gas to within 5% for Inferno. (*c*) H_2S analyzed colorimetrically from samples collected in titanium major samplers. High scatter is attributed to degassing in the major samplers. Solid line is regression of all Inferno data points. Dashed line is regression of all Virgin Mound data points. Dot-dashed line is regression of Inferno data points with $P_{CO_2} < 1$ bar (Mg > 20 mmol/kg). Dotted line is extrapolation through single data point for Virgin Mound with $P_{CO_2} < 1$ bar. (*d*) H_2S estimated by weighing mercuric sulfide precipitate in gas-tight sample flasks. (*e*) Helium versus magnesium. The value in parentheses for Virgin Mound was measured on the same subsample described in Figure 3*b* above.

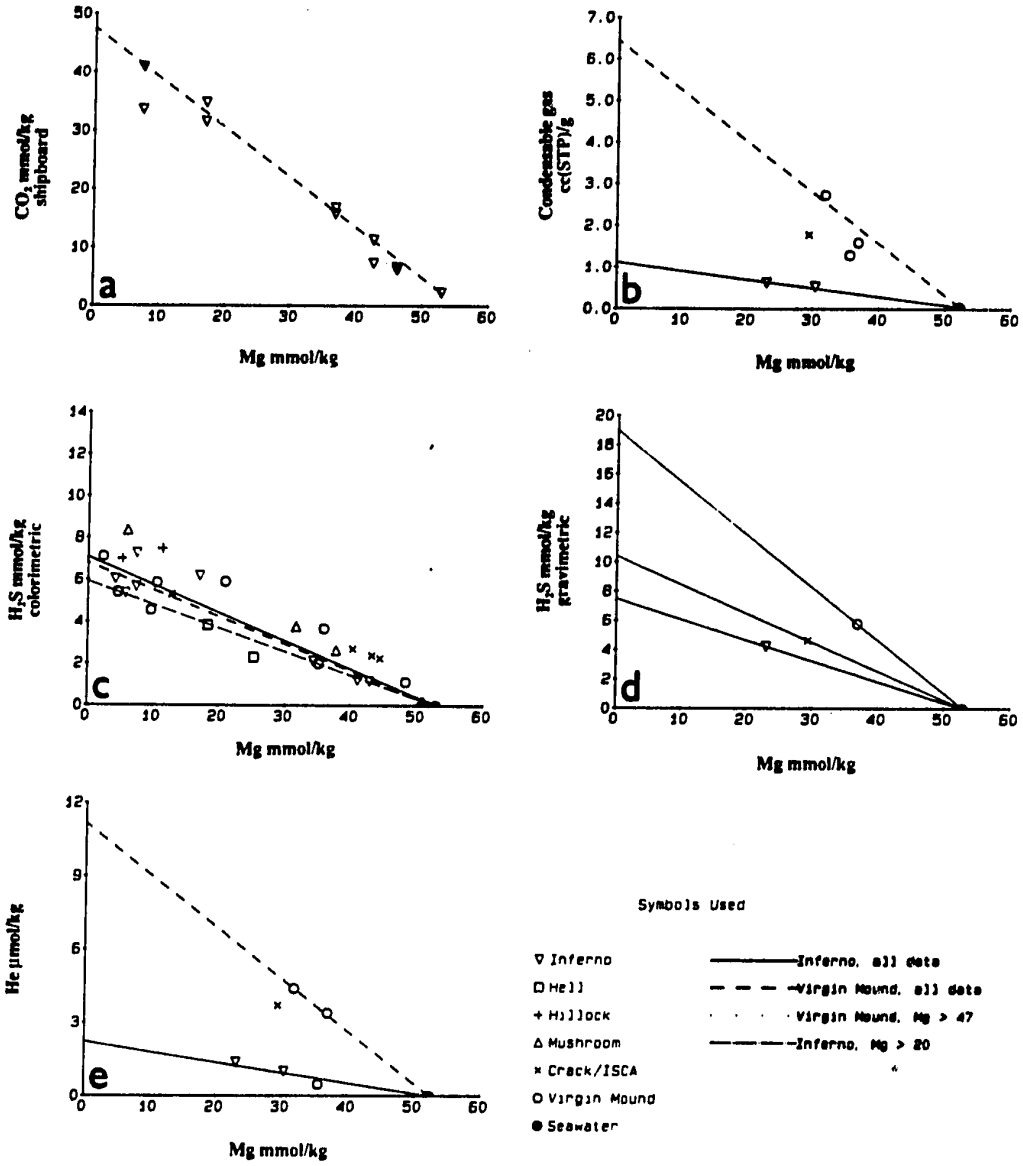
a
CO_2 mmol/kg shipboard
Mg mmol/kg
b
Condensable gas cc(STP)/g
Mg mmol/kg
c
H_2S mmol/kg colorimetric
Mg mmol/kg
d
H_2S mmol/kg gravimetric
Mg mmol/kg
e
He µmol/kg
Mg mmol/kg
Symbols Used
▽ Inferno
□ Hell
+ Hillock
△ Mushroom
× Crack/ISCA
○ Virgin Mound
● Seawater
Inferno, all data
Virgin Mound, all data
Virgin Mound, Mg > 47
Inferno, Mg > 20

Based on the total condensable gas measurements (Figure 2.2*b*), all vent fluids from ASHES are extremely high in CO_2, with the highest measured concentration at Virgin Mound (285 mmol/kg) and the lowest at Inferno (50 mmol/kg). These concentrations are higher than any other reported values for seafloor hydrothermal systems (see Table 2.3 for comparison), except Loihi Seamount, where the CO_2 content of 30°C fluids is 300 mmol/kg at a magnesium concentration of 50.3 mmol/kg [*Karl et al.*, 1988]. (Extrapolating the Loihi value back to zero magnesium yields an endmember concentration of 6-8 mol/kg!) CO_2 is the major dissolved component in Virgin Mound fluids, higher in concentration than any other dissolved species.

We have data from samples taken with the UCSB gas-tight samplers for three vents (Inferno, Virgin Mound, and Crack); volatile concentrations in the other vents are poorly constrained. We estimated endmember concentrations of CO_2 in the other vents by extrapolating the available data for the most diluted samples; these estimates are shown in parentheses in Table 2.2.

H_2S. There is considerable scatter in the sulfide data (Figure2.2*c*), which can be attributed to a number of factors. Probably the most important source of error in the measurement of H_2S is degassing prior to measurement. Gas levels are extremely high in all fluids from the ASHES vent site (50-285 mmol/kg CO_2 in the endmember fluids), so that even samples which have been diluted with >50% seawater are supersaturated with CO_2 at atmospheric pressure (saturation concentration is approximately 30 mmol/kg, based on the Henry's law constant for CO_2 of *Drummond* [1981]). Even though samples were removed directly from the titanium sample bottles with gas-tight syringes and analyzed or preserved within 2 hours (and often within minutes of removal from the major sampler), formation of a head space gas phase probably occurred in the major sampler before the sample could be

TABLE 2.3. Comparison of Gas Concentrations From Several Hydrothermal Systems.

	Temp, °C Maximum Observed	CO_2 mmol/kg	He µmol/kg	CH_4 µmol/kg	He/CO_2 $x10^6$
Axial Virgin Mound	299	285	11.2	NA	39
Axial Inferno	328	50	2.45	25	49
Axial Crack	218	179	8.44	NA	47
Loihi[a]	30	300	NA	7	
EPR, 21°N[b]	350	5.72	0.94	51-65	164
SJdF[c]	285	3.92-4.46	0.89	82-118	200-227

Reported gas concentrations are zero-magnesium end-members, except Loihi data, which are values at 30°C.
[a] *Karl et al*, 1988.
[b] *Welhan and Craig* [1983] and *Kim et al.*, [1984].
[c] *Evans et al.* [1988] and *Von Damm and Bischoff* [1987].

analyzed. In some cases, gas bubbles were seen escaping from the major samplers during ascent from the seafloor. Degassing errors make it difficult to estimate accurately endmember concentrations of H_2S. The H_2S endmembers estimated from the shipboard measurements must be considered minimum values. Negative errors may also be caused by precipitation of metal sulfides from solution in the major samplers.

If we regress separately all of the data for Inferno and Virgin Mound (Figure 2.2*c*), then the two vents do not differ significantly in H_2S (7 ± 1 mmol/kg). However, if we consider only the samples for which the partial pressure of CO_2 is $\leq$ 1 atmosphere (Mg>20 mmol/kg for Inferno, Mg>47 mmol/kg for Virgin Mound, Figure 2.2*c*), then Virgin Mound has an endmember concentration of 13 ± 2 mmol/kg (based on a single data point) and Inferno is 6 ± 1 mmol/kg. (Uncertainties for endmembers obtained from single data points are estimated by extrapolating the analytical uncertainty.) We were able to estimate gravimetrically the H_2S content of samples collected in gas-tight samplers (Figure 2.2*d*) by assuming that H_2S was quantitatively removed and that all of the precipitate in the flasks was mercuric sulfide. (Approximately 1 g of solid mercuric chloride was placed in each flask; this quantity is enough to precipitate H_2S completely in concentrations up to 24 mmol/kg, which is more than twice any of the levels measured in this way. The solubility of mercuric chloride in water is 6g/100 mL, so no solid $HgCl_2$ should remain. The presence of other metal sulfides precipitated from solution would introduce a negative error.) Because of the way the samples were processed, we have only three data points for this method, but they clearly show a significant difference between the three vents represented (Virgin Mound = 19.5 ± 3, Crack = 10.5 ± 1, and Inferno = 7.5 ± 0.8). The three H_2S endmembers estimated for Inferno agree to within the uncertainty of the data, supporting the inference from the shipboard CO_2 data that

degassing was less severe in Inferno samples, and lending credibility to the extrapolation of the gravimetric data for the other vents. We conclude that endmember H_2S in Virgin Mound is 2 to 3 times higher than Inferno.

Helium. Helium (Figure 2.2*e*) was measured on samples from gas-tight samplers only. As for CO_2, the levels of helium at ASHES are quite high; relative to other vent fields, twofold to tenfold enrichments were observed (Table 2.3). Virgin Mound has the highest endmember helium content at ASHES (11.2 μmol/kg), while the Inferno endmember (2.45 μmol/kg) is lowest.

Anions

Chloride. Chloride clearly shows multiple mixing lines between seawater and the high-temperature fluids from different vents (Figure 2.3*a*). The highest endmember chloride concentration (624 mmol/kg) is seen in Inferno vent fluids and the lowest in Virgin Mound (176 mmol/kg). Other vents plot along separate and distinct mixing lines between these extremes, and are tabulated in order of decreasing chlorinity in Table 2.2. The data show no change during the two-year period in which samples were collected. The Virgin Mound fluids have the lowest chloride content of any seafloor hydrothermal system yet sampled and the observation of such large variations in chlorinity within a single vent field is unprecedented.

Throughout this paper we will group the vent fluid data into three groups based on their chloride concentrations. Inferno is the only vent sampled with a chloride concentration significantly above the seawater value of 540 mmol/kg and will be referred to as chloride-enriched or high-chlorinity. Hell, Hillock, and Mushroom comprise the chloride-normal group and range from 550 to 480 mmol/kg. Virgin Mound, Crack and ISCA have chloride concentrations below 260 mmol/kg and comprise the chloride-depleted or low-chlorinity group. Although chlorinity in these vent fluids is not related to salinity in a constant, well-defined manner as in seawater,

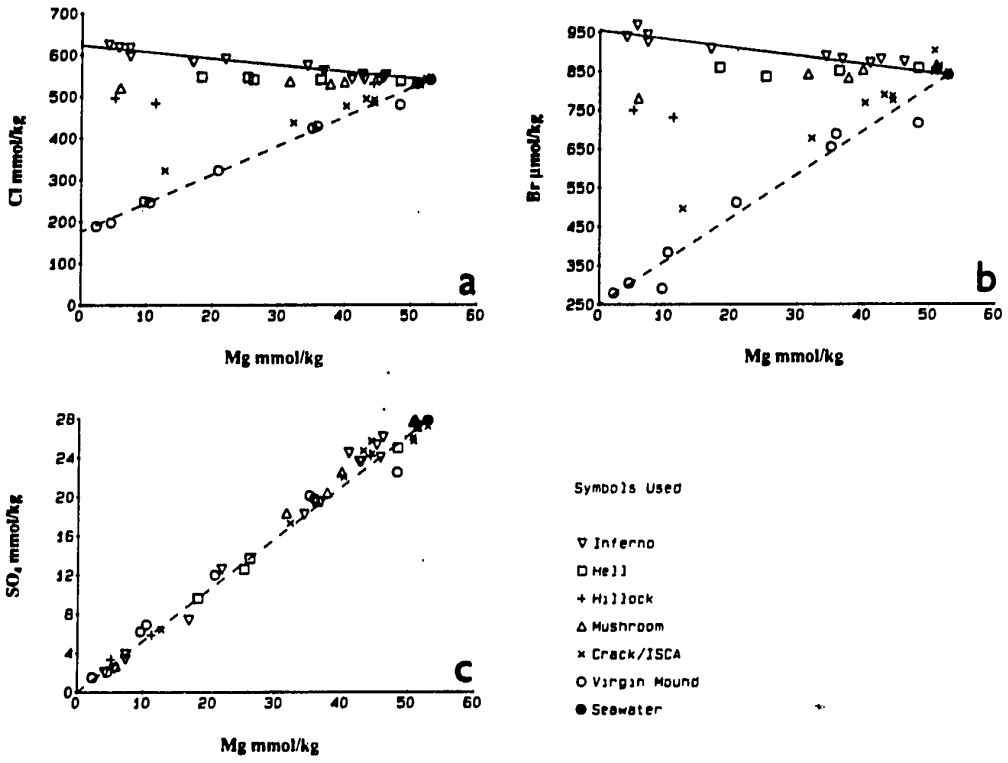

Figure 2.3. Plot of anion concentrations versus magnesium for ASHES fluids, 1986-1988. Symbols listed in Figure 3. Lines drawn represent linear least squares fit to data for Inferno vent (solid line) and Virgin Mound vent (dashed line). (*a*) Chloride shows very distinct trends for each vent, with no discernible change over the period sampled. ASHES is the first documented vent field to show significant positive and negative chloride anomalies. Inferno vent has the highest concentration of all nonvolatile elements, while the lowest levels are found in Virgin Mound. (*b*) Bromide concentrations follow chloride concentrations very closely. End-member Br/Cl ratios are close to the seawater value for all vents. (*c*) Sulfate concentrations extrapolate to zero for all vent fluids. Dashed line is drawn between seawater composition and the origin.

chloride is the major anion in the vent fluids and chlorinity is an approximate measure of the total dissolved salts. Grouping the vents together is a matter of convenience; they exhibit a range of endmember compositions within each group which are clearly distinguishable for many elements, but they are very similar in some respects.

Bromide. Bromide concentrations (Figure 2.3*b*) follow the same pattern as chloride. Inferno fluids are approximately 112% of seawater bromide concentration and Virgin Mound fluids are about 30% of the seawater value. The Br/Cl ratio of all of the high-temperature vent fluids is $0.00150 \pm .00005$ (mean $\pm 1\sigma$), compared to the seawater ratio of 0.00155. Though the calculated Br/Cl ratio of Virgin Mound fluids is only 1.42, it is not statistically distinguishable from the Br/Cl ratio of the other vent fluids because there is a high degree of scatter in the Br data for Virgin Mound.

Sulfate. There are no significant differences between vents for sulfate ion, which extrapolates to zero concentration in all of the vents (Figure 2.3*c*). Departures of the measured sulfate concentration from what would be expected due to seawater mixing are less than the analytical uncertainty ($2\sigma = 4\%$) in all but a few cases. Because there is no discernible excess sulfate over what can be expected from mixing with seawater, entrainment of anhydrite particles during sampling was minimal. There was no detectable difference in sulfate between samples which had been purged with nitrogen to remove sulfide and those which were simply stored in plastic bottles with no treatment, so it appears that oxidation of sulfide was not a source of error.

Cations

Lithium. Lithium (Figure 2.4*a*) is highly enriched over seawater in all vent fluids from ASHES. As for the other nonvolatile elements, Li is highest in Inferno (0.636 mmol/kg) and lowest in Virgin Mound (0.184 mmol/kg).

Sodium. Sodium (Figure 2.4*b*) was calculated by charge balance. Inferno endmember is 500 mmol/kg and Virgin Mound is 148 mmol/kg. Sodium shows the same trend as chloride.

Potassium. Potassium (Figure 2.4*c*) is enriched in Inferno (26.4 mmol/kg) and depleted in Virgin Mound (6.98 mmol/kg) relative to ambient seawater (9.79 mmol/kg).

Magnesium. Our data are consistent with the hypothesis that magnesium is absent from the high-temperature fluids as found in experimental studies [*Bischoff and Dickson,* 1975; *Mottl and Seyfried,* 1980] and verified by the collection of samples with near-zero magnesium at other mid-ocean ridge vent sites. Our lowest measured magnesium concentration was 2.31 mmol/kg (4.3% seawater) from a sample collected at Virgin Mound, which was visibly the most vigorous vent in the field. In most cases, the vent orifices were only about 2 cm in diameter and entrainment of seawater during sampling was difficult to avoid.

Calcium. Calcium (Figure 2.4*d*) is highly enriched in Inferno fluids (46.8 mmol/kg) and is nearly identical to seawater in Virgin Mound samples (10.2 mmol/kg). Using calcium data corrected for excess sulfate does not significantly change the calcium endmembers, and since the uncertainty in the sulfate data used to correct the data is large ($2\sigma = 4\%$), we report endmembers based on extrapolation of the uncorrected Ca data.

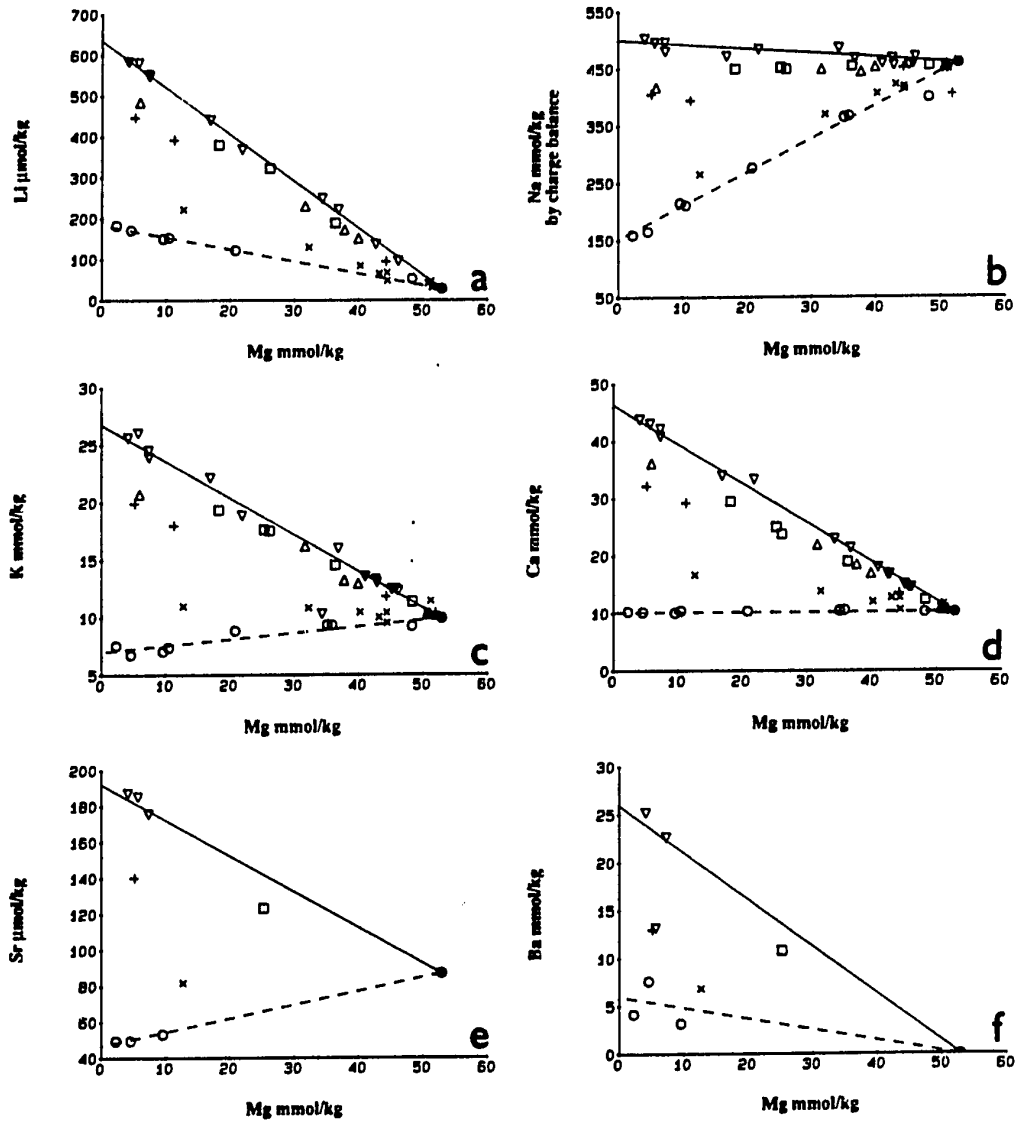

Figure 2.4. Plot of cation concentrations versus magnesium for ASHES fluids, 1986-1988. Symbols listed in Figure 3. (*a*) Lithium is enriched over seawater in all vent fluids. (*b*) Sodium, which was calculated by charge balance, ranges from 108% of seawater concentration in Inferno down to 33% of seawater in Virgin Mound. (*c*) Potassium is nearly 3 times seawater concentration in Inferno and about 30% less than seawater in Virgin Mound. (*d*) Calcium ranges from more than 4 times seawater concentration in Inferno to nearly equal to seawater in Virgin Mound. (*e*) Strontium (measured on a subset of nine samples by ICP). (*f*) Barium (measured on a subset of nine samples by ICP).

Strontium. Results of ICP analysis for strontium (Figure 2.4*e*) show that it behaves similarly to many of the other cations. Inferno (180 μmol/kg) is enriched 200% over seawater, and Virgin Mound (46.4 μmol/kg) is significantly lower than seawater (87 μmol/kg). The Sr/Ca ratio is slightly higher in Virgin Mound (0.00455) than Inferno (0.00410). These ratios are similar to the Sr/Ca ratios in other mid-ocean ridge vent fluids (Table 2.4).

Barium. We have analyzed barium by ICP in 9 of the least diluted samples (Figure 2.4*f*). As shown by *Von Damm et al.* [1985], barium is subject to barite solubility control during dilution with seawater and therefore will be under-estimated by linear extrapolation to zero magnesium. The highest measured concentration in Inferno was 25 μmol/kg, compared to only 7.6 μmol/kg in Virgin Mound. These values have very likely been lowered by mixing with seawater in the subsurface or during sampling. The extrapolated endmembers reported in Table 2.2 should be considered as minima.

Other Constituents

Silica. In 1986 and 1987 silica was determined on shore from samples stored undiluted in plastic bottles. It is evident that samples with silica content greater than about 2 mmol/kg underwent polymerization during storage (Figure 2.5*a*). These samples were diluted 1:100 in 0.01M HNO_3 and analyzed periodically over several months. The measured silica content gradually increased, but did not reach levels predicted by the samples with silica less than 2 mmol/kg.

In 1988, silica was measured shipboard on samples which were diluted for measurement within twelve hours of sampling. These data (Figure 2.5*b*) show very little difference between the low- and high-salinity vent fluids. Using only the 1988 data, we calculate endmember concentrations of 15.1 ±0.5 mmol/kg for Inferno and 13.5±0.6 mmol/kg for Virgin Mound (Figure 2.5*b*). We also analyzed a subset of the

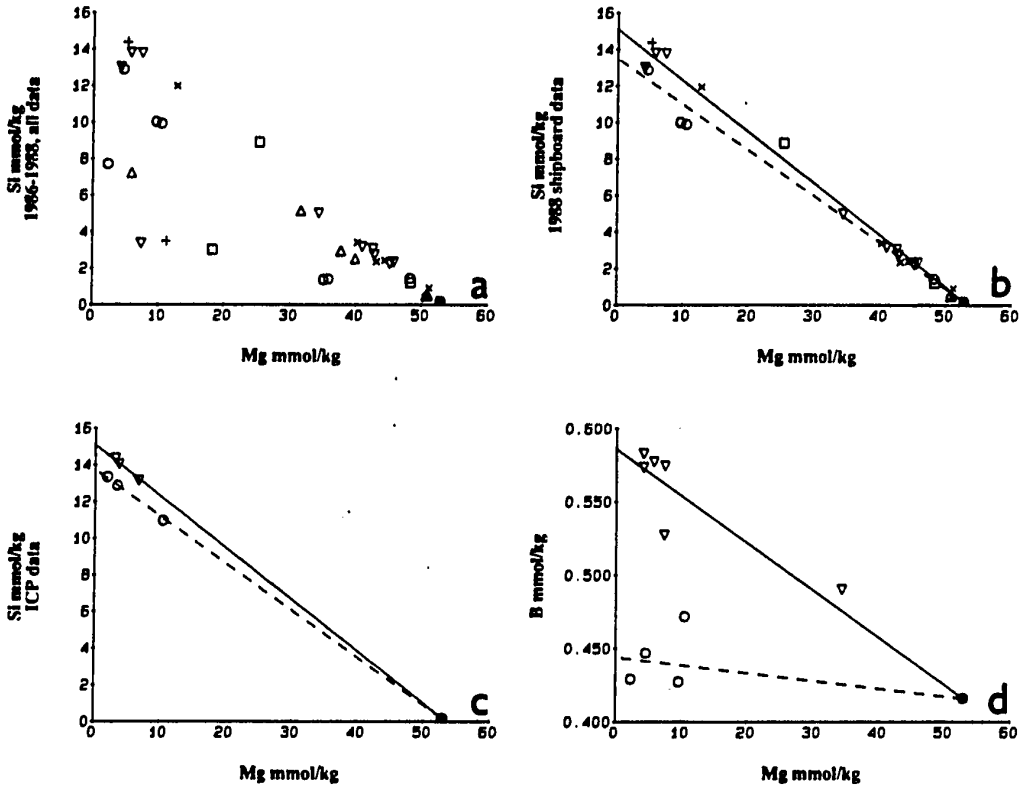

Figure 2.5. Elemental concentration or chemical property versus magnesium for ASHES fluids. Symbols listed in Figure 3. (*a*) Silica versus magnesium. Data from all 3 years. Data points which fall below the trend of the high-magnesium samples have been affected by silica polymerization during storage and were not used for calculating end-member concentrations. (*b*) Silica versus magnesium, 1988 shipboard data. Regressions for Inferno (solid line) and Virgin Mound (dashed line) show a small but significant difference between the two vents. (*c*) Silica versus magnesium from subset of lowest magnesium samples analyzed by ICPAES, which is not affected by polymerization. End-member silica concentrations calculated from ICP data agree well with 1988 shipboard data. (*d*) Boron versus magnesium. Data for Inferno and Virgin Mound only are shown. Some boron data courtesy of Ian Jonasson and Gwendy Hall, Geological Survey of Canada.

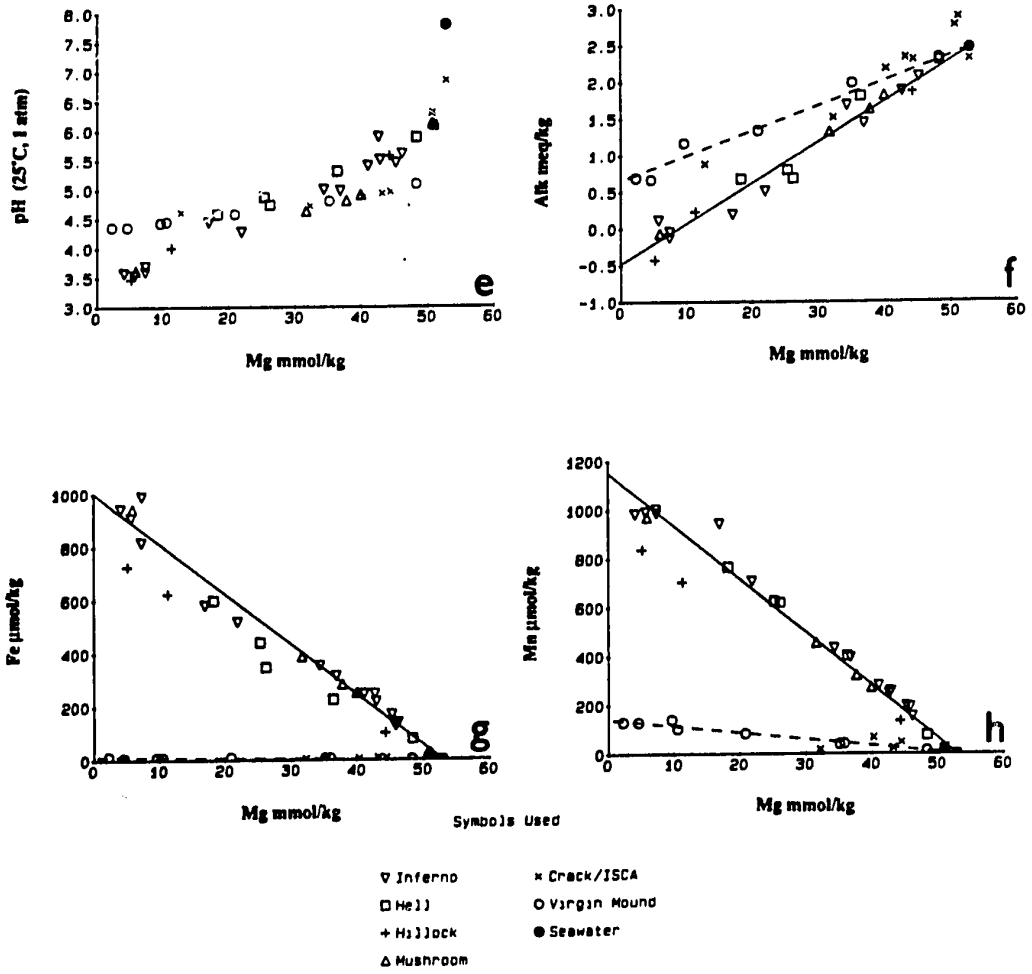

Figure 2.5. (continued) (*e*) *p*H (25°C, 1 atm) versus magnesium. (*f*) Alkalinity versus magnesium. (*g*) Total iron versus magnesium. Iron is present at very low concentrations in the low-chlorinity fluids. (*h*) Manganese versus magnesium.

samples by ICP (Figure 2.5*c*), which is not sensitive to silica polymerization. The endmembers calculated from these data (Inferno = 15.1 mmol/kg, Virgin Mound = 13.8 mmol/kg) agree very well with the shipboard data and the extrapolation of the most diluted samples .

Unlike the other major ions, there is only a small difference in silica content between the low-chlorinity and high-chlorinity fluids (see discussion).

Boron. Boron was measured in two laboratories (U.W. and Geological Survey of Canada, Ottawa) by ICP Atomic Emission Spectrometry. We have data for a total of 8 samples, of which 2 were measured by both labs (Figure 2.5*d*). Boron is elevated over seawater concentration (0.416 mmol/kg) in both Inferno (0.59 mmol/kg) and Virgin Mound (0.45 mmol/kg).

Alkalinity. It was necessary to modify the Gran method [*Dyrssen,* 1965] of calculating the alkalinity from the acidimetric titration data to account for the very large quantities of CO_2 in the samples. Specifically, the assumption that the hydrogen ion concentration is much larger than the bicarbonate concentration beyond the CO_2 endpoint is not valid, so we included a term for the bicarbonate concentration as a function of pH and total CO_2 at each step and plotted the following function against volume of acid added:

$$(v_o + v)\left[10^{-pH} - C_T\left(10^{pH-K_1}\right)\right] \qquad (1)$$

where v_o is the volume of sample, v is the volume of acid added, C_T is the total CO_2 content, and K_1 is the first dissociation constant for carbonic acid, taken from *Stumm and Morgan* [1981].

It was clear from the bubbly appearance of some samples that they were supersaturated with gas (largely CO_2 and H_2S), and we conclude that considerable CO_2 had been lost before the alkalinity titration was initiated. We calculated the CO_2

concentration in each sample using the endmember CO_2 value for each vent (see results for gases) and the measured Mg concentration for the sample. Using the Henry's law constant at 25°C of *Drummond* [1981], we calculate that the CO_2 saturation concentration at atmospheric pressure is approximately 30 mmol/kg in seawater. In order to allow for some supersaturation we set an upper limit on the CO_2 concentration in the alkalinity samples. If the calculated CO_2 concentration exceeded 50 mmol/kg in the sample, then we set CO_2 equal to 50 mmol/kg for the alkalinity calculation; if CO_2 was less than 50 mmol/kg we used the calculated value. Degassing and the CO_2 correction procedure may introduce errors as large as 5% in alkalinity.

The results for alkalinity are shown in Figure 2.5*e*. Inferno and the chloride-normal vents have very similar alkalinities, and the endmember for Hell, Hillock, Mushroom, and Inferno taken together is -0.48 meq/kg. The low-chloride vents, Virgin Mound and Crack, have positive alkalinities of +0.66 and +0.40 meq/kg, respectively.

pH. There are two trends in the plot of measured *p*H versus magnesium (Figure 2.5*f*). The normal salinity fluids lie along a dilution curve which points to an endmember *p*H (25°C, 1 atm) of about 3.5. Virgin Mound and Crack vents form a curve which points to a higher, apparent endmember *p*H near 4.4.

The very high gas content of these fluids has significant effects on the measured *p*H; exsolution of CO_2 can cause large positive errors in the measured *p*H, especially for samples with positive alkalinities. In Figure 2.6 we have plotted the effect of loss of CO_2 on *p*H along lines of constant alkalinity. The measured *p*H values are inconsistent with the measured alkalinity and the CO_2 content predicted by the data from samples taken in the UCSB gas-tight bottles (see below). The measured *p*H of samples from Virgin Mound are almost certainly elevated up to 0.8 *p*H units above

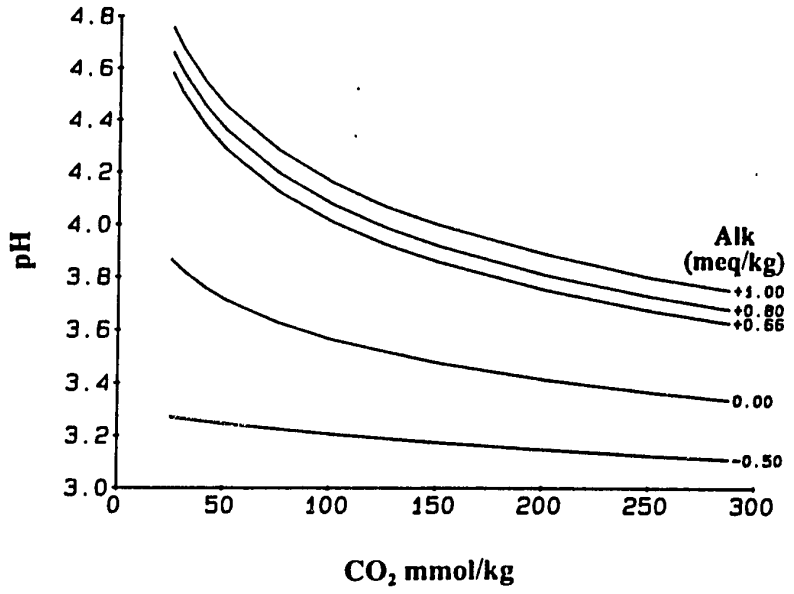

Figure 2.6. Plot of *p*H versus total CO_2 (mmol/kg) along curves of constant alkalinity (labelled in meq/kg). Solutions are saturated with CO_2 at 25°C and 1 atm at approximately 30 mmol/kg CO_2. The measured *p*H of the low salinity samples (4.4) is consistent with a *p*H of about 3.7 prior to degassing to a CO_2 concentration near saturation. >98% of total CO_2 is undissociated over the entire *p*H range shown.

their value before degassing (Figure 2.6). The negative alkalinity samples are initially lower in CO_2 and their change in *p*H due to degassing is less than 0.1 *p*H units for the least diluted samples. We conclude that the actual *p*H of Virgin Mound fluids at room temperature prior to degassing is in the range 3.65-3.70.

Although the alkalinity of the low-salinity fluids at ASHES is high relative to fluids from other ridge-crest hydrothermal fields, the *p*H prior to degassing is buffered near 3.7 by the high levels of CO_2. Using the aqueous chemical speciation program MINEQL [*Westall et al.*, 1976], modified for high-temperatures as described in *Tivey* [1988], I have calculated an *in situ p*H for Virgin Mound (at 300°C) of 3.95.

Iron. Iron (Figure 2.5*g*) attains concentrations of approximately 1 mmol/kg in Inferno and the chloride-normal vents. Inferno is highest in iron (1065 μmol/kg), while Hell and Hillock are somewhat lower (868 and 873 μmol/kg).

The iron content of the chloride-depleted vents is less than 3% of the value of the chloride-normal or chloride-enriched vent fluids. Virgin Mound has the lowest iron concentration (12 μmol/kg).

The major samplers typically had a small amount of coarse-grained particles in the dregs, which were retrieved from the dismantled samplers and saved for future analysis. The relatively large size of these particles leads us to believe that they are entrained chimney fragments broken loose during sampling and not particles formed by precipitation in the sampler. Samples were typically clear when expressed into the trace metal sample bottles, and acidification to *p*H <1.8 effectively kept the metals dissolved. With time, a fine, black precipitate formed in some unacidified samples. These observations suggest that loss of trace metals in the samplers was probably not significant.

The lower iron content in fluids from Hell vent may indicate that iron has precipitated prior to or during sampling. The lowest Mg concentration for samples from Hell vent was 19 mmol/kg, suggesting that some subsurface mixing with seawater may have occurred.

Manganese. Manganese is highest in Inferno (1150 μmol/kg) and lowest in Virgin Mound (142 μmol/kg). The Fe/Mn ratio is close to 1 for Inferno and the chloride-normal vents (Table 2.2), with the exception of Hell, for which Fe/Mn=0.76, consistent with the hypothesis that some iron has been lost due to precipitation of sulfide minerals. The chloride-depleted vents have much lower Fe/Mn ratios (Table 2.2), indicative of large-scale subsurface precipitation of iron.

Zinc. Zinc attains levels of 106 to 134 μmol/kg in Inferno and the chloride-normal fluids, while the chloride-depleted fluids contain only 2 to 3 μmol/kg (Table 2.2). Hell vent has the highest zinc concentration and Virgin Mound has the lowest (2.2 μmol/kg).

Copper. Inferno and the chloride-normal vent fluids have endmember copper concentrations near 10 μmol/kg, with the exception of Hell vent, which has an endmember of only 1.2 μmol/kg. This is consistent with the lower iron content of Hell fluids and is further evidence for subsurface precipitation of sulfides.

Comparison to Other Vent Fields

The composition of Inferno and the normal chlorinity vent fluids from ASHES is within the range of compositions found at other mid-ocean ridge hydrothermal areas (Table 2.4), though the gas content is higher (Table 2.3). (Lower levels of silica in ASHES fluids may be attributed to the significantly shallower depth.) The low-chlorinity, metal-depleted, gas-enriched fluids at ASHES have no counterparts in the literature on mid-ocean ridge hot springs, and the observation of such

TABLE 2.4. Chemical Comparison of ASHES Vent Fluids With Other Mid-ocean Ridge Hydrothermal Systems.

Vent	ASHES		13°N[a]	21°N[b]		SJFR[c]	Mid-Atlantic Ridge[d]	
	Inferno	Virgin Mound		NGS	OBS	Plume	TAG	MARK-1
*p*H, 25°C	3.5	4.4	3.2	3.8	3.4	3.2		3.9
T, °C	328	299	320	273	350	224	290-321	350
Cl mmol/kg	624	176	740	579	489	1087	659	559
Li µmol/kg	636	184	688	1033	891	1718	411	843
Na mmol/kg	501	151	560	510	432	796	584	510
K mmol/kg	26.8	6.98	29.6	25.8	23.2	51.6	17.6	23.6
Ca mmol/kg	46.8	10.2	55.0	20.8	15.6	96.4	26.0	9.9
Sr µmol/kg	192	46.4	175	97	81	312	99	50
Sr/Ca x1000	4.10	4.55	3.18	3.76	5.19	3.24	3.81	5.05
Mn µmol/kg	1150	142	1090	1002	960	3585	1000	491
Fe µmol/kg	1065	12	1450	871	1664	18,739	1640	2180
H_2S mmol/kg	7.1	(18)	NA	6.5	7.3	3.50	NA	5.9
Si mmol/kg	15.1	13.5	22.0	19.5	17.6	23.3	22.0	18.2

Value in parentheses is an estimate.

[a] *Michard et al.*, [1984].

[b] *Von Damm et al.*, [1985].

[c] *Von Damm* [1988].

[d] *Campbell et al.* [1988].

chemically diverse fluids within a few meters of each other is unprecedented.

Discussion

Our interpretation of the data focuses on the subsurface mixing of vapor and liquid endmembers created by adiabatic boiling of a hydrothermal fluid. We will begin by briefly reviewing the phase relations of aqueous salt solutions and the earlier work on phase separation in hydrothermal systems and then proceed to develop a model to account for the observed chemistry of ASHES fluids.

Properties of the H_2O-NaCl System

Experimental studies have determined the phase relations in the system H_2O-NaCl over a very wide range of pressure and temperature conditions [*Sourirajan and Kennedy*, 1962; *Khaibullin and Borisov*, 1966; *Bischoff and Rosenbauer*, 1984, 1988]. *Bischoff and Rosenbauer* [1984] have shown that the bulk properties of 3.2 wt % NaCl in H_2O are very similar to the properties of seawater.

A key difference between the phase behavior of pure water and that of the binary system H_2O-NaCl is that phase transitions may occur in the binary system beyond the critical point of the system. The critical point is the point in pressure-temperature-composition space where the properties of liquid and vapor are identical. For 3.2 wt % NaCl the critical point is reached at 407°C and 298.5 bars [*Bischoff and Rosenbauer*, 1988]. When a hot salt solution decompresses and encounters the two-phase curve at temperatures below the critical point (Figure 2.7), the result is subcritical phase separation or boiling, formation of nearly pure water vapor from saline liquid. When the same fluid crosses the extension of the two-phase boundary at temperatures higher than the critical point (called the condensation-point curve by *Fournier* [1987]), the result is condensation of a small

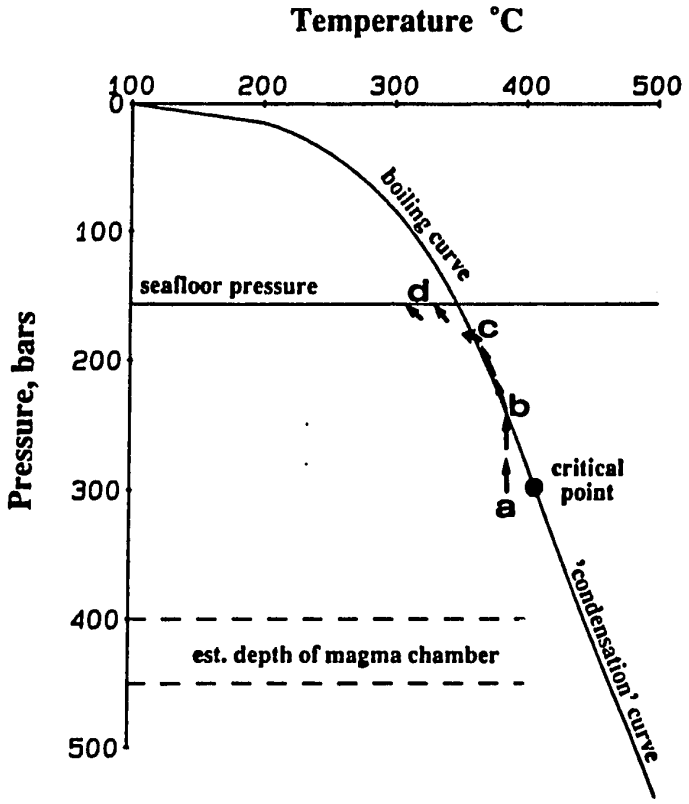

Figure 2.7. Two-phase boundary curve for 3.2 wt % NaCl, with a proposed fluid pathway for ASHES fluids. A fluid which intersects the two-phase curve at temperatures below the critical point as a result of adiabatic decompression (along the path from a to b) will boil and generate a low-salinity vapor phase. The liquid phase becomes enriched in salt as adiabatic boiling proceeds (from b to c), and the system cools due to the enthalpy of vaporization. Boiling stops when the fluid is cooled by heat loss to the surrounding rock or by mixing with cold seawater (point c) and the liquid and recondensed vapor exit the seafloor (point d). A fluid which is hot enough to intersect the two-phase curve beyond the critical point will undergo supercritical phase separation by condensing a small amount of highly saline brine from a vapor-like fluid of near-seawater salinity. Data for two-phase curve are from *Bischoff and Rosenbauer* [1988]. Estimated depth to the magma chamber from *Dixon et al.* [1989], assuming hydrostatic pressure.

amount of highly saline brine from a vapor-like fluid. In the binary H_2O-NaCl system it is appropriate to refer to this brine condensation as supercritical phase separation, though the term is oxymoronic when applied to a pure substance.

As the critical point is approached from lower temperatures and pressures, boiling produces a vapor which contains progressively more salt. *Khaibullin and Borisov* [1966] and *Sourirajan and Kennedy* [1962] have studied the distribution of salt (NaCl and KCl) between liquid and vapor under P-T conditions up to and beyond the critical point and have shown that the amount of salt in the vapor is much less than in the liquid until the boiling temperature approaches to within 10-15°C of the critical point.

Effect of gases. Studies of the system H_2O-NaCl-CO_2 [*Ellis and Golding*, 1963; *Takenouchi and Kennedy*, 1964, 1965; *Gehrig et al.*, 1979; *Drummond*, 1981] have shown that addition of CO_2 moves the critical point of the system to higher pressures and lower temperatures. For the level of CO_2 in ASHES fluids, the critical point is shifted by less than 3°C and 10 bars.

The boiling point can be substantially lowered by the measured amounts of CO_2 (Figure 2.8), but all measured temperatures at ASHES are still within the single phase region. CO_2 is by far the most abundant gas in ASHES fluids, but the cumulative effect of other dissolved gases (H_2S, N_2, CH_4, He, etc.) may also contribute to a higher vapor pressure and a lower boiling temperature.

Phase Separation in Hydrothermal Systems

A variety of evidence including fluid inclusion data, salinity variations and pressure-temperature measurements suggests that phase separation occurs in hydrothermal systems. Alternative mechanisms of rock hydration and precipitation/dissolution of a chloride-bearing mineral phase can explain some of the observed salinity variations.

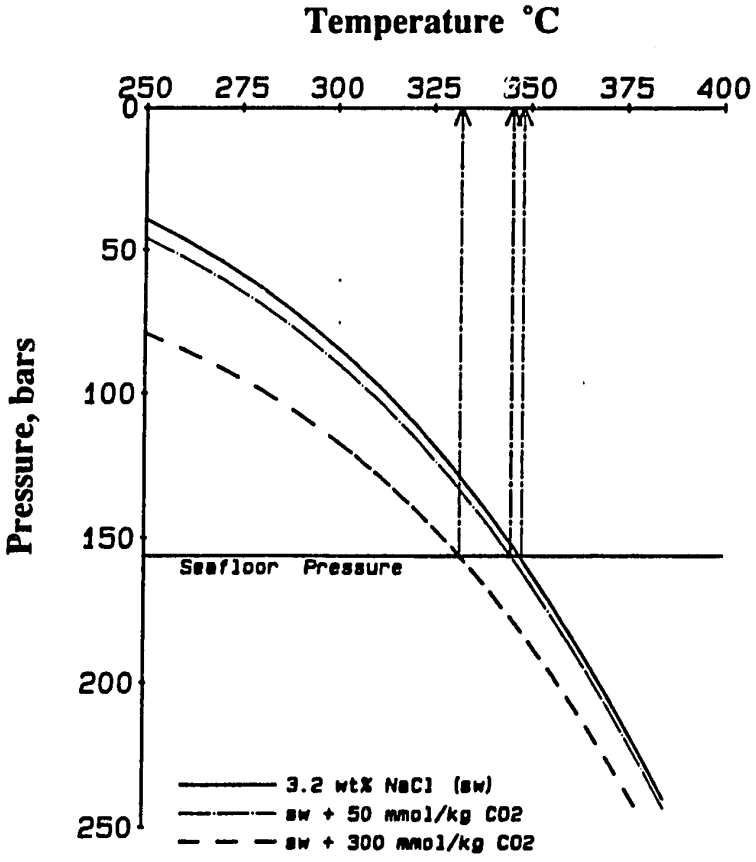

Figure 2.8. Effect of CO_2 on pressure. Two-phase curves for 3.2 wt % NaCl (solid curve) [*Bischoff and Rosenbauer*, 1988], and 3.2 wt % NaCl plus 50 (dot-dashed curve) and 300 (dashed curve) mmol/kg CO_2. Vertical dot-dashed lines intersect the ordinate at the boiling temperature at 156 bars total pressure for each composition. Addition of 50 and 300 mmol/kg CO_2 lowers the boiling temperature at 156 bars by 3° and 16°C, respectively. As boiling proceeds and CO_2 partitions into the vapor phase, the two-phase curve for the system will approach the two-phase curve for a gas-free NaCl solution.

Fluid inclusions. There is sufficient evidence from fluid inclusion data [*Delaney et al.*, 1987; *Kelley and Delaney,* 1987; *Ramboz et al.*, 1988; *Cowan and Cann,* 1988] to suggest that both subcritical phase separation (boiling) and supercritical phase separation (condensation) occur in hydrothermal systems. *Kelley and Delaney* [1987] have identified two-phase fluid inclusions in gabbros from the Mid-Atlantic Ridge with salinities from 1 to 50 wt % NaCl equivalent and formation temperatures from 400° to 700°C. These inclusions are interpreted to be a result of condensation of highly saline brines from hydrothermal fluids at 1000 to 1200 bars.

Ramboz et al. [1988] have studied fluid inclusions in anhydrite recovered in sediment cores from the Atlantis II Deep in the Red Sea. They interpret these inclusions to be the result of trapping a mixture of liquid and condensed vapor generated by boiling of a 19 wt % brine at 390 to 403°C and ~223 bars. These conditions are below the critical point for such a brine (540°C, 700 bars). It is suggested that the 19 wt % brine may have formed during isothermal boiling near a magmatic heat source and then may have undergone isenthalpic boiling while rising adiabatically. The pure vapor phase was not trapped in fluid inclusions during this process, presumably due to its much higher mobility and undersaturation with respect to mineral formation.

Cowan and Cann [1988] have interpreted two- and three-phase fluid inclusions from the Troodos ophiolite to represent trapped mixtures of seawater and the vapor and brine phases formed by supercritical phase separation (condensation) of a hydrothermal fluid at 500-525°C and 350-400 bars.

Chlorinity variations. Large positive and negative deviations from seawater chlorinity have been observed in hydrothermal fluids from the Galapagos Spreading Center, the East Pacific Rise, and the Southern Juan de Fuca Ridge [*Edmond et al.*, 1979; *Michard et al.*, 1984; *Von Damm et al.*, 1985; *Von Damm and Bischoff,* 1987;

Bowers et al., 1988], raising the possibility that hydrothermal circulation may be a source or sink of chlorinity equal to or greater than the river flux [*Edmond et al.*, 1979]. Rock hydration and precipitation/dissolution of a chloride-bearing mineral [*Seyfried et al.*, 1986] have been cited as possible explanations for the variations on the East Pacific Rise and at Galapagos, but these mechanisms are not adequate to explain the magnitude of observed chlorinity variations, which range from 200% of seawater at SJFR [*Von Damm and Bischoff*, 1987] to 33% of seawater at ASHES.

Von Damm [1988] and *Cowan and Cann* [1988] both proposed that the observed chlorinity variations in hydrothermal systems could be accounted for by mixing of seawater, hydrothermally evolved seawater, and the vapor and brine phases produced during phase separation of hydrothermal fluid. These models not only require that phase separation occur, but that the phases must also become segregated and follow different pathways to the surface. Unless sampling strategies have missed the vapor phase at SJFR (there is some evidence that a vapor phase may be venting from warm vents there (G. J. Massoth and J. E. Lupton, unpublished data, 1989; K. L. Von Damm, unpublished data, 1989)) then the chemistry of SJFR fluids (i.e., a brine phase with no attending vapor) implies that phase separation is episodic, resulting in the buildup and release of brine pools. During the times when the hypothetical brine pool is accumulating, there would be a net release of vapor. Though phase separation may produce the entire range of chlorinities observed at mid-ocean ridge hydrothermal sites, it should not affect the balance of chlorinity in the oceans unless brine pools are permanently sequestered in the crust, possibly by a mechanism similar to that proposed by *Goldfarb and Delaney* [1988], whereby high-salinity brines accumulate in small fractures or micro-cracks by virtue of their surface-coating characteristics.

Pressure-temperature measurements. The histogram of measured vent fluid temperatures presented by *Campbell et al.* [1988] shows that the majority of temperature measurements at mid-ocean ridge vents are below the boiling point. However, temperatures clearly within the two-phase region have been reported on two occasions at Endeavour Ridge [*Delaney et al.*, 1984; *Spindel et al.*, 1988; *Tivey et al.*, 1990]. There are significant chloride variations among the vents at the Endeavour Ridge site, but the available gas data are not negatively correlated with chloride to the same degree as the ASHES fluids (see chapter 3). The temperature measurements and chemical data at Endeavour are consistent with phase separation at supercritical temperatures and pressures.

It has been argued that precipitation/dissolution of a chloride-bearing mineral phase (as opposed to phase separation) may cause the observed salinity variations at 13°N EPR [*Seyfried et al., 1986; Bowers et al.*, 1988] because of the lack of correlation between chlorinity and gas content in some vent fluids. However, the ASHES data, as we shall see, do show chlorinity-gas content correlations strongly suggesting active phase separation in the ascending hydrothermal fluids. Furthermore, under some conditions phase separation does not produce large changes in gas content with chlorinity, and other processes may be responsible for causing variability in gas content between systems.

Vapor-Liquid-Seawater Mixing Model

We propose that a hydrothermal fluid rising through the ocean crust has boiled and generated vapor and liquid (brine) phases which have become physically segregated and followed different pathways to the seafloor, cooling and mixing to varying degrees along the way with cold seawater, which has percolated into the

interstitial matrix of the ocean crust. In order to evaluate this hypothesis, we will compare the chemistry of ASHES hydrothermal fluids with mixtures of model-generated vapor and liquid phases and cold seawater.

Assumptions of phase separation model. By creating a simple boiling model to describe the partitioning of dissolved solids and gases between vapor and liquid, we can compare the mixing of theoretically generated vapor and liquid endmembers with the actual mixing patterns observed in the ASHES fluids. The treatment here follows that of *Drummond* [1981].

The elements of a simple boiling model may be stated in two assumptions:

1. When boiling occurs, the salt remains entirely in the liquid phase, so that the vapor produced is essentially distilled water and gas.

2. Gases partition between liquid and vapor according to Henry's law.

The first assumption is valid in a normal (subcritical) boiling regime [*Sourirajan and Kennedy,* 1962; *Khaibullin and Borisov,* 1966] when the boiling is more than about 15°C or 30 bars below the critical point (i.e., up to about 390°C for seawater). Under near-critical or supercritical P-T conditions, significant concentrations of salt may exist in the "vapor" phase. In the mixing model, the vapor component will have zero concentration of nonvolatile elements, while the residual liquid will be enriched over its starting composition by a factor of $1/(X)$, where X is the mass fraction of water remaining in the liquid phase after the fraction $(1-X)$ has been removed as vapor. If we can place reasonable constraints on the starting composition of the hydrothermal fluid, then we can estimate the minimum amount of boiling which has occurred.

The critical pressure of 300 bars is approximately 1.5 km below the seafloor at the ASHES site, assuming hydrostatic pressure. The depth to the magma chamber based on the solubility of CO_2 in basaltic glass has been estimated to be 2.7 km

below the seafloor [*Dixon et al.*, 1988], which does not prohibit circulation of fluids in the supercritical region. We cannot preclude that supercritical phase separation (condensation) has taken place, but the data neither require nor suggest that it has.

Endmembers in the ASHES system. Much of the chemical variability between vents in the ASHES field can be explained by a simple, three-endmember, conservative mixing model similar to that proposed by *Von Damm* [1988]. In nearly any property-property plot (Figures 2.2, 2.3, and 2.4), it can be seen that most of the data points fall within a triangular area defined by the composition of seawater and the endmember compositions of Virgin Mound and Inferno vents; thus nearly all of the data can be explained by mixing of these three components. While we have focused attention on the data from Inferno and Virgin Mound, because these two vents represent the extremes of composition found at the ASHES site, it is certainly possible that more extreme compositions may exist in the subsurface.

If we remove the seawater component in the mixing diagrams by extrapolating the data for each vent to zero magnesium (Figure 2.9), we can see that the data points cluster tightly about a line drawn between the Inferno endmember and the origin for each of the nonvolatile components considered. This is consistent with mixing a fluid with Inferno composition with a fluid of zero salinity. This strongly suggests that a fluid of near-zero salinity exists somewhere in the system but is not completely segregated from the liquid. Likewise, a component more saline than the most saline fluid sampled may also exist in the subsurface, with incomplete segregation preventing us from sampling the most extreme fluids.

If all nonvolatile components behave ideally and are not affected by reactions occurring after phase separation, then all of the ASHES endmembers, as plotted in Figure 2.9, should lie on a line between Inferno composition and pure water. (In the absence of data describing the partitioning of nonvolatile components between liquid

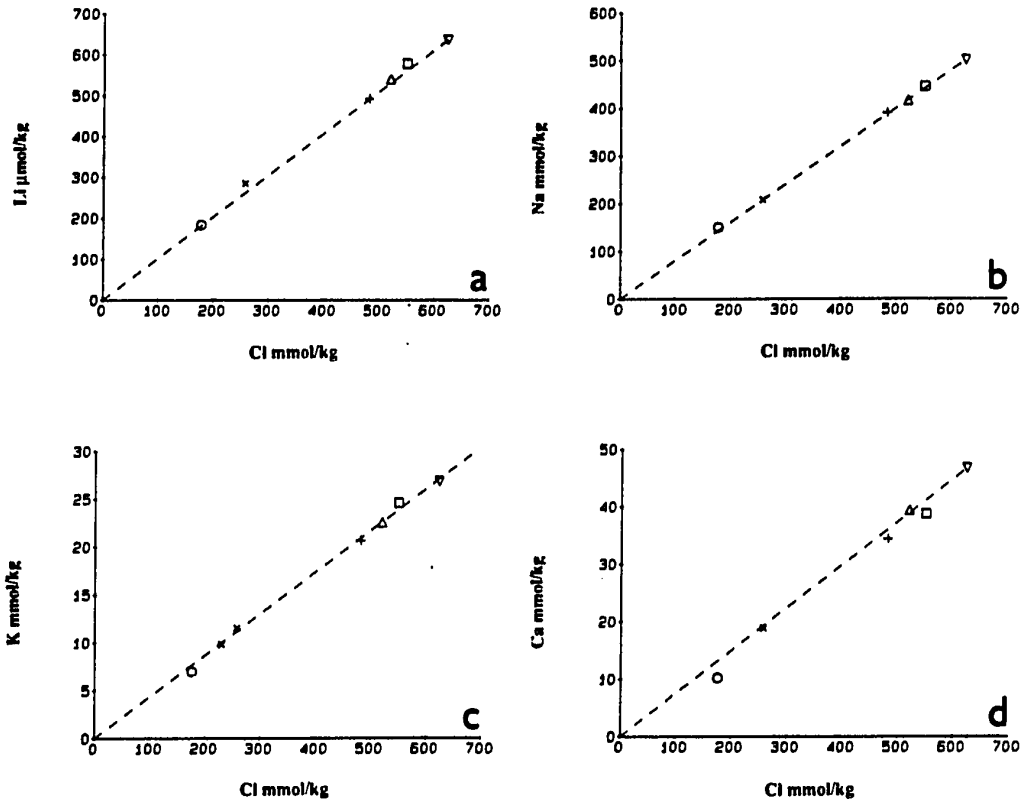

Figure 2.9. Plot of endmember elemental concentrations versus endmember chloride concentration for individual vents. By extrapolating the data points for each vent to zero magnesium, the seawater component is removed, revealing a mixing line between Virgin Mound and Inferno compositions. For many elements, the end-members for the different vents lie very close to a line connecting Inferno composition with the origin, which is consistent with the mixing of a brine with a vapor of near-zero salinity. The simple boiling model assumes that all end-members will lie on this mixing line; deviations from this ideal behavior are used to infer relative loss or gain of elements by the hydrothermal fluids. (*a*) Lithium. (*b*) Sodium. (*c*) Potassium. (*d*) Calcium.

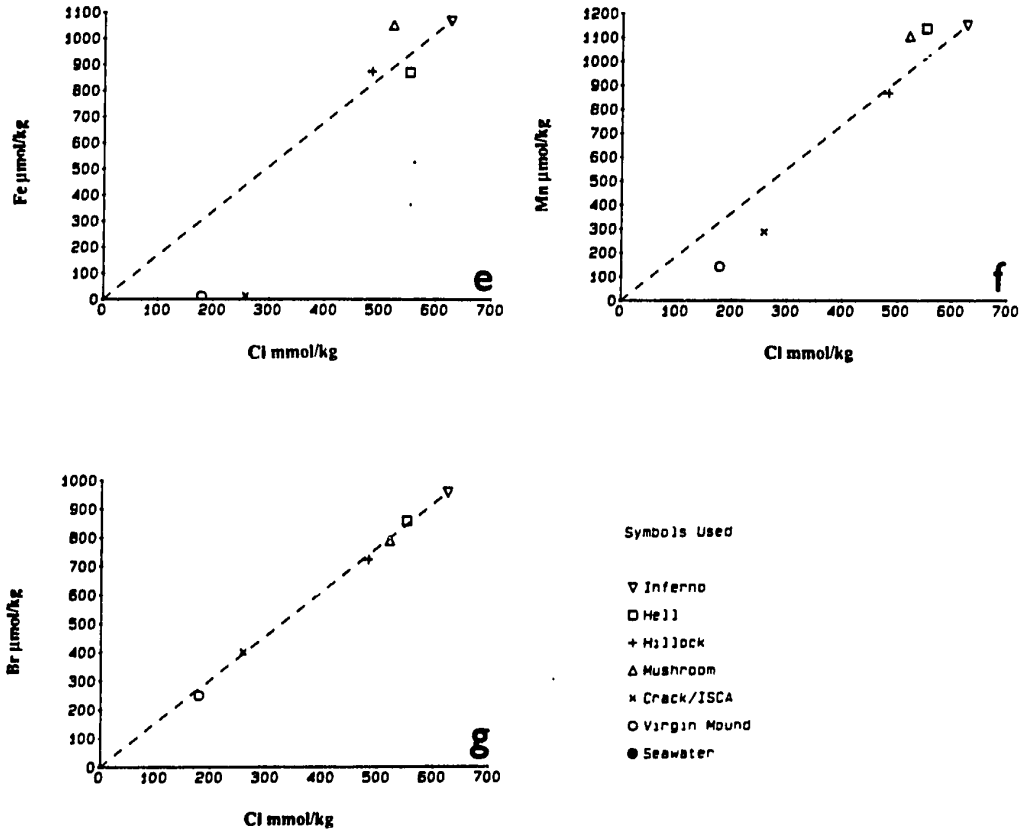

Figure 2.9. (continued) Endmember elemental concentrations versus endmember chloride. (*e*) Iron. (*f*) Manganese. (*g*) Bromide.

and vapor, we assume that all nonvolatiles have an equal, very low affinity for the vapor phase. In the specific cases where we have data on the distribution of components between phases, we have explicitly calculated how the fluids are affected.) However, if the fluids continue to react, there will be deviations from this ideal behavior. We have assumed in drawing the lines in Figure 2.9 that the ratios of dissolved components remain unchanged by the boiling process. Even if this assumption is not valid, the chemical deviations from this ideal behavior will reflect relative changes between vents.

High gas content of ASHES fluids. The levels of CO_2 and Helium in all ASHES fluids are considerably higher than other mid-ocean ridge sites, and the ratio of helium to CO_2 is smaller at ASHES (Table 2.3). What is the source of these gases?

The CO_2 content of basalts from Axial Seamount reported by *Dixon et al.* [1988] show a maximum value of 360 ppm CO_2 by weight, which is equivalent to about 8 mmol/kg. To reach the levels of CO_2 observed in Virgin Mound fluids by leaching CO_2 from the basalt would require a water/rock ratio of about 0.03, which is much lower than indicated by the fluid chemistry at ASHES and at other ridge-crest hydrothermal sites [*Von Damm,* 1988]. It is very unlikely that the high concentrations of gases in the ASHES fluids could be derived solely from leaching of basalt.

Small gas enrichments could also be achieved if the hydrothermal system is not closed to mass and a saline, gas-depleted brine is left behind to accumulate in the crust. This would cause all of the venting fluids to be enriched in volatiles and depleted in nonvolatiles. Because of the magnitude of gas enrichment and because even the higher salinity fluids are enriched in gases, loss of a gas-depleted brine is not a likely explanation for the high gas levels at ASHES, but since we have not

measured a tracer known to be conservative throughout the entire process of hydrothermal circulation, the possibility that the system is open to mass cannot be ruled out. Argon measurements may help to resolve this issue [*Evans et al.*, 1988].

High gas levels in ASHES fluids may be due to magmatic exsolution of a CO_2-rich fluid and injection into the circulating hydrothermal fluids. This is consistent with a magma at CO_2 saturation rising up into the volcanic edifice of Axial Seamount and exsolving a fluid upon decompression. (The much higher concentrations of CO_2 at Loihi Seamount [*Karl et al.*, 1988] (Table 2.3) may be the result of this same process.) Because the maximum measured H_2O content of basalt at Axial Seamount [*Dixon et al.*, 1989] is below the solubility of H_2O in basaltic melts even at pressures as low as 250 bars [*Burnham*, 1979], an exsolved magmatic fluid should be mostly CO_2 and other gases. Since the maximum CO_2 content of ASHES fluids is only about 1.3 wt %, we may eliminate the hypothesis that the observed salinity variations at ASHES are due to mixing of a hydrothermal fluid with a low-salinity, CO_2-enriched fluid of magmatic origin.

Gas partitioning. When boiling occurs in a hydrothermal system, volatile components will be preferentially partitioned into the vapor phase. This partitioning can be described by Henry's law:

$$K_H^p = f_g / m_g \qquad (2)$$

where K_H^p is the Henry's law constant at pressure p, f_g is the fugacity of the volatile component and m_g is the molality of the volatile component in the aqueous phase. The partial pressure of all gases in the ASHES fluids is less than 50 bars, which places them in the region of Henry's law behavior for temperatures up to 350°C [*Ellis and Golding*, 1963; *Drummond*, 1981].

As an additional tool for looking at the distribution of a gaseous component between liquid and vapor, we may use the volatility ratio [*Ellis and Golding,* 1963; *Drummond,* 1981] :

$$VR = \frac{(n_{gv} \times n_{wl})}{(n_{gl} \times n_{wv})} \tag{3}$$

where n_{gv} is the number of moles of gas per unit volume in the vapor, n_{gl} is the number of moles of gas per unit mass (kg) in the liquid, n_{wv} is the number of moles of water per unit volume in the vapor, and n_{wl} is the number of moles of water per unit mass in the liquid. The volatility ratio is related to the Henry's law coefficient by

$$VR = \frac{(K_H \times V_{wv})}{(\theta Z R T)} \tag{4}$$

where V_{wv} is the specific volume of water vapor, θ is the fugacity coefficient, Z is the compressibility factor of the gas, R is the gas constant, and T is temperature in Kelvin.

Drummond has calculated VR for H_2, CH_4, CO_2, H_2S, and SO_2 and fit each of them to a linear equation of the form

$$\log VR = A + BT \tag{5}$$

where A and B are constants. These regressions are obtained from data for solubility in distilled water. In order to apply the equations to a saline system, we first convert the actual temperature to a reduced temperature scale by the principle of corresponding states:

$$T' = T \times (T^{o}_{crit})/(T_{crit}) \tag{6}$$

where T^o_{crit} is the critical temperature of pure water, and T_{crit} is the critical temperature of the solution. T' is then substituted for the actual temperature, T, in equation (4).

Although in theory VR is unity at the critical point, Drummond's data only extend to 350°C and equation (4) gives a value greater than 1 at the critical temperature for all gases except SO_2. Use of equation (4) near the critical point will result in overestimating the gas content of the vapor phase and underestimating the gas content of the liquid phase.

Evolution of gas content in the liquid phase with boiling differs in open and closed systems. Briefly, a closed system is one in which the vapor and liquid phases always remain in contact as the system evolves; the vapor and liquid follow the same flow path during closed-system boiling and the two phases remain in equilibrium. In an open system, the vapor is continuously removed from the liquid as boiling proceeds, and is therefore in equilibrium with the liquid only at the moment it is formed.

For either type of system, one can calculate the residual concentration of gas in the liquid as a function of degree of boiling [*Drummond,* 1981] by using the volatility ratio. For a closed system we have

$$m_g = \frac{m_g^o}{(X + VR(1-X))} \tag{7}$$

where m_g is the molality of gas in liquid equilibrated with water vapor, m_g^o is the initial molality of gas in liquid, and X is the mass fraction of water remaining in the liquid phase. For an open system (Rayleigh distillation) the relation is

$$m_g = m_g^o \times X^{(VR-1)} \tag{8}$$

We can then calculate the molality of gas in the recondensed vapor (since that is what we actually measure) by mass balance.

As boiling proceeds, the liquid loses heat to the vapor phase and the system cools rapidly. The cooling rate depends on the enthalpy of vaporization and is temperature dependent. The closer the system is to the critical temperature, the smaller the enthalpy of vaporization and the smaller the cooling rate. If the temperature interval is small, the cooling rate can be considered constant over the interval without introducing significant error. In our calculations, we have matched the initial and final temperatures with the degree of boiling by conservation of enthalpy using regression equations for enthalpy of liquid and vapor as a function of temperature and salinity [*Drummond,* 1981].

Evolution of system composition with boiling. By using the experimental solubility data of Drummond, we can predict the partitioning of the major gases between liquid and vapor. Given an initial composition, we can calculate the composition of vapor and liquid as a function of the degree of boiling.

The results of these calculations are shown in Figures 2.10 and 2.11. Figure 2.10*a* shows the CO_2 concentration of the liquid and vapor for both open and closed systems. It is evident that the liquid is depleted in gas much faster in the open system than in the closed system. By the time 15% of the water has been transferred to the vapor phase (an amount consistent with the measured chlorinity enrichment of Inferno fluids), the gas content of the liquid is 50% of its initial value in a closed system, and only 25% in an open system (Figure 2.10*a*). Figure 2.11 shows the evolution of chloride and CO_2 as boiling proceeds in a closed system, compared to the endmember concentrations of chloride and carbon dioxide for Inferno, Virgin Mound, and Crack vents. The point for Inferno falls nearly directly on the line for the pure liquid in a closed system and the point for Virgin Mound lies near mixing lines for 15 and 20% boiling.

Figure 2.10. (*a*) Dissolution of CO_2 during boiling in open and closed systems. Concentrations of CO_2 in liquid (lower lines) and vapor phases as a function of the percent of water removed as vapor. CO_2 concentration axis is relative to the initial concentration in the liquid prior to the onset of boiling. Concentrations are calculated using equations (4)-(7) with these conditions: initial temperature = 390°C, cooling rate = 1.25°C/% boiling. (*b*) Dissolution of hydrogen (analogue for helium, see text) during boiling in open and closed systems. Note that the partitioning of hydrogen between liquid and vapor is very similar to that of CO_2. (*c*) Dissolution of H_2S with boiling. The higher solubility of H_2S results in less enrichment in the vapor phase than is predicted for hydrogen and CO_2. Solubility data are from *Drummond* [1981].

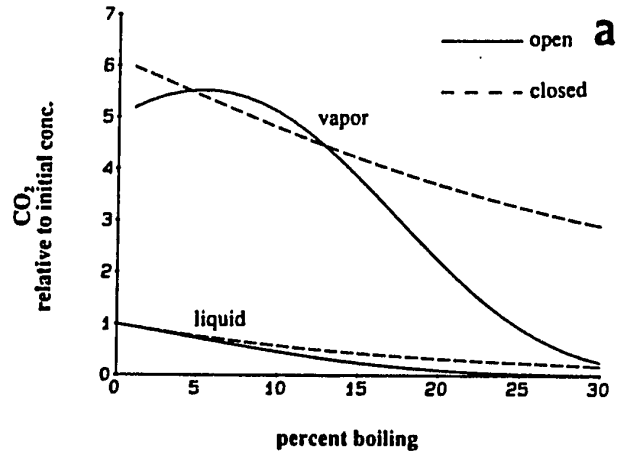
a
open
closed
vapor
liquid
CO_2
relative to initial conc.
0
1
2
3
4
5
6
7
0
5
10
15
20
25
30
percent boiling

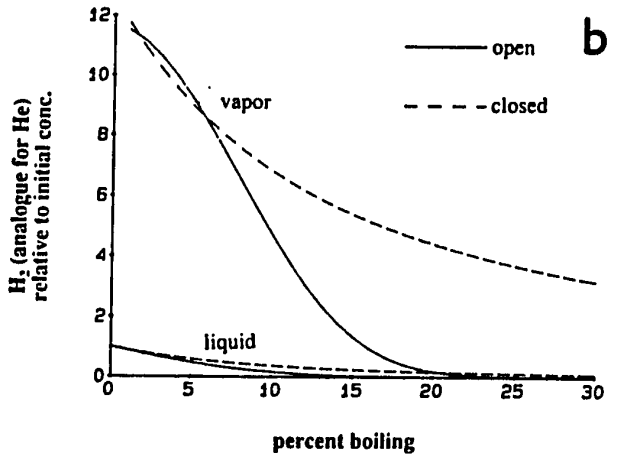
b
open
closed
vapor
liquid
H_2 (analogue for He)
relative to initial conc.
0
2
4
6
8
10
12
0
5
10
15
20
25
30
percent boiling

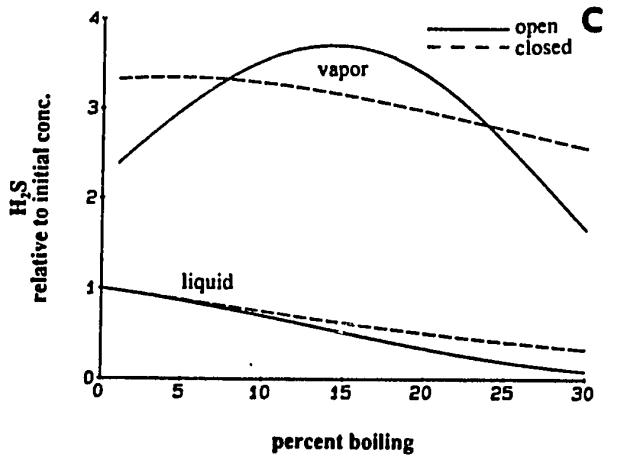
c
open
closed
vapor
liquid
H_2S
relative to initial conc.
0
1
2
3
4
0
5
10
15
20
25
30
percent boiling

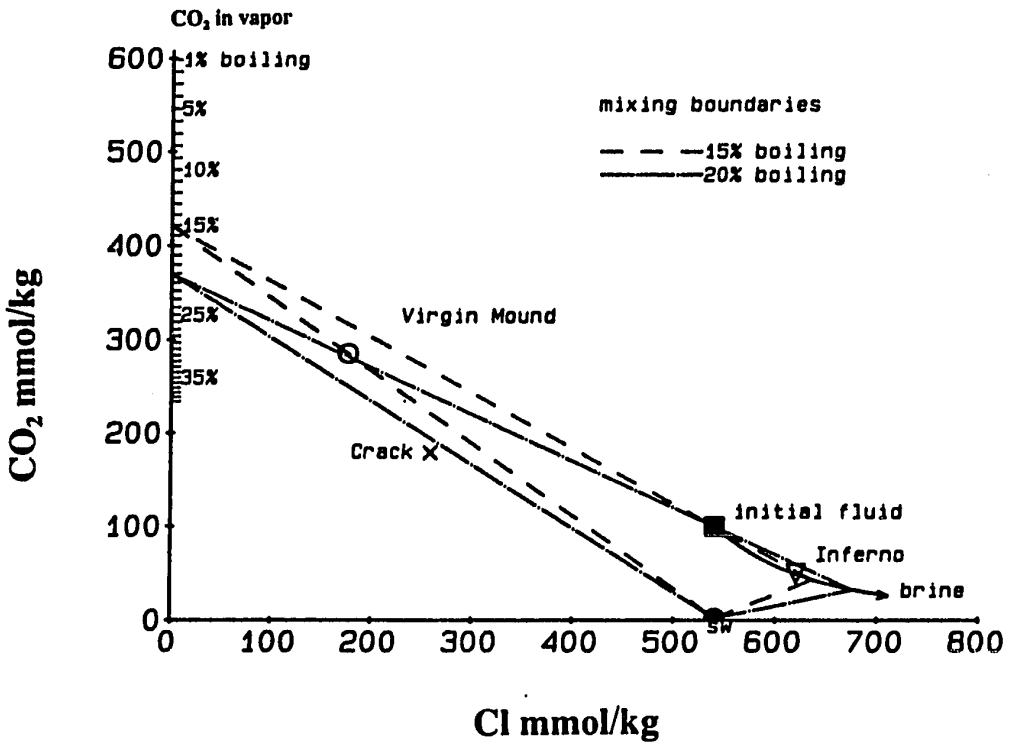

Figure 2.11. Evolution of Cl and CO_2 with boiling in a closed system. We have set the initial chloride content equal to seawater concentration and assumed that the initial CO_2 is 100 mmol/kg, but the shape of the mixing areas is not affected by the absolute quantity of CO_2 in the system. The CO_2 content of the vapor for a closed system is superimposed on the *y* axis (since Cl=0 in the vapor). A point is marked for each percent of water removed as vapor. The evolving composition defines a set of mixing lines connecting the pure liquid (solid curve) with the pure vapor for a given degree of boiling. Note that each of these lines passes through the point which represents the initial system composition. If boiling proceeds as in a closed system for some time before the vapor and liquid segregate and follow separate paths to the surface, then mixtures of these two end-members will lie along the mixing line for the given degree of boiling and the extent to which the two phases unmix will determine how closely they approximate the pure end-members. Mixing lines between vapor, liquid, and seawater are drawn for 15 and 20% boiling, and the plotted data points for Virgin Mound, Inferno, and Crack vents lie very close to these mixing areas. The CO_2 content of the vapor (tic marks along CO_2 axis) decreases as boiling proceeds. Temperature at onset of boiling for these calculations is 390°C.

The data point for Crack vent falls slightly below the line for mixing of pure liquid and vapor, but close to the mixing zone for liquid-vapor-seawater, suggesting that fluids from Crack vent may have mixed with seawater in the subsurface (consistent with their lower maximum temperature). Alternatively, the lower gas content of Crack vent may reflect the partially open nature of the hydrothermal system: Crack vent fluids may be the result of a later stage of boiling than Virgin Mound. By partially open we mean that adiabatic boiling may proceed for some time with the vapor and liquid maintaining contact before a vapor-enriched component becomes segregated from a liquid- or brine-enriched component. If Inferno represents the closest approximation to a brine in this system, then the high gas content which remains in Inferno argues that boiling has proceeded in a manner more closely approximating a closed system than an open system.

The gravimetric H_2S data indicate that Virgin Mound fluids are enriched roughly 2.5 times over Inferno, which is somewhat less than the approximately fourfold enrichment that we would expect if H_2S is assumed to behave conservatively during boiling. Although H_2S levels in the fluids may be reduced by subsurface precipitation of metal sulfides, there is not enough iron in the fluids to account for all of the H_2S deficiency, assuming that the original unboiled fluid did not contain significantly more iron than the maximum measured concentration of iron in the vent fluids.

The helium data provide another constraint on volatile behavior during phase separation, but there is very little experimental data on helium solubility at high temperatures and virtually no data above 300°C [*Himmelblau,* 1960; *Potter and Clynne,* 1978]. At low temperatures (<75°C), helium is by far the most insoluble gas common to hydrothermal fluids, but the solubility increases rapidly with temperature so that at 200°C, N_2, O_2, Ne, Ar, and CH_4 are all less soluble than He [*Himmelblau,*

1960; *Potter and Clynne,* 1978]. The solubility of helium (and other gases) near the critical point is poorly known. Because helium solubility is close to hydrogen solubility at temperatures >250°C [*Himmelblau,* 1960], we will use the volatility ratio of hydrogen [*Drummond,* 1981] for comparison.

Figure 2.10*b* shows the dissolution path of hydrogen (a proxy for helium) as boiling proceeds in both open and closed systems. Note that the calculated helium enrichments in the vapor phase are only slightly higher than those for CO_2 under closed system conditions in the 15 to 20% boiling range.

The ASHES gas data (Table 2.3) show that the low-chlorinity fluids are slightly less enriched in helium than in CO_2. One possible explanation for this observation is that phase separation has taken place in a temperature region where helium is more soluble than CO_2. The solubility of helium in aqueous salt solutions is less than the solubility of CO_2 at temperatures below 350°C, but helium solubility increases rapidly with temperature. Near the critical point, the difference in solubility between the two gases will be smaller, since the volatility ratio for all gases approaches 1 at the critical point. The observed He/CO_2 ratios may imply that phase separation has taken place in a temperature range where there is a reversal in the relative solubilities of these two gases, and that the solubility of helium may increase more rapidly than that of carbon dioxide as the critical point is approached. More gas solubility measurements in the near-critical region are needed to evaluate this hypothesis.

Both the helium and CO_2 enrichments in the low-chlorinity fluids are roughly consistent with the boiling model for initial boiling temperatures near 390°C. The ability of this simple closed-system boiling model to explain the covariation of chloride and carbon dioxide, the major anion and dissolved gas in ASHES fluids, argues strongly that phase separation has taken place.

Application of boiling model to experimental results. To test the ability of our model to predict the partitioning of gas between liquid and vapor in a closed system, we compare the model output with CO_2 and Cl concentrations measured during an experimental study of phase separation [*Bischoff and Rosenbauer,* 1987] (Figure 2.12). In the two experiments conducted, boiling is initiated at higher temperatures (~415°C) than we envision for the subsurface at ASHES and the extent of boiling is much higher (52 and 66%), but the model results are very close to the experimental results, indicating that the assumptions inherent in our model are reasonable and that the CO_2 solubility data are adequate even at temperatures as high as 390°C.

The nonvolatile elements reported in *Bischoff and Rosenbauer* [1987] (Figure 2.13) generally exhibit the ideal partitioning between liquid and vapor which we have inferred to take place during subseafloor boiling at ASHES (Figure 2.9). The measured chlorinities of the experimental vapor phases are very low, so that even if cations have different relative affinities for the vapor phase, a line drawn through brine and vapor will pass very near the origin.

Pressure-temperature constraints. In order to constrain the pressure-temperature history of ASHES fluids, we must know what the composition of the fluid was prior to the onset of boiling. Since we are not certain that we have a direct measure of the unboiled fluid, we are forced to make an assumption. In the discussion of the evolution of system composition with boiling we have taken the ambient seawater value for the initial chloride content of the high-temperature fluids and shown that the ASHES data are consistent with a simple closed system boiling model. We have neglected other processes (rock hydration, chloride-bearing mineral precipitation) which might change the chloride content of the fluids. The ability of this simple boiling and mixing model to explain most of the data argues that boiling is the dominant process in altering the chloride content in the ASHES hydrothermal

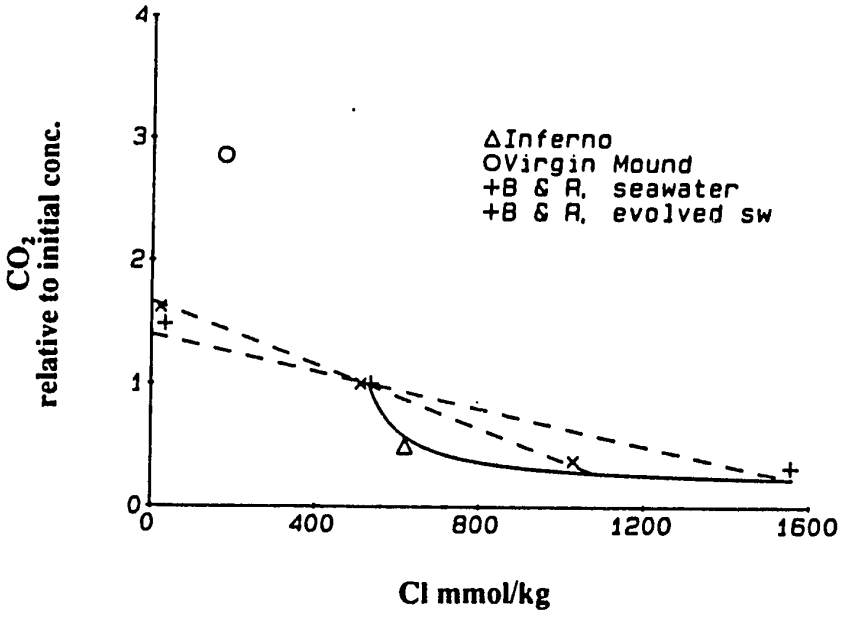

Figure 2.12. CO_2 versus Cl, comparison of boiling model output with experimental data from *Bischoff and Rosenbauer* [1987]. (CO_2 concentrations have been normalized to facilitate comparison.) Experimental data points are plotted for the original fluid, prior to boiling, and for the final brine and vapor in equilibrium. The solid curve represents the composition of the brine as boiling proceeds in a closed system at 390°C; the final temperatures of equilibration were 392°C for the natural seawater experiment and 388°C for the evolved seawater experiment. Dashed lines connect the model output of brine and vapor compositions for the same percent boiling as in the experiments. The data points from Inferno and Virgin Mound are shown to illustrate the effect of the percent boiling on gas partitioning.

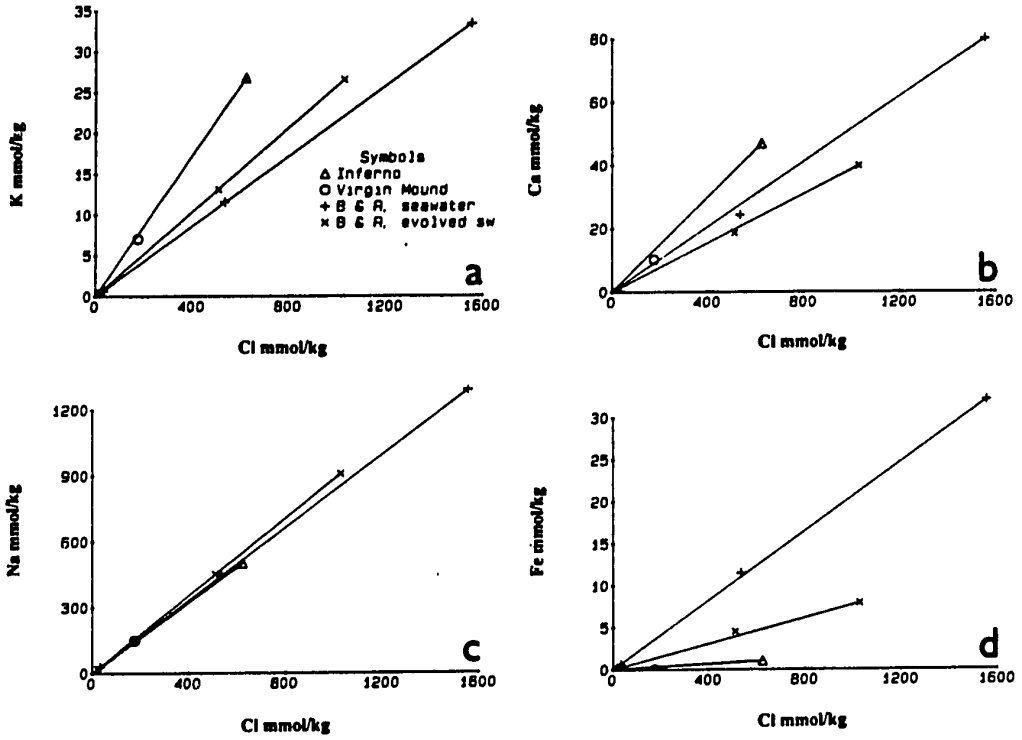

Figure 2.13. Comparison of major ions from ASHES with experimental data of *Bischoff and Rosenbauer* [1987]. Lines are drawn between most concentrated data point and the origin. (*a*) Potassium versus chloride. (*b*) Calcium versus chloride. (*c*) Sodium versus chloride. (*d*) Iron versus chloride. ASHES data and experimental data very closely fit the ideal mixing between brine and vapor expected in our model.

system. Formation of a Cl-bearing phase should raise the Br/Cl ratio of the low-chlorinity fluids [*Seyfried et al.*, 1986], but there is no discernible systematic variation of Br/Cl with chlorinity at ASHES. Since we have not measured any component that is known to be conservative throughout the entire cycle of hydrothermal circulation, the simplest and best assumption we can make is that chloride does not vary except due to phase separation, so that the unboiled hydrothermal fluid has the same chlorinity as seawater.

Given the limitations of this assumption, we can place some rough constraints on the P-T path of the boiling fluids. The Inferno chloride endmember is about 15% higher than ambient seawater, implying a minimum of 15% boiling if we do not consider rock hydration. In Figure 2.11, the data points for all of the vents lie close to the mixing area for 20% boiling. Our working hypothesis is that 15 to 20% of the original water has been vaporized. This is consistent with a crude estimate of the relative mass flux of low-, normal-, and high-chlorinity fluids in the ASHES vent field based on the number of observed high-temperature vents of each type.

To estimate a pressure and temperature for the onset of boiling, we will consider the two cases where boiling proceeds with conservation of enthalpy or conservation of entropy. We have plotted the enthalpy of 3.2 wt % NaCl along the boiling curve using the data of *Bischoff and Rosenbauer* [1985] (Figure 2.14*a*). The minimum temperature for initiation of boiling is found by assuming that boiling continues in the subsurface until just below the seafloor. By the method of *Tanger and Pitzer* [1989], we obtain the enthalpy of mixtures of 15 and 20 wt % vapor with the corresponding chloride-enriched liquid. We project the enthalpy of the vapor-liquid mixture onto the enthalpy of 3.2 wt % NaCl at vapor saturation and find the temperature at the onset of boiling. An analogous calculation is done for conservation of entropy (Figure 2.14*b*). In order to transfer 15-20% of the water to

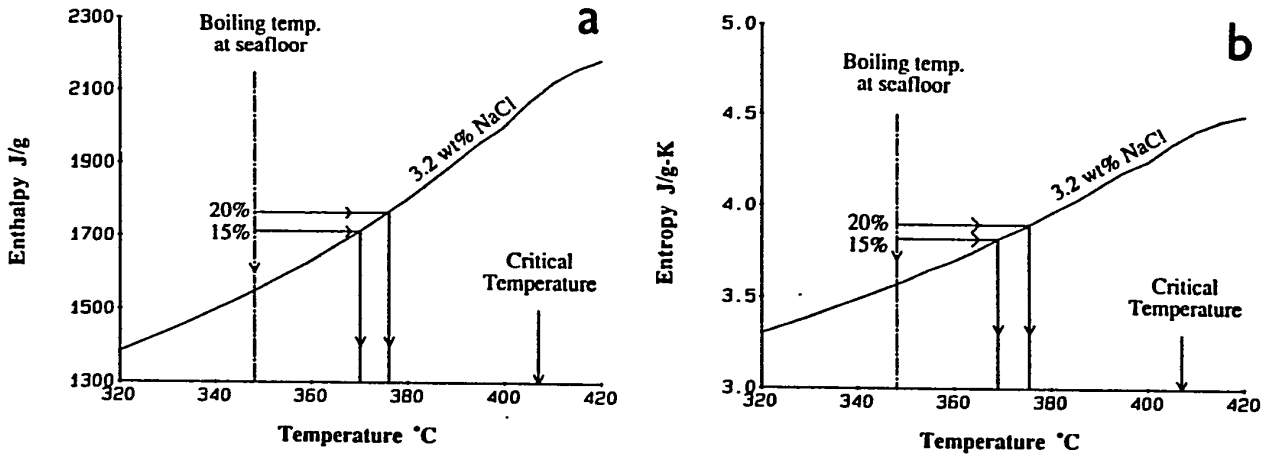

Figure 2.14. Calculation of minimum temperature range for onset of boiling. Based on the maximum measured chlorinity enrichment over seawater and the covariation of CO_2 and chloride (Figure 12), we assume a range of 15-20% boiling has occured. (*a*) Solid curve is the enthalpy of 3.2 wt % NaCl (seawater analog) along the boiling curve. Assuming conservation of enthalpy, we calculate the enthalpies of mixtures created by 15-20% isenthalpic boiling and find the minimum temperature at the onset of boiling by matching the enthalpies of the 15 and 20% mixtures at their seafloor boiling temperature with the enthalpy for seawater along the boiling curve. Initial fluid of seawater salinity must have been in the range 370°-376°C in order to boil away 15-20% of the original mass of water into the vapor phase. (*b*) Assuming conservation of entropy yields a minimum temperature range of 369°-375°C. Enthalpy and entropy data for 3.2 wt % NaCl are from *Bischoff and Rosenbauer* [1985] and the data needed to calculate the enthalpy and entropy of the 15 and 20% mixtures are from *Tanger and Pitzer* [1989] (J. C. Tanger, written communication, 1989).

the vapor phase, boiling must start at a minimum temperature in the range of 369°-376°C. This corresponds to pressures along the boiling curve for 3.2 wt % NaCl between 200 and 215 bars [*Bischoff and Rosenbauer*, 1985], or a depth of approximately 0.5-0.65 km below the seafloor, assuming hydrostatic pressure.

The observed venting temperatures are below the boiling point by >15°C, indicating that the fluids have cooled somewhere in the subsurface. That magnesium is very low in the sampled fluids suggests that if mixing is responsible for the cooling, then the mixing did not occur with cold, Mg-bearing, ambient seawater in the very near subsurface. The consistent, high silica contents of the ASHES fluids also argue that they have been in contact with rock surfaces long enough after segregation to approach equilibrium with respect to quartz. These observations support a deeper onset for boiling, moving the initial boiling temperature higher than the minimum estimated range of 369°-376°C.

When we look to the chemistry in order to estimate a maximum temperature for the onset of boiling, it is difficult to envision a P-T pathway through the supercritical region which could generate the salinities observed in the ASHES vent field. Supercritical phase separation would generate a highly saline brine and a liquid of somewhat less than seawater salinity, while we see evidence for a nearly fresh vapor component and a liquid (brine) of slightly more than seawater salinity. Hypothesized P-T pathways originating in the supercritical region require considerable cooling to have taken place and are unjustifiably complex. The simplest hypothesis consistent with the data is that hydrothermal fluids at ASHES have undergone subcritical boiling.

Fluid-Rock Interaction in the Upflow Zone

Although the covariation of chloride and CO_2 in ASHES fluids is explained by our simple model of salt and gas partitioning during boiling, other elements do not

conform to model predictions (Table 2.5). The exceptions may point to weaknesses in our basic assumptions about volatile and nonvolatile behavior, and, more importantly, to processes occurring subsequent to phase separation.

Silica. In contrast to the majority of nonvolatile elements, silica contents are very similar in Virgin Mound and Inferno vents (Figure 2.5 and Tables 2.2 and 2.5). This observation suggests two hypotheses: (1) silica behaves as a volatile component and partitions into the vapor phase, or (2) fluid-rock interaction subsequent to phase separation has resulted in the dissolution of silica into the vapor-enriched fluid.

Bischoff and Rosenbauer [1987] observed significant concentrations of silica in the vapor phase during an experiment on the interaction of basalt and seawater under conditions of supercritical phase separation. Although the P-T conditions of their experiment are different from the conditions we envision for the subsurface at ASHES, there is some basis for comparison. Using the equations of *Fournier* [1983], it is possible to calculate the solubility of quartz given the solution density, salinity and temperature. Bischoff and Rosenbauer used Fournier's equations to compare the predicted concentration of silica in the liquid and vapor phases with their experimental observations and obtained rough agreement (see Table 2.6). We have chosen a temperature of 370°C along the vapor saturation curve for 3.5 wt % NaCl for comparison. If we take these results as roughly representative of the partitioning of silica, we would expect no more than about 2 mmol/kg Si in the pure vapor component at ASHES. Admixture of 30% of the residual liquid (represented by Inferno composition) yields an initial composition for Virgin Mound of 6 mmol/kg Si, less than half of the observed concentration.

Some quartz may have precipitated and the silica content of the liquid phase at depth may have been higher than the levels measured at Inferno due to the initially

Table 2.5. Comparison of Calculated and Measured Fluid Composition of Virgin Mound

Composition of Inferno fluids is taken as representative of the residual liquid phase. Fluid composition of Virgin Mound is calculated in two ways: (1) as a mixture of 28.2% Inferno fluid and 71.8% vapor and (2) as a mixture of 24% Inferno, 5% seawater, and 71% vapor. When seawater is mixed in we assume that all sulfate is precipitated as anhydrite. Boron concentration in the vapor is calculated using the partition coefficient of *Glover* [1988] at 370°C. Silica in the vapor estimated with the equations of *Fournier* [1983]. Also tabulated are the ratios of concentration in Virgin Mound to Inferno concentration for each element and the ratio of measured to calculated concentration.

Component	Unit	Seawater	Virgin Mound	Inferno	Ratio VM/Inf	Vapor	Inferno + Vapor	Ratio meas/calc	Inferno + Vapor + Seawater	Ratio meas/calc
Cl	mmol/kg	540	176	624	0.282	0	176	1.000	176	1.000
Ca	mmol/kg	10.25	10.2	46.8	0.218	0	13.20	0.773	10.20	1.000
K	mmol/kg	9.8	6.98	26.5	0.263	0	7.47	0.934	6.8	1.027
Na	mmol/kg	467	148	500	0.296	0	141	1.050	142.8	1.036
Li	µmol/kg	26	184	636	0.289	0	179.3	1.026	152.39	1.207
B	mmol/kg	0.416	0.447	0.587	0.761	0.182	0.30	1.509	0.29	1.541
Sr	µmol/kg	87.0	46.4	192	0.242	0	50	0.857	50	0.927
Br	µmol/kg	839	250	956	0.262	0	269.6	0.927	270.3	0.925
Si	mmol/kg	0.178	13.5	15.1	0.894	2	5.69	2.371	5.02	2.692
CO_2	mmol/kg	2.4	285	50	5.7	380	286.9	0.993	281.8	1.011

TABLE 2.6. Comparison of Experimental and Predicted Partitioning of Silica Between Liquid and Vapor.

	Bischoff and Rosenbauer 392°C, 251 bars		Bischoff and Rosenbauer 388°C, 240 bars		Axial 370°C, 209 bars	
	Liquid	Vapor	Liquid	Vapor	Liquid	Vapor
Density	0.630	0.186	0.585	0.176	0.590	0.163
NaCl, wt %	9.05	0.192	6.02	0.134	3.50	0.020
m_{Si}, meas	0.029	0.006	0.020	0.0028	0.0151	
m_{Si}, calc	0.0192	0.0022	0.0169	0.0019	0.0152	0.0014

Densities for Axial conditions from *Khaibullin and Borisov* [1966]. Calculated silica concentrations are from the method of *Fournier* [1983].

higher temperature. However, even if the initial level in the liquid were as high as 25 mmol/kg, there would still be substantially less silica in the vapor-enriched phase than we observe, and extraction of silica from rock is still required.

We cannot account for the observed levels of silica by invoking partitioning of silica into the vapor phase. We infer that most of the dissolved silica in the vapor-enriched fluids at ASHES derives from water-rock interaction subsequent to phase separation and segregation, and that silica can be rapidly dissolved from the rock. Dissolution rates should be a function of temperature, degree of disequilibrium (undersaturation), water to rock ratio (surface area of rock/volume of water), and quality of rock surface exposed (altered or fresh, glassy or crystalline).

According to model calculations incorporating the kinetics of silica dissolution from quartz and basaltic glass [*Wells and Ghiorso,* 1988; J. T. Wells, personal communication, 1989], a solution which initially contained no silica at 350°C, rising through 1 km of crust in a 2 cm wide crack at 1 m/s could increase to about 7 mmol/kg if the surface was lined with quartz and up to 20 mmol/kg (or quartz saturation) if the surface was fresh basaltic glass. Dissolution of basalt glass is about an order of magnitude faster than dissolution of quartz. These calculations suggest that it is not unreasonable to expect the silica content of the vapor-enriched fluid to be close to quartz saturation, even if it contained only 2-6 mmol/kg silica at the time of segregation from the bulk of the liquid phase.

The degree of quartz saturation may be critical in controlling water-rock interaction at ASHES. If the source of hot fluid does not vary, then we would expect the boiling horizon to be thermodynamically controlled and boiling would initiate at a fixed depth. Furthermore, because the vapor and liquid ultimately follow separate pathways to the surface (based on our observations), then the vapor phase (which should be initially undersaturated with respect to quartz) might flow through a region

of relatively exposed, uncoated basalt. If there is a large thermodynamic driving force for dissolution of the basalt along the flow path of the vapor-enriched fluid, then silica (and other elements) would be rapidly taken up into solution. The residual liquid phase would be supersaturated with quartz (due to the effects of cooling and concentration attendant to boiling) and could be expected to deposit quartz on the rock surface, as observed by *Delaney et al.* [1987] in greenstone breccias recovered from the Kane Fracture Zone. We would expect the vapor-enriched fluid to continue to react with the wall substrate, while precipitation of quartz from the brine might insulate it from further interaction with the rock. Though all fluids may continue to react with the host rock, the measured compositions still reflect relative changes.

Both Virgin Mound and Inferno fluids are slightly supersaturated with respect to quartz at the measured exit temperatures. Using *Fournier*'s [1983] quartz solubility equations and the density data of *Potter and Brown* [1977] as a geobarometer indicates that Inferno fluids (at 325°C) would be in equilibrium at 240-280 bars pressure, or approximately 1 km below the seafloor, assuming a hydrostatic pressure gradient. The same calculation for Virgin Mound fluids (at 300°C) yields a pressure of 400-450 bars. If the actual temperature for Virgin Mound were just 5 degrees higher, the calculated pressure of reaction would be 300 bars, so that a small amount of cooling could significantly change the result of the quartz geobarometer.

If our interpretation of the history of ASHES fluids is correct, then the key assumptions inherent in the geobarometer have been violated. Based on comparison of measured temperatures with the boiling temperature, both low- and normal-salinity fluids have cooled by 20°-50°C, either by conductive cooling or by mixing with seawater. Both cooling mechanisms cause solutions which are at quartz

saturation to become supersaturated [*Janecky and Seyfried,* 1984]. It is possible that the difference between the two endmembers does reflect quartz solubility control; the lower concentration in Virgin Mound could be attributed to the combined effects of lower temperature and lower salinity, both of which decrease the solubility of quartz. However, given the probable convoluted history of these fluids, a straightforward application of the quartz geobarometer is not instructive about the maximum depth of reaction. We believe that the low-salinity fluids have increased their silica content due to water-rock reaction in the upflow zone.

We would not expect silica dissolution to occur unaccompanied by other changes in measurable properties of the fluids. In particular, we would expect a concomitant increase in the "soluble" or extractable elements K, Li, and B [*Seyfried et al.*, 1984; *Spivack and Edmond,* 1987; *Von Damm,* 1988] and an increase in one or more of the major cations if net dissolution of silicate minerals is responsible for the increase in dissolved silica. We would also expect the alkalinity of the vapor-enriched phase to increase as silicate hydrolysis reactions proceed.

Major cations. A generic reaction to describe dissolution of a sodium-bearing mineral may be written

$$4NaAlSi_3O_8 + 4H^+ + 2H_2O \leftrightarrow Al_4Si_4O_{10}(OH)_8 + 8SiO_2 + 4Na^+ \qquad (9)$$

Alternatively, we may represent exchange of calcium for sodium by the following reaction proposed by *Seyfried* [1987]:

$$NaAlSi_3O_8 + Ca^{++} \leftrightarrow 2Na^+ + 2CaAl_2Si_2O_8 + 4SiO_2 \qquad (10)$$

These reactions are not intended to represent actual reactions occurring in the hydrothermal system but rather to reflect generic processes of dissolution and ion exchange which may alter the fluid chemistry.

In our model, the composition of the high-temperature fluid prior to boiling controls the initial composition of the brine produced. Because we do not have a direct measure of the composition of the unboiled fluid and since we cannot unambiguously infer what the original composition was, we assume that the elemental ratios in Inferno fluids are the same as in the parent fluid (a reasonable assumption judging from Figure 2.9). Because the nonvolatile components are uniformly enriched by removal of water vapor and because nonvolatiles are practically absent from the pure vapor, then, at the time of segregation, a mixture of liquid and vapor would inherit the elemental ratio of the parent fluid. According to our model, measured differences in elemental ratios between vent fluids reflect relative changes since phase separation and segregation.

Though the uncertainty in the endmember sodium concentration is large, so that small increases could go undetected, when we compare the predicted versus the measured sodium concentrations in Virgin Mound (Table 2.5), there is an excess of between 3.5 and 5%. The activity ratios of a_{Na^+}/a_{H^+} and $a_{Ca^{++}}/a^2_{H^+}$ calculated from the computer programs MINEQL and EQ3 [*Westall et al.*, 1976; *Wolery*, 1979] indicate that both Virgin Mound and Inferno fluids are undersaturated with respect to sodium and calcium fixation reactions proposed by *Seyfried* [1987], although this calculation is subject to the considerable uncertainty in the high-temperature thermodynamic database. The data suggest that the excess silica in Virgin Mound fluids may be the result of dissolution of a sodium-bearing phase.

Extractable elements. The elements K, Li and B increase in solubility (or "extraction efficiency") in the order K<Li<B [*Seyfried et al.*, 1984]. The concentrations of these elements and their ratios in the different vent fluids at ASHES provide another constraint with which to evaluate post-segregation water/rock interaction. If we are correct in our interpretation that the vapor-enriched

fluids have reacted with the rock lining the flow-path, then we would expect to see an increase in the Li/K ratio in the low-salinity fluids. A plot of Li/K ratio versus chloride (Figure 2.15) shows that this is in fact the case.

The situation for boron is somewhat more complicated since boron is not strictly nonvolatile. The distribution of B between liquid and vapor can be described by a distribution coefficient:

$$K_D = \frac{[B]_v}{[B]_l} \tag{11}$$

where $[B]$ represents the concentration of B (per kg) and the subscripts v and l refer to the vapor and liquid phases. *Glover* [1988] has fit the available data and determined that K_D is related to the density, ρ, of each phase by

$$\log(K_D) = -0.947 \log\left(\frac{\rho_l}{\rho_v}\right) + 0.0547\left(\log\left(\frac{\rho_l}{\rho_v}\right)\right)^2 \tag{12}$$

Using the densities for liquid and vapor reported in *Khaibullin and Borisov* [1966] for 3.5 wt % NaCl at 370°C as an approximation for the in situ densities at ASHES, we calculate $K_D = 0.308$. Assuming 20% boiling and using the calculated distribution coefficient, we would predict that a mixture of 30% brine and 70% vapor would have an initial boron concentration somewhat less than 30% of the brine and that the initial B/K ratio of the 30/70 mixture would be nearly identical to the ratio in the brine. What we observe is that the boron concentration of Virgin Mound (the 30/70 mixture) is about 70% of Inferno (the brine) and that the B/K ratio of VM is nearly three times the ratio in Inferno. Even allowing for considerable uncertainty in this calculation, the data clearly indicate that there has been substantial water/rock interaction in the low-salinity fluids after becoming segregated from the brine-enriched fluids.

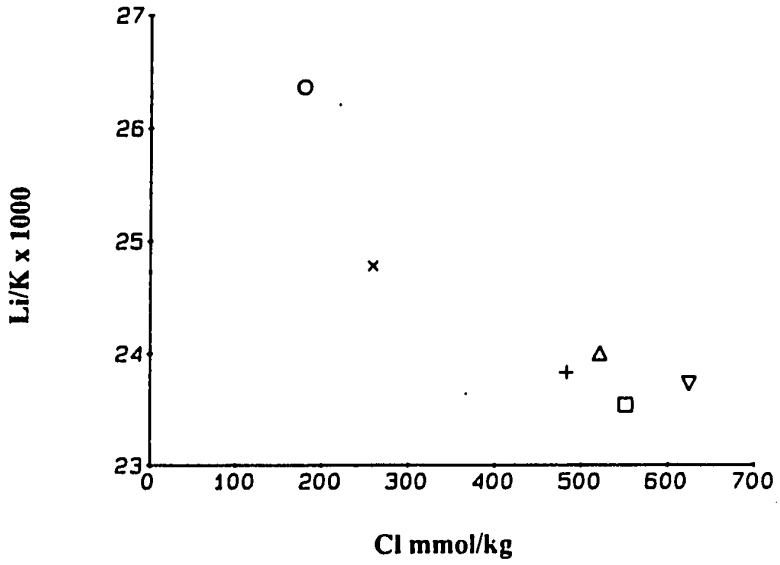

Figure 2.15 End-member lithium to potassium ratio versus end-member chloride for ASHES vents. We assume that Li and K partition equally between vapor and liquid during boiling, so that the Li/K ratio at the time of segregation would be the same in all fluids. The increase in Li/K in the low-chlorinity fluids is consistent with continued leaching of extractable elements from the wall substrate into the low-chlorinity, vapor-enriched fluids relative to the higher-chlorinity fluids.

Potassium may not behave as a strictly soluble element [*Von Damm,* 1988], and it is possible that removal of potassium from the vapor-enriched fluid into a mineral could cause the Li/K and B/K ratios to increase. However, this process would affect both ratios equally and this is not what we observe. The Li/K ratio in Virgin Mound is 11% higher than Inferno, while B/K is nearly 300% higher, in agreement with the order of solubility. We conclude that most of this variation is due to leaching of the extractable elements from the rock.

Although boron isotopic data for ASHES fluids is unavailable, we would predict that the boron in Virgin Mound fluids would have a larger portion of rock-derived boron than the Inferno fluids and should therefore have a lower $^{11}B/^{10}B$ ratio [*Spivack and Edmond,* 1987]. At the high temperatures in this system, we would not expect a significant boron isotopic fractionation associated with phase separation.

Alkalinity. The observation that the Virgin Mound fluids have a notably higher *p*H and alkalinity is qualitatively consistent with the silicate hydrolysis reactions needed to increase the silica content from the predicted level of 6 mmol/kg to the observed 13.5 mmol/kg. As the alkalinity (and *p*H) of the solutions increases due to hydrolysis reactions, we would expect the rates of dissolution to decrease. In order to reach the measured alkalinity of +0.66 meq/kg from the predicted value near zero, we would need to increase the total cations in solution by less than 1 meq/kg, assuming a 1:1 stoichiometry of hydrogen ion exchange for cations, and ignoring for the moment other reactions (precipitation of iron sulfide minerals, for example) which might change the alkalinity. Given the cumulative analytical uncertainties of the measured cations, 1 meq/kg would go undetected.

Mineral Precipitation and Mixing

In contrast to the silica data, several elements are depleted in the low-salinity fluids relative to what would be expected by the conservative mixing model which accounts for many of the measured elements (Figure 2.9 and Table 2.5). These depletions may be attributed to precipitation of minerals due to decreases in temperature and increases in *p*H caused by some combination of conductive cooling, mixing with cold alkaline groundwater, and hydrolysis of silicate minerals.

Calcium depletion. While the ratio of concentration in Inferno to that in Virgin Mound is very similar for many of the nonvolatile elements (0.280 ± .017 for Na, K, Li, Cl, and Br), this ratio for calcium is only 0.218, indicating that some process has removed calcium relative to the other major cations. In addition, the alkalinity of the low salinity fluids is positive (+0.66 for Virgin Mound), which would not be expected based on a mixture of pure vapor (Alk=0) and a liquid with negative alkalinity (Inferno=-0.48 meq/kg). We identify two major processes which could explain these observations: hydrolysis of silicate minerals (discussed above) and admixture of cold groundwater of composition close to seawater.

The low Ca and lower temperature at Virgin Mound are consistent with subsurface mixing of cold alkaline seawater, which would cool the solution and precipitate anhydrite. If we assume that both calcium and chloride remain entirely in the liquid phase during phase separation, and that mixing seawater into a high temperature fluid will precipitate all sulfate as anhydrite, then we can solve for the amount of seawater needed to generate the observed depletion in calcium:

$$Cl_{VM} = xCl_{Inf} + yCl_{sw} \tag{13}$$

$$Ca_{VM} = xCa_{Inf} + y(Ca_{sw} - SO_{4_{sw}}) \tag{14}$$

x and y are the mass fractions of Inferno endmember and seawater, respectively, and all of the other quantities have been measured. We could substitute another conservative element for chloride (e.g., sodium or bromide) in the two equations above without altering the result significantly. The vapor fraction is absent from these equations since it does not contribute any of the nonvolatile components.

To account for the observed calcium anomaly requires a mixture of 24% liquid (Inferno composition), 5% seawater, and 71% pure vapor, which would also lower the temperature by approximately 18°C, close to the observed difference between Inferno and Virgin Mound. Alkalinity is not conserved during mixing if mineral precipitation occurs and can only be used as a qualitative guide to subsurface processes, but admixture of 5% seawater is insufficient to raise the alkalinity to the observed value even if no metal sulfides precipitate. Furthermore, addition of seawater would result in only a temporary increase in *p*H; if subsequent high-temperature reactions remove magnesium, a net decrease in *p*H would occur. For this reason it appears that the difference in alkalinity (and *p*H) between Inferno and Virgin Mound fluids may be a result of the different nature and/or extent of fluid-rock interaction in the two fluids, rather than a result of different degrees of mixing with seawater.

Iron depletion. Iron has been nearly completely stripped from the low-salinity fluids; the iron content of Virgin Mound is less than 1% of the iron in Inferno. The iron concentrations are consistent with solubility control by iron sulfide minerals (pyrrhotite or pyrite). Initial results of equilibrium speciation calculations of ASHES fluids (at 350°C and 250 bars) using the program MINEQL [*Westall et al.*, 1976] indicate that both Inferno fluids (in situ *p*H = 4.11) and Virgin Mound fluids (in situ *p*H = 4.63) are slightly supersaturated with respect to pyrrhotite. Calcium complexing with chloride and bicarbonate is important in determining the in situ *p*H

and thus the mineral saturation state, of ASHES fluids, and uncertainties in the thermodynamic data for calcium complexes introduces large uncertainties in the calculated *p*H. Increased chloride complexing of calcium could raise the *p*H by shifting the equilibrium of the following reaction to the right:

$$CaHCO_3^+ + H^+ + Cl^- \leftrightarrow CaCl^+ + H_2CO_3 \qquad (15)$$

The effect of boiling under conditions similar to what we envision in the subsurface at ASHES (360°-390°C, initial *p*H ~4.0, high CO_2) is to lower the *p*H in the liquid slightly [*Drummond,* 1981; *Drummond and Ohmoto,* 1985]. This decrease in *p*H, combined with the lowered H_2S levels, would act to maintain dissolved metals in solution. The driving forces for mineral precipitation from the liquid phase under these conditions are cooling and concentration by removal of water as vapor. Subsurface loss of iron from the vapor-enriched phase has occurred in the subsurface at ASHES, consistent with the higher measured *p*H and H_2S in the low-chlorinity fluids. Some loss of iron from the normal- and high-chlorinity fluids may have occurred as a result of the cooling associated with boiling.

Geographic Distribution of Venting

The six major vents in the ASHES field are arranged roughly along the perimeter of a circle 60m in diameter. The lowest salinity fluids exit the seafloor in the eastern half of the circle (farthest from the caldera wall), and there is a salinity gradient from SE to NW.

We may distinguish between two ideal mechanisms for physically segregating the vapor from the liquid phase. On one extreme, we may envision a system of large (cm-scale) conduits of focused fluid flow and on the other an isotropic porous medium. In the first case, two phases travelling along a non-vertical conduit may partially segregate by virtue of their differing buoyancies and when a branch point is

encountered, the lighter fluid mixture will follow the more vertical route, resulting in vapor-enriched fluid segregating from liquid-enriched fluid (this type of mechanism is discussed in some detail by *Delaney et al.* [1987]). In the second case, the relative permeability of the porous medium will be different for the two phases [*Grant et al.*, 1982; *Fox,* 1990], and the more mobile vapor phase will tend to migrate away from the liquid. The second mechanism should operate when the fluids flow through a system of small (sub-millimeter) cracks, and the first when fluids flow along a highly permeable zone. Both mechanisms may operate in a real hydrothermal system.

If we accept the listric faulting mechanism to explain caldera subsidence [*Walker,* 1988], then the proximity of the ASHES vent field to the caldera wall suggests that the primary caldera boundary fault should extend directly under the vent field. If the fault is associated with a high permeability zone, then the vapor phase may separate from the liquid by the first mechanism discussed above (see Figure 2.16). The salinity distribution among the vents is roughly consistent with this mechanism of fluid segregation. This reasoning might also suggest that venting should be found at the base of the wall; a search of the base of the wall revealed some warm vents and dead clam shells, but no high-temperature venting.

Low-chlorinity fluids in the form of diffusely flowing warm vents (e.g., ISCA vent) are also found very close to some of the large sulfide structures (see Figure 2.1) which are venting fluids of normal chlorinity. This may be evidence for the mechanism of phase segregation proposed by *Fox* [1990]. More detailed analysis of the chlorinity/temperature distribution at ASHES combined with geothermal reservoir modeling [*Pruess,* 1988] may serve to evaluate the roles played by the relative permeability mechanism and the buoyancy mechanism.

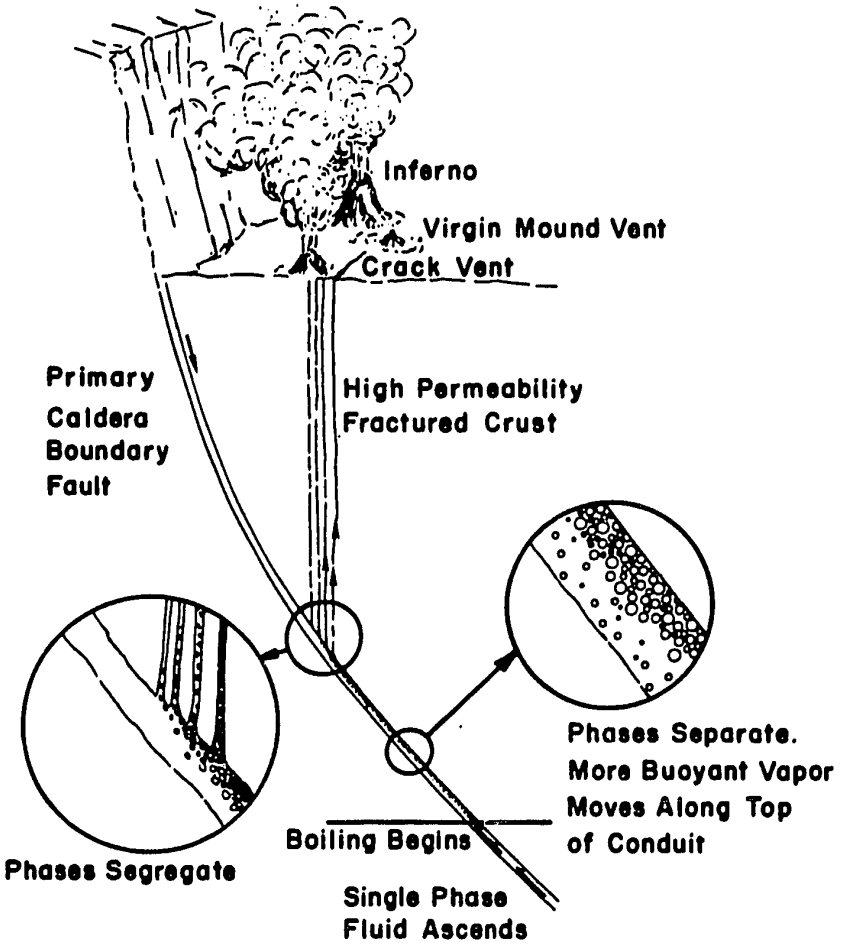

Figure 2.16. Cutaway view schematic of Axial Seamount caldera, showing relative location of major low- and high-chlorinity vents in relation to the western caldera wall. Geographic distribution of venting is roughly consistent with segregation of vapor and liquid phases by buoyancy difference. *Fox* [1990] notes that the proximity of low-chlorinity warm vents to normal-salinity, high-temperature vents suggests an alternative mechanism for phase segregation based on differential relative permeability.

Conclusions

We have collected fluids from a single vent field which vary from 33 to 116% of seawater chlorinity and from 50 to 288 mmol/kg CO_2. The inverse correlation of chlorinity and gas content, and the covariation of all major non-volatile elements is compelling evidence that we have sampled fluids enriched in vapor and liquid phases which have separated during adiabatic boiling and have become physically segregated. This supports the hypotheses that active phase separation occurs in hydrothermal systems [*Welhan and Craig*, 1979; *Delaney and Cosens*, 1982] and that the two phases may physically segregate [*Delaney et al.*, 1987] and follow separate pathways to the surface.

The data suggest that phase separation initiated at a temperature at least as high as 370°C and possibly very near the critical point. Though we cannot determine whether boiling proceeded in an open or closed system, most of the chemical variation between vents at ASHES can be explained by a closed system model of phase separation which partitions gases according to Henry's law and assumes that all nonvolatile components remain entirely in the liquid phase.

Important discrepancies between this simple model and the ASHES data point to processes occurring in the upflow zone after the phases have partially segregated:

Unexpectedly high levels of silica, boron and lithium in the vapor-enriched phase suggest that substantial water/rock interaction has taken place in the upflow zone subsequent to phase separation and segregation.

That the low-chlorinity, vapor-enriched fluids have substantially increased in dissolved silica since segregating from the high-chlorinity fluids implies very rapid kinetics of dissolution of silicate minerals from the wall rock. The higher alkalinity

of the vapor-enriched phase may be due to the hydrolysis reactions required to elevate silica to the observed level, and a slight elevation in sodium suggests that dissolution of sodium-rich phase (e.g., albite) may be occurring.

The fluids have probably cooled due to sub-surface mixing with cold seawater, resulting in the depletion of calcium in the vapor-enriched fluid by precipitation of anhydrite.

Iron has been lost from the low-chlorinity fluids due to precipitation of sulfide minerals.

The geographical distribution of vents is consistent with models of phase segregation by buoyancy difference as in Figure 2.16 or by migration of vapor away from liquid by differential relative permeability [*Fox*, 1990].

Chapter 3

ENDEAVOUR VENT FIELD: SUPERCRITICAL PHASE SEPARATION.

Geologic setting.

The Endeavour vent field is located near 47°57'N on the Endeavour Segment of the Juan de Fuca Ridge and is situated on the axial valley floor at a depth of ~2200 m. There are many large, steep-sided active and inactive sulfide structures situated within 150 m of the western axial valley wall, roughly distributed along the strike of the wall (020°) for a distance of ~450 m [Tivey and Delaney, 1986; Delaney *et al.*, manuscript in preparation]. Both the size of the sulfide structures and the quantity of high-temperature fluid discharge at the Endeavour site are much larger than at Axial Seamount and most other hydrothermal areas [Tivey and Delaney, 1986]. There are many structures with multiple high-temperature vents at Endeavour which contain 1000-10000 m^3 of sulfide material compared to a maximum of ~100 m^3 per structure at ASHES. There is a much larger hydrothermal plume over the Endeavour site [Lupton 1990, Baker *et al.*, 1990]. There is very little evidence of recent volcanic activity at the Endeavour vent field [Tivey and Delaney, 1986], which appears to be geologically much older and hydrothermally more mature than the ASHES site. Unlike ASHES, vent structures at Endeavour are fairly clearly associated with faults and fissures (Figure 3.1).

Navigation within the vent field.

High-temperature (345 - 400°C) fluids were recovered from the Endeavour vent field from DSV *Alvin* in 1984, 1987, and 1988, with the number of samples collected increasing in each successive year. A different navigational array was used in each year, so the fixes recorded for sampling are not directly comparable across years. However, work is being done (R. E. McDuff and V. A. Atnipp) to reconcile

Figure 3.1 a) Geologic map of the Endeavour vent field (simplified). X-Y grid is in meters. Structures from which fluid samples were obtained are labelled A through E (large letters) from northeast to southwest in the vent field. Some individual vents are labelled. Visible faults run predominantly parallel to the base of the western wall (~020°), and venting is clearly associated with the faults. (Map provided by V. Robigou, J. R. Delaney, and R. E. McDuff)

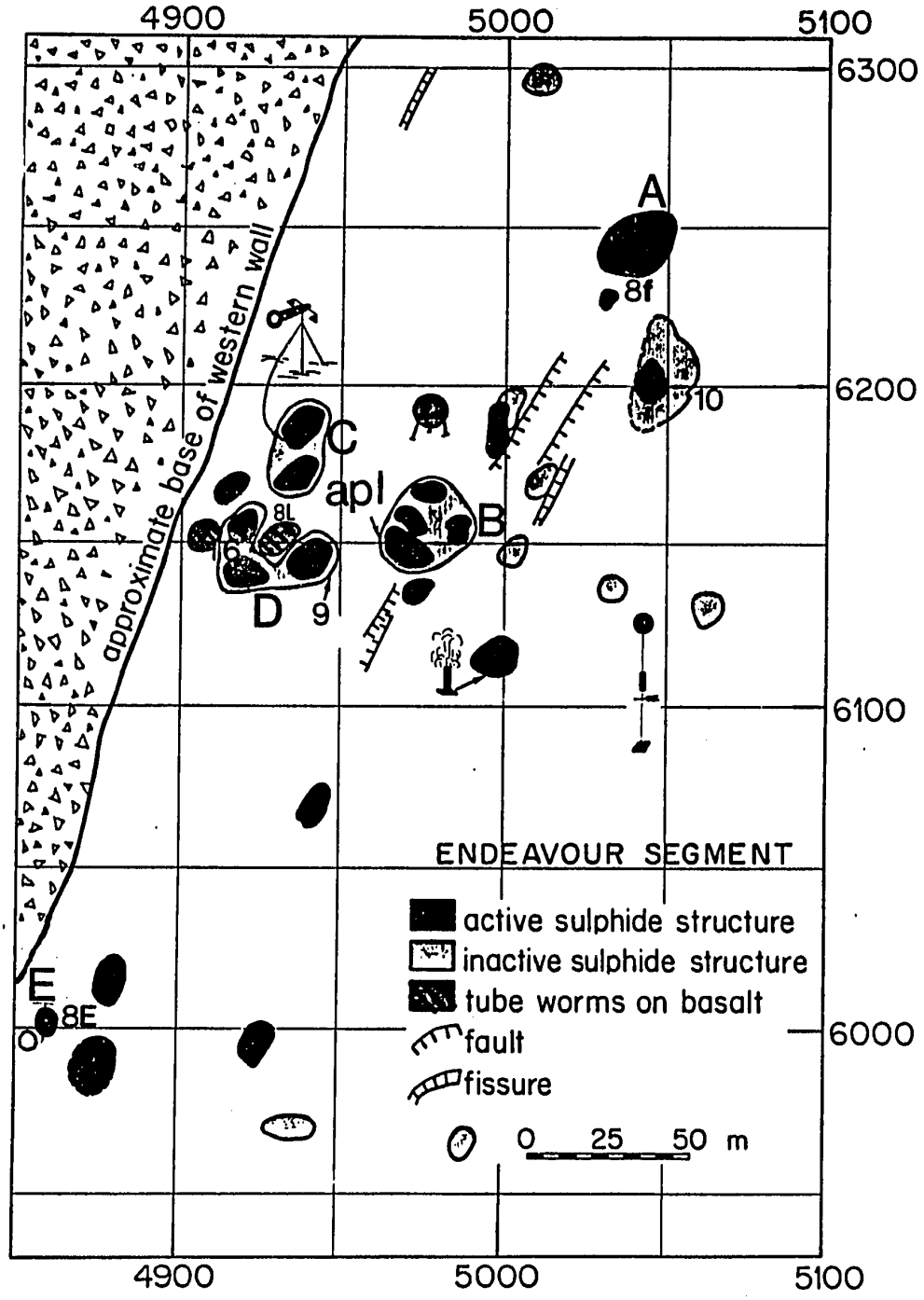
4900
5000
5100
6300
6200
6100
6000
A
8f
10
C
apl
B
8L
6
D
9
approximate base of western wall
E
8E
ENDEAVOUR SEGMENT
active sulphide structure
inactive sulphide structure
tube worms on basalt
fault
fissure
0 25 50 m

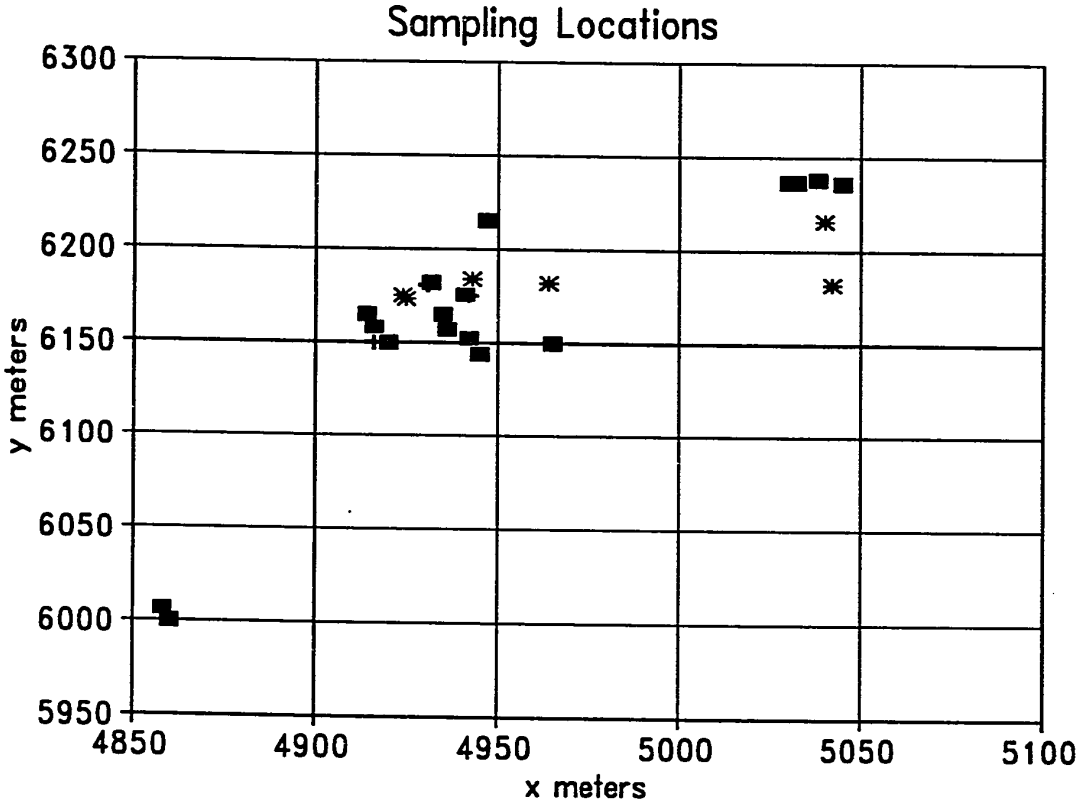

Figure 3.1 (continued) b) Map showing locations of some of the hydrothermal fluid samples taken. Coordinates are in the 1988 grid. X increases to the east, Y increases to the north. Uncertainty in 1988 fixes is ± 2 m; for 1987 fixes, ± 5 m; for 1984 fixes, ± 15 m.

navigation between years using the Alvin in-sphere transponder travel times, which yield very accurate fixes (within ~1 m). In some cases, vents have been identified by markers which have been revisited from year to year. For this study, I will use the recorded (x,y) fixes from each year adjusted to the 1988 grid (since we have a very detailed geologic map on the 1988 grid courtesy of V. Robigou, J. R. Delaney, and R. E. McDuff) by using a marker of known position.

The 1984 Long-term Ocean Bottom Observatory (LOBO) vent site was revisited in 1988 [R. E. McDuff, personal communication], so I translated the 1984 ship fixes by equating the position of the smoker sampled in 1984 on dive 1447 at the LOBO vent ((x,y)= (4111,5084) in 1984 coordinates) with the 1988 in-sub position (4933,6182). The precision of the shipboard fixes is probably no better than 20 m. Judging from the resulting position of the 1984 sample fixes on the 1988 map, this translation is not very accurate, since it places some high temperature vents in the talus of the western axial valley wall. Discussions with participants on the 1984 Alvin dive series at Endeavour have convinced me that two high-temperature vent fluid samples were taken from structure C and two from the northern side of structure D. The remaining high-temperature sample was taken approximately 100 m to the east and slightly north, which is somewhere between the structures I have labelled A and B. There are two known high-temperature venting sites on the geologic map between A and B: one at (5000,6180) which is marked 8P and another unmarked site at (5050,6200). Major sample 1438-9 almost certainly comes from the latter of these two sites, near marker 10, since the structure marked 8P was not seen until 1988.

To translate the 1987 data, I looked at the dive track fixes taken on board Atlantis II for dive 1933, where a number of samples were taken from what was called smoker 16 in 1987. The average position for the time interval between 12:00

and 12:10, when Alvin was working on the bottom near smoker 16, was $(x,y)_{1987}$ = (3454,1992). I equated this with the 1988 coordinates given for smoker 16 on the geologic map of the vent field, (4914,6149). The 1987 shipboard fixes were then offset to match the 1988 grid ($(x,y)_{1987}$ + (1460,4157) = $(x,y)_{1988}$). Detailed dive tracks obtained with this translation are in very good agreement with the 1988 geological map.

A summary of sample locations for all years is given in Figure 3.1.

Results of chemical analysis: calculation of endmembers.

Summary

All of the calculated endmember concentrations for the Endeavour vent field fall within the range of previously measured values for mid-ocean ridge hydrothermal systems. However, the Endeavour field does have some distinctive chemical characteristics. One of the most notable aspects of the chemistry of Endeavour vent fluids is that the endmember chloride content varies from ~255 to ~505 mmol/kg (~47%-~94% of seawater chloride content), and most of the major ions are strongly correlated with chloride, which increases from the SW to the NE. Any model of the origin of these fluids must explain both the intra-field range of chlorinity and the offset from seawater chlorinity. In addition, the ammonia content at Endeavour is higher than at any sediment-starved ridge-crest and the lithium and manganese contents are somewhat low.

The 1988 results are presented as zero-magnesium endmembers by vent structure in Table 3.1. The endmembers for 1984 and 1987 generally agree with the 1988 data; differences are discussed in the text.

Table 3.1. Endeavour Endmembers by Structure

	Structure				
	A	B	C	D	E
Temp, °C	322	341	350	357	345
Cl, mmol/kg	506 ± 3	455 ± 3	429 ± 3.4	432 ± 7.8	255 ± 5
Br, µmol/kg	875 ± 8	760 ± 10		743 ± 10	
Li, µmol/kg	455 ± 10	390 ± 10	373 ± 4	372 ± 12	178 ± 7
Na, mmol/kg	391 ± 10	361 ± 10	339 ± 10	339 ± 10	203 ± 10
K, mmol/kg	27.4 ± 1.7	24.4 ± 0.2	23.5 ± 1.7	24.4 ± 0.7	16 ± 2
Ca, mmol/kg	43.0 ± 1.3	34.5 ± 0.3	31.9 ± 1.5	33.4 ± 0.9	18 ± 1.4
Sr, µmol/kg	154 ± 6	137 ± 7	136 ± 3.5	132 ± 5.6	
NH_3, µmol/kg	500 ± 20	582 ± 20	606 ± 15	663 ± 35	577 ± 20
Fe, µmol/kg	500 ± 20	1013 ± 24		913 ± 144	
Mn, µmol/kg	195 ± 5	297 ± 10	295 ± 10	295 ± 9	
H_2S, mmol/kg	3.17 ± 0.19	5 ± 0.1	5.16 ± 0.2	5.15 ± 0.44	6.8 ± 1.3
Si, mmol/kg	16.9 ± 0.3	16.2 ± 0.2	16 ± 0.4	15.8 ± 0.8	5 ± 1.2
pH	4.25 ± 0.05	4.25 ± 0.05	4.2 ± 0.1	4.2 ± 0.1	
Alk	-0.45 ± 0.05			-0.14 ± 0.22	
CO_2, mmol/kg	9.98 ± 0.2			14.3 ± 0.4	13.6 ± 3

Reported uncertainties are 1σ esitmates from linear regressions of property versus magnesium. Reported temperatures are maximum values obtained in vents from the different structures at the time that water samples were collected in 1988. Higher temperatures were recorded at other times (see text).

Anions

Chloride. For all vents and in all years, a plot of chloride vs. magnesium (Fig. 3.2) shows that all Endeavour vent fluids sampled were depleted in chloride relative to seawater. The zero-magnesium endmember chloride concentration covers a rather wide range of values, with most of the samples extrapolating to approximately 420 mmol/kg. Considering only the samples which have very little entrained seawater ([Mg] < 35 mmol/kg) gives a range of chloride endmembers from 400 - 505 mmol/kg. Including the more diluted samples extends the range to ~255 mmol/kg.

In order to facilitate comparison of the samples, I will break them down by their proximity to one of the major sulfide structures in the vent field (Fig 3.1a). We took samples from or near 5 different large sulfide structures. Starting in the NE, I will refer to the sulfide structure which includes smoker 8F as structure A. Moving SSW along some normal faults, the next major structure encountered (marked with 8D and 8J) is centered at (4975,6155) and will be referred to as structure B. Structure C lies about 40 m to the NW near the western wall and bears markers 8A, 12, and 14. Structure D is the largest mapped sulfide structure in the vent field and is identified by markers 8C, 9, 16 and 3. The southern-most structure sampled, structure E, is situated about 10 m from the western wall near (4860,6000) and bears marker 8E. Over 80% of all the samples were taken from structures C and D in the central portion of the mapped vent field near the western wall. In comparing the sampling locations from year to year, it is clear that the widest area was sampled in 1988, ranging from vent 8E in the SW portion of the vent field to 8F in the NE. In 1987, vent fluid samples were taken from the central part of the vent field, mostly from structures C and D, and possibly some from the area between A and B. In 1984, fluids were sampled from near the central structures C and D and from an area just south of structure A, as well as from some smaller warm vents.

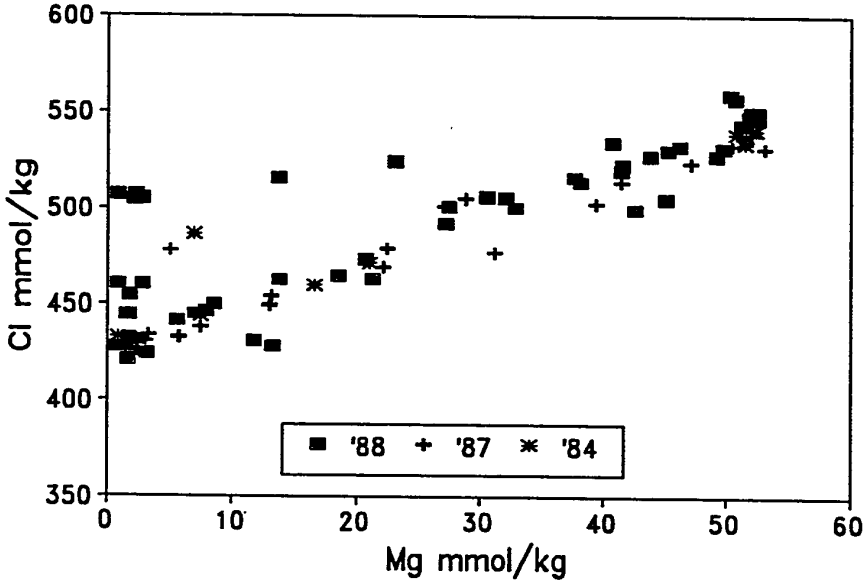

Figure 3.2. Plot of chloride versus magnesium for all years. Most of the samples were taken from the central structures and plot near a mixing line with an end-member chloride concentration of 420-430 mmol/kg, showing no significant change over the 4-year period of sampling. Samples taken from the northeast part of the vent field have higher chlorinity, while samples taken from vent 8E in the southwest are significantly lower.

1984 Results.

We have relatively few samples from 1984, but there were two distinct chloride endmembers sampled. The translation of the 1984 navigation onto the 1988 map suggests, and 1984 Alvin dive participants confirm, that four of the high-temperature samples were taken within a ~40 m diameter area surrounding structures C and D, while one high-temperature sample and one warm vent sample were taken between structures A and B. All samples fall close to a mixing line with an endmember chloride concentration of ~425 mmol/kg, except the two samples taken to the NE, which have an endmember chloride concentration of ~478 mmol/kg. Most of the 1984 samples cannot be assigned to a particular vent orifice, but it is reasonably certain that four high-temperature samples are from structures C and D and the fifth high-temperature sample is from just south of structure A near marker 10 (5050,6200). Fluids with two distinct chloride endmembers were sampled, and the higher chlorinity fluids came from the NE part of the vent field.

1987 Results

The dive tracks from 1987 cover a very large range in the vent field, including territory nearly 1 km to the south of the central part of the vent field, several hundred meters to the east, and areas on the western axial valley wall. However, with the possible exception of dive 1932, vent fluid sampling appears to have been restricted to the central structures B, C, and D and areas within several meters of these structures. Sampling locations from dive 1932 are in doubt because the navigation system was not working properly for most of that dive. A total of 20 major samples were taken in 1987, of which all but three fall close to a dilution line extrapolating to a chloride endmember of ~422 mmol/kg. The three other samples were all taken on dive 1932, so their origin is unknown. These three samples extrapolate to an

endmember chloride concentration of ~470 mmol/kg. The higher chlorinity fluids sampled in 1984 and 1987 are very similar and may come from the same structure, but the uncertainties in the navigation do not allow a direct comparison.

1988 Results

Due to the emphasis on vent fluid microbiology and chemistry in 1988, and to the availability of a good geologic map, samples were recovered from a much larger area and in greater number than in the other two years (a total of 53 titanium major samplers). In addition, the improvements in the navigation software made continuous, high-precision fixes available in the sphere so that sampling locations are very well known. I will organize all of the data by vent structure, since the data from each structure appear to lie along single dilution lines.

In 1988, high-temperature fluids were sampled from all of the major structures (A-E) and several warm vents were sampled. Samples from structure A (site 8F) yield a chloride endmember of 505 mmol/kg (Fig. 3.3). A single sample from the west side of structure B (site APL1, where the APL corrosion experiment measured transient temperatures of >400°C) yields an endmember chloride concentration of 455 mmol/kg. The high-temperature samples from structures C and D plot close to a mixing line with an endmember chloride concentration of 425 mmol/kg (Fig. 3.3). Two warm vent samples (T = 27°C, Mg = ~49) taken 10 m north of 8E and one diluted smoker sample (T = 345°C, Mg = 45) taken at marker 8E yield an endmember chlorinity of 254 ± 5 mmol/kg (Fig. 3.3), significantly lower than anything sampled in '84 or '87. This establishes a very clear and significant gradient of chlorinity from SW to NE.

M. Mottl [personal communication, 1990] sampled several vents in the Endeavour field on an Alvin dive series immediately following the 1988 Archaebacteria cruise. His chloride data matches ours very well for the vents that we

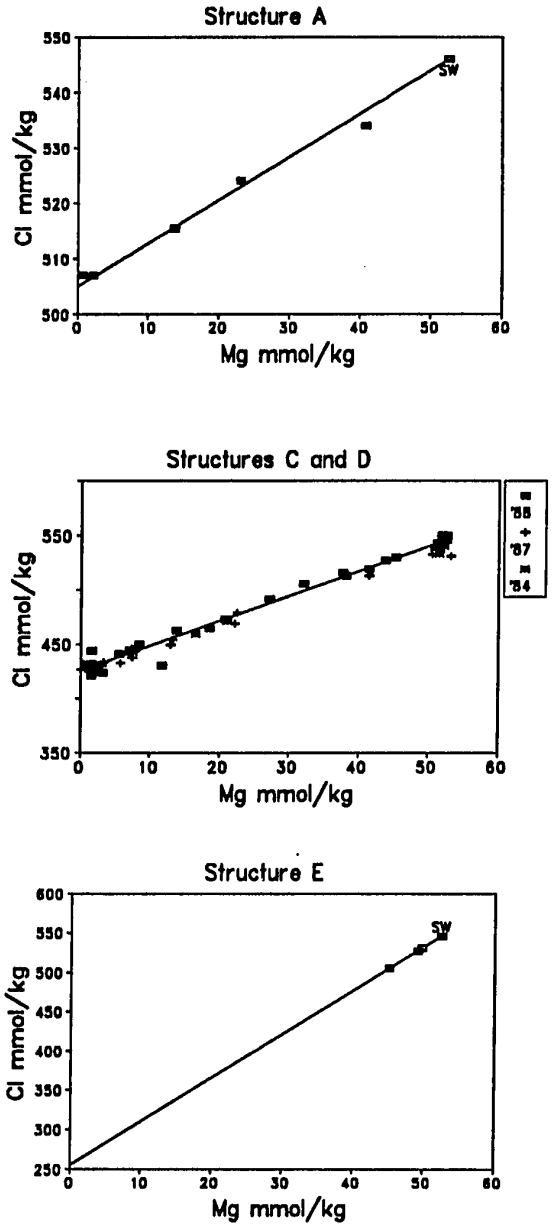

Figure 3.3. Plot of chloride versus magnesium for different sulfide structures. Chloride clearly decreases from structure A to structure E (see Figure 3.1a for locations).

both sampled (8E, near 8D on structure B, and near 8F on structure A). Mottl also obtained samples from smokers near marker 8K (4925,6025) and marker 8Q at (5000,6110), with approximate chloride endmembers of 370 and 354 mmol/kg, respectively.

Bromide The results of the colorimetric Chloramine-T/phenol red analysis of bromide on Endeavour fluids were highly variable and difficult to reproduce. Results suggest that the Br/Cl ratio decreases with decreasing chloride concentration. The measured (Chloramine-T) Br/Cl ratios are significantly lower than any reported values for mid-ocean ridge hydrothermal fluids. J. Gieskes and Chen-Feng You of Scripps Institute of Oceanography have measured Br on sample cuts from Endeavour and ASHES fluids by an (unpublished) iodometric titration method which they have shown to be without any major systematic interference. Their results indicate that, within the analytical uncertainty of 3%, Endeavour and ASHES fluids fall on the same trend as all other vent fluids on a plot of Br against Cl. They have found that the Chloramine-T method gives low results in the presence of dissolved organic carbon (DOC in Endeavour vent fluids is a few hundred μmol/kg, M. Lilley, personal communication, 1990), and further that there may be a negative Br error for fluids with low chlorinity. The iodometric analysis of a subset of representative samples from each of the major structures indicates that there are no significant intra-field variations in the Br/Cl ratio in Endeavour vent fluids (Figure 3.4). The best samples from 8E are too diluted with seawater to estimate a reliable bromide endmember.

Sulfate I measured sulfate by ion chromatography on major ion samples, which were simply stored in polyethylene bottles with no treatment, and on samples which had been purged with nitrogen gas to remove H_2S. On a plot of sulfate vs. magnesium for the major ion samples, there is some excess sulfate in the low-Mg

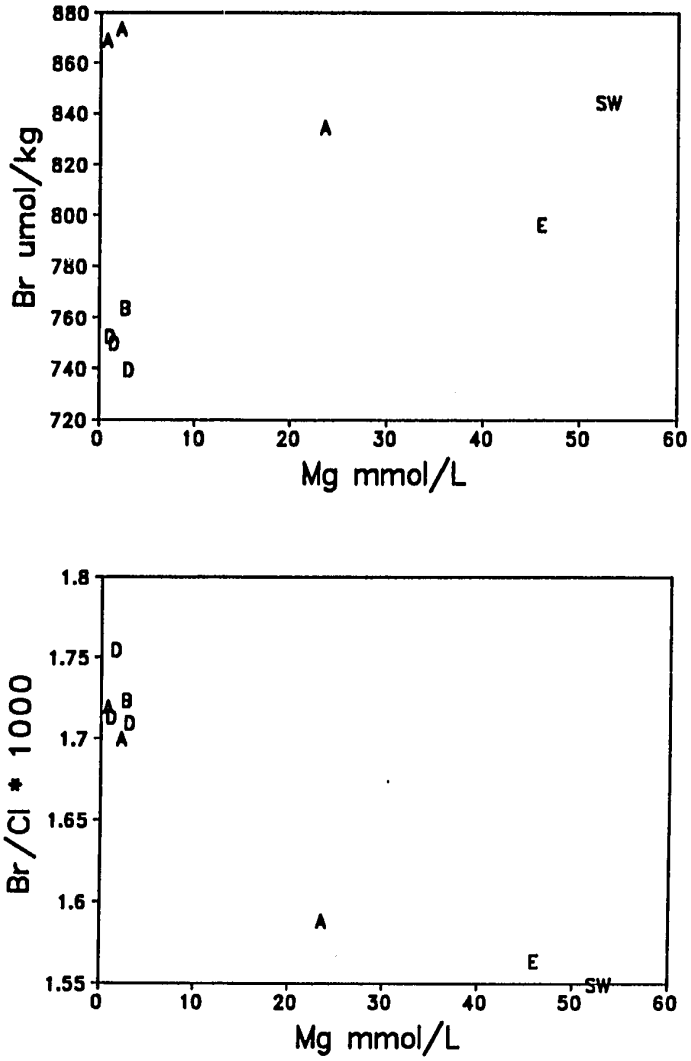

Figure 3.4. Bromide and bromide/chloride ratio versus magnesium. Data points are represented by letters corresponding to the structures from which they came. Bromide analyzed at Scripps Institution of Oceanography by J. Gieskes and C.-F. You. All samples have Br/Cl elevated over the seawater ratio, but there are no apparent differences in Br/Cl between vents.

samples over the level expected by mixing of seawater with a sulfate-free hydrothermal fluid (Figure 3.5a). This excess sulfate does not appear on the same plot for the purged samples (Figure 3.5b). I attribute the excess sulfate in the un-purged samples to oxidation of sulfide in the sample bottles. The analysis of the purged samples indicates that the high-temperature endmembers do not contain measurable levels of sulfate (i.e., sulfate and magnesium go to zero together).

Cations

Lithium Lithium endmembers range from 178 ± 8 μmol/kg at 8E to 455 ± 10 μmol/kg at structure A (Table 3.1, Figure 3.6). Lithium is typically enriched 10 to 40 times over the seawater concentration in hydrothermal fluids. The 1984 data give an endmember of close to 400 umol/kg for all samples except the one taken in the NE part of the field, which extrapolates to ~425 umol/kg.

Sodium Sodium was calculated by charge balance after all other major elements were analyzed (Figure 3.7). Sodium endmembers range from ~390 mmol/kg at structure A to ~203 mmol/kg at structure E.

Potassium Potassium is highest in the fluids from structure A (27.4 mmol/kg) and decreases with chlorinity to a value of 16 ± 2 mmol/kg in the fluids from structure E (Figure 3.8). Potassium concentrations from structures C and D in 1988 are indistinguishable to within the uncertainty of the linear regression extrapolation. Potassium in the only major element to show a significant change in endmember concentration from 1984 to 1988 (Fig. 3.8).

Calcium Calcium ranges from 43.0 mmol/kg at structure A to 18 mmol/kg at structure E (Figure 3.9). The calcium endmembers for structures C and D are the same to within the uncertainty of the extrapolation (31.9 ± 1.5 and 33.4 ± 0.9 mmol/kg).

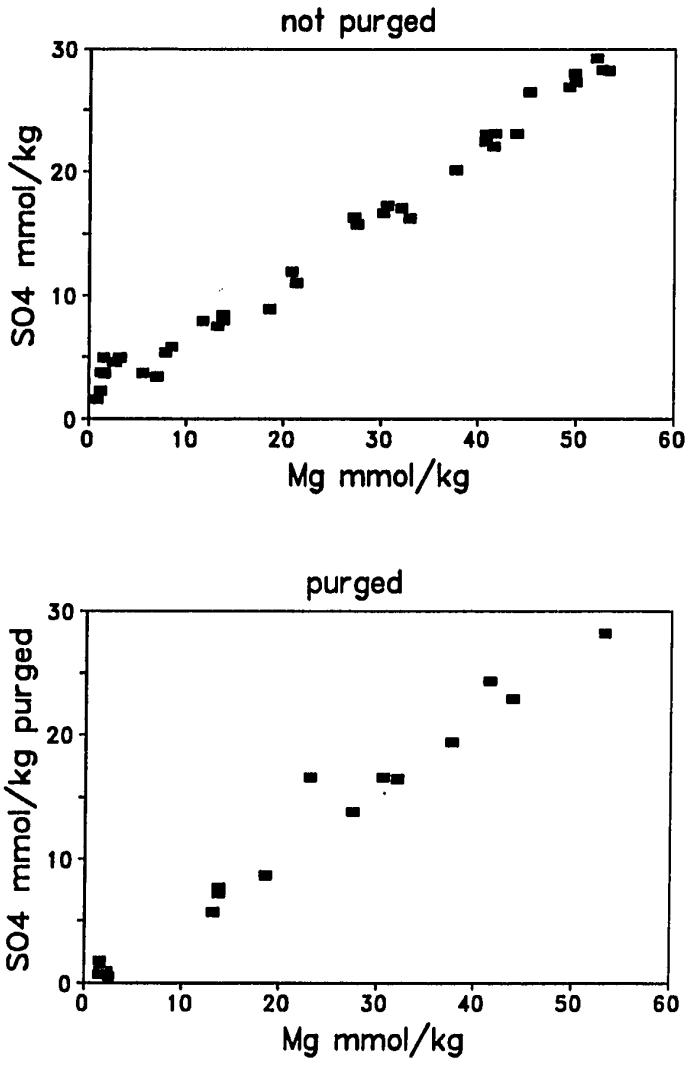

Figure 3.5. Sulfate versus magnesium for all structures. Samples which were not purged to remove hydrogen sulfide show evidence of excess sulfate due to oxidation in the sample bottle. Purged samples show no excess sulfate over the expected contribution from seawater mixing.

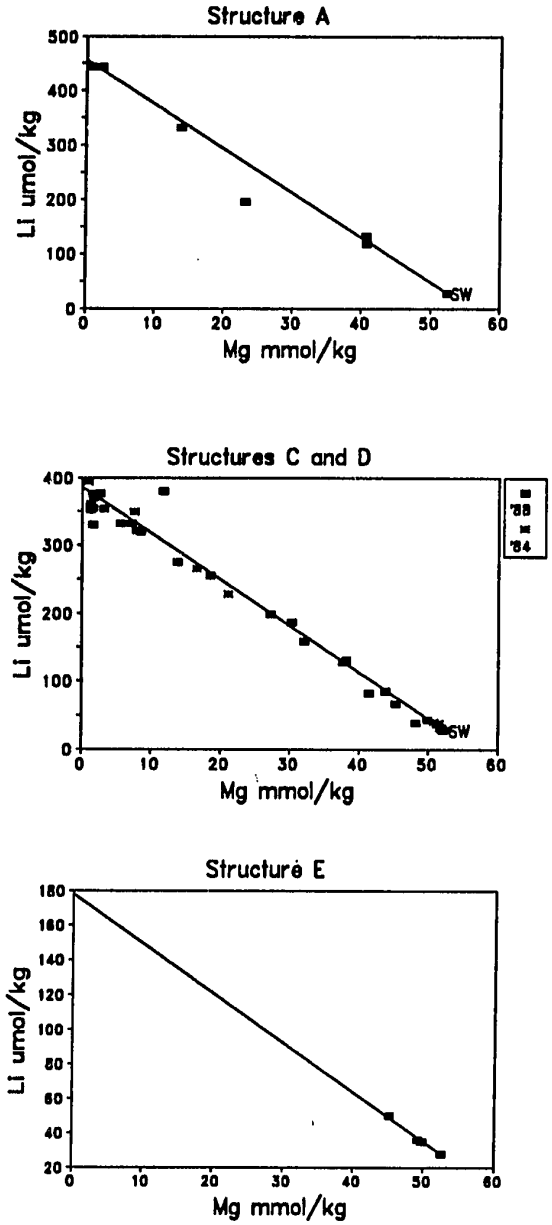

Figure 3.6. Plot of lithium versus magnesium for different sulfide structures. Least squares best fit lines drawn between seawater and zero-magnesium endmembers.

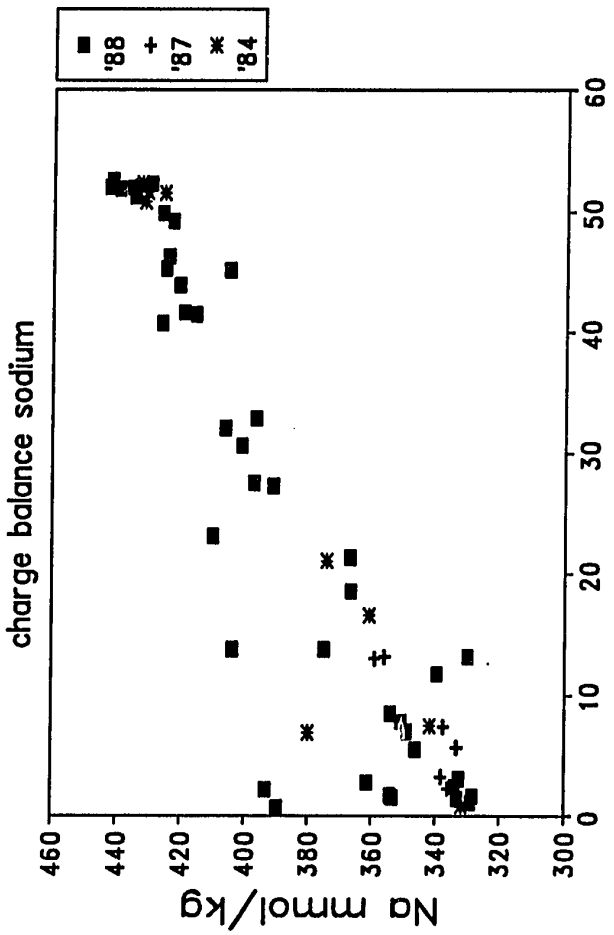

Figure 3.7. Plot of sodium (calculated by charge balance) versus magnesium for all years. Though there is more scatter, the sodium data follow the same patern as the chloride data (Figure 3.2).

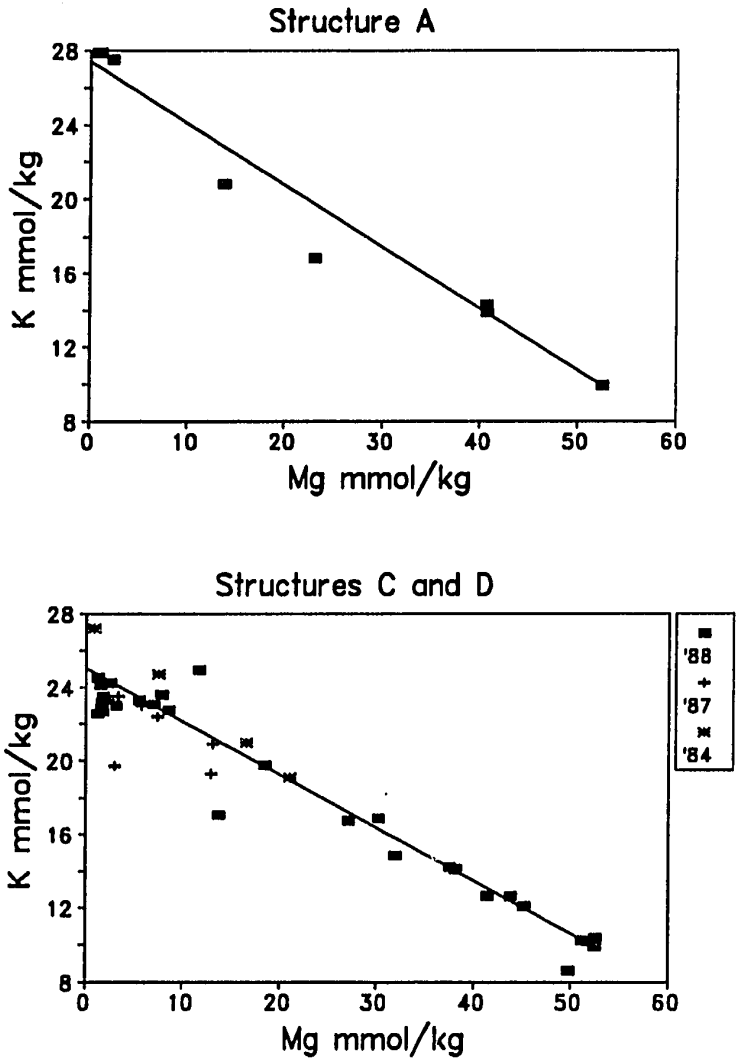

Figure 3.8. Potassium versus magnesium for structures A, C, and D.

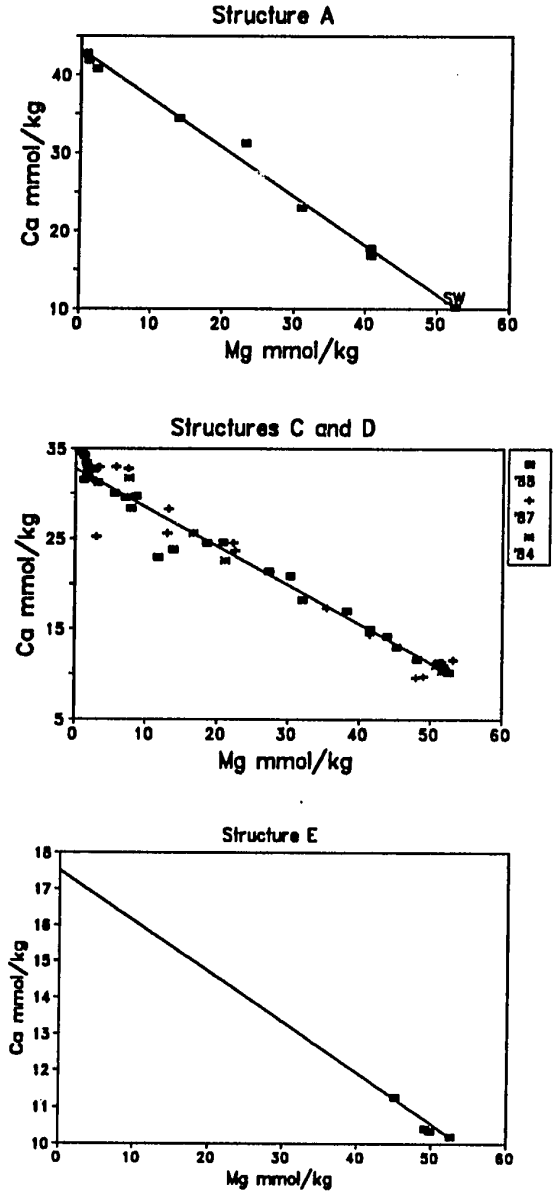

Figure 3.9. Plot of calcium versus magnesium for the different sulfide structures.

Strontium Strontium reaches a level of 154 µmol/kg at structure A, and decreases to ~133 µmol/kg at structures C and D (Figure 3.10). The data were too scattered to make the long extrapolation for the fluids from structure E. The 1984 data for vents on structures C and D give an endmember strontium concentration of 135 ± 5 µmol/kg, which is identical to the 1988 value.

Manganese and Iron The manganese content of the Endeavour fluids does not correlate with chlorinity as do most of the major elements. Manganese data for all of the vents except 8F cluster about a single dilution line with an endmember concentration of ~290 µmol/kg (Figure 3.11). The concentration in vent 8F is distinctly lower at ~195 µmol/kg. There are no data for structure E, and the endmember for structure B is based on the single sample (Mg = 2.8 mmol/kg) taken there, so it is not clear whether the trend of Mn vs. Cl extends to lower chlorinities.

The 1984 Mn data all plot close to a single mixing line with an endmember Mn concentration of ~245 µmol/kg. (One sample, probably from structure D, has a slightly higher concentration.) The sample with the higher chloride endmember falls on the same trend as the other samples.

The iron data show considerably more range and scatter than the manganese data. Some of the moderately diluted samples (Mg between 5 and 30 mmol/kg) show some evidence of iron loss. This is probably due to precipitation in the major samplers, or in some cases to sub-seafloor precipitation of iron sulfides.

The 1988 iron data (Figure 3.12) from structures B, C, and D fall roughly on a single dilution line with an endmember of ~1000 µmol/kg. The samples from structure A extrapolate to ~500 µmol/kg. It appears that the 8F fluids have lost both iron and manganese. A plot of the Fe/Mn ratio (Figure 3.12) shows that iron has been lost preferentially to Mn in fluids from structure A.

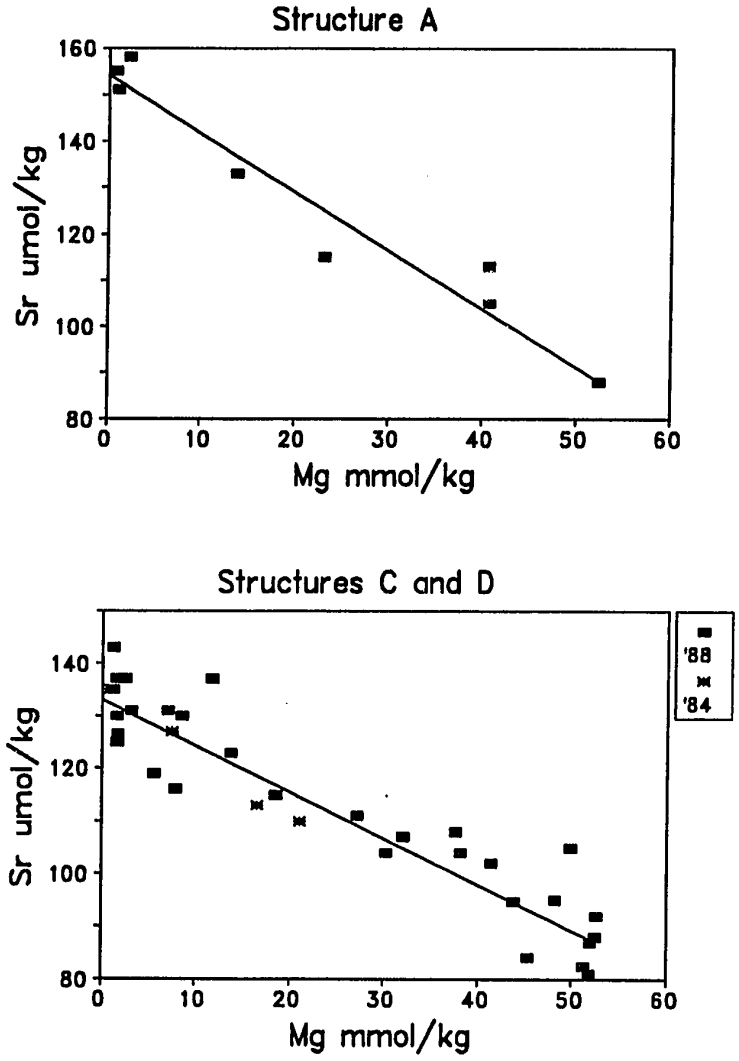

Figure 3.10. Strontium versus magnesium for structures A, C, and D.

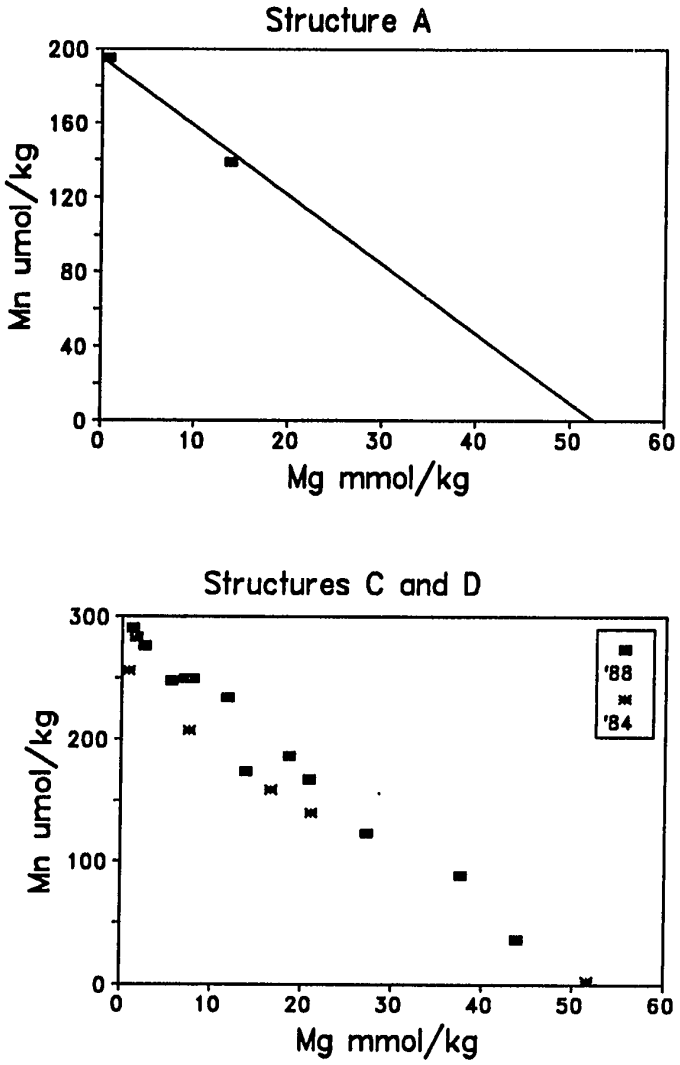

Figure 3.11. Mn versus magnesium for structures A, C, and D.

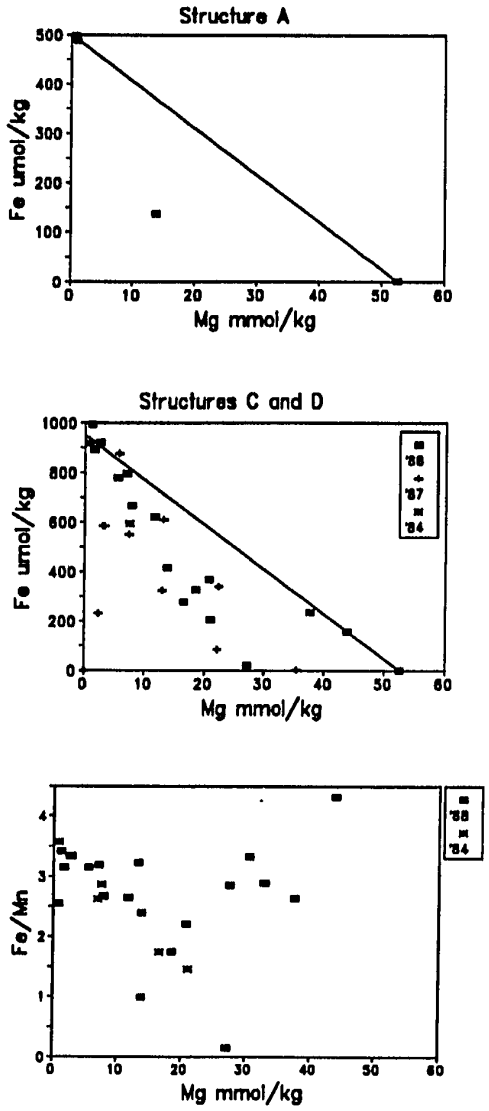

Figure 3.12. Iron versus magnesium for structures A, C, and D. Lines drawn between seawater and best estimate of high-temperature endmembers. Also shown is the iron to manganese ratio versus magnesium.

The 1984 iron data also show some iron loss in the intermediate Mg samples. The least diluted 1984 sample (Mg < 1 mmol/kg), which probably comes from structure D, has an endmember iron concentration of ~925 μmol/kg and an Fe/Mn ratio of ~3.5, neither of which is significantly different from the 1988 value. All of the other samples plot below the line connecting seawater and the 925 μmol/kg Fe endmember. The Fe/Mn ratio for 1984 samples continuously decreases with increasing Mg content, probably reflecting loss of iron at the time of sampling or during sample storage. The higher chlorinity sample taken from the eastern part of the vent field had a temperature of only 270°C, so there may have been some sub-surface precipitation due to cooling and/or seawater mixing.

Iron was analyzed on cuts taken from untreated major samples from the 1987 dive series, but Mn has not yet been analyzed for these samples. There is considerable scatter in the Fe data, most likely due to precipitation in the polyethylene storage bottles prior to removing and acidifying the sub-sample, which was done approximately one month after the samples were taken. The samples with the lowest Mg, which have the highest measured iron content, yield an endmember concentration of ~950 μmol/kg.

In summary, the endmember iron and manganese concentrations for the central structures B, C, and D are approximately the same in all years. The iron and manganese contents of the highest chlorinity fluids sampled in 1988 from vent 8F are significantly lower than the trend for the other vents.

Other constituents

Hydrogen sulfide There is quite a bit of scatter in the sulfide data, which is probably due to a combination of precipitation, oxidation, and degassing in the samples prior to analysis. The H_2S data for 1988 show a single major trend for structures B, C, and D with an endmember concentration of 5.5 ± 0.7 mmol/kg

(Figure 3.13). The H_2S endmember for structure A is significantly lower at 3.2 mmol/kg. The highest trend extrapolates to an endmember of 5.5 ± 0.5 mmol/kg. Sample 1438 falls well below the other data points and gives an endmember of 3.4 ± 0.2 mmol/kg.

Ammonia The 1988 ammonia data (measured by shipboard FIA) show scatter about a single trend on a plot of ammonia versus magnesium (Figure 3.14). All of the high-temperature vents have endmember ammonia concentrations of 500-700 μmol/kg, which is much higher than other unsedimented hydrothermal systems. There is no discernible geographical gradient of ammonia in the vent field and no correlation with chlorinity.

Silica In 1988, silica was analyzed shipboard by the methylene blue FIA method. Samples were diluted within 8 hours of reaching the surface and run within 48 hours. The scatter in the data (Figure 3.15) results in fairly high uncertainty in the calculation of endmember silica concentrations for some vents. This scatter can be attributed to variable delay times between sampling and dilution and between sampling and analysis. Long delays before dilution can result in low measurements due to polymerization of silica in the sample bottle. This was a serious problem in 1984 and 1987, when silica was analyzed on shore from undiluted samples. For this reason, silica endmembers for 1984 and 1987 cannot be estimated with the available data. It is still possible to measure silica in these samples by ICP Atomic Emission Spectrometry, which is not affected by polymerization.

The 1988 data show a trend of increasing silica with increasing chloride content. Vent 8F has the highest concentration of silica (17.1 ± 0.3 mmol/kg). Structures B, C, and D have endmembers of 16.2 ± 0.2, 16.0 ± 0.4, and 15.8 ± 0.8, respectively. Based on one data point, vent 8E has an endmember silica concentration of 5 ± 1.2 mmol/kg. The silica endmembers for structures A, B, C,

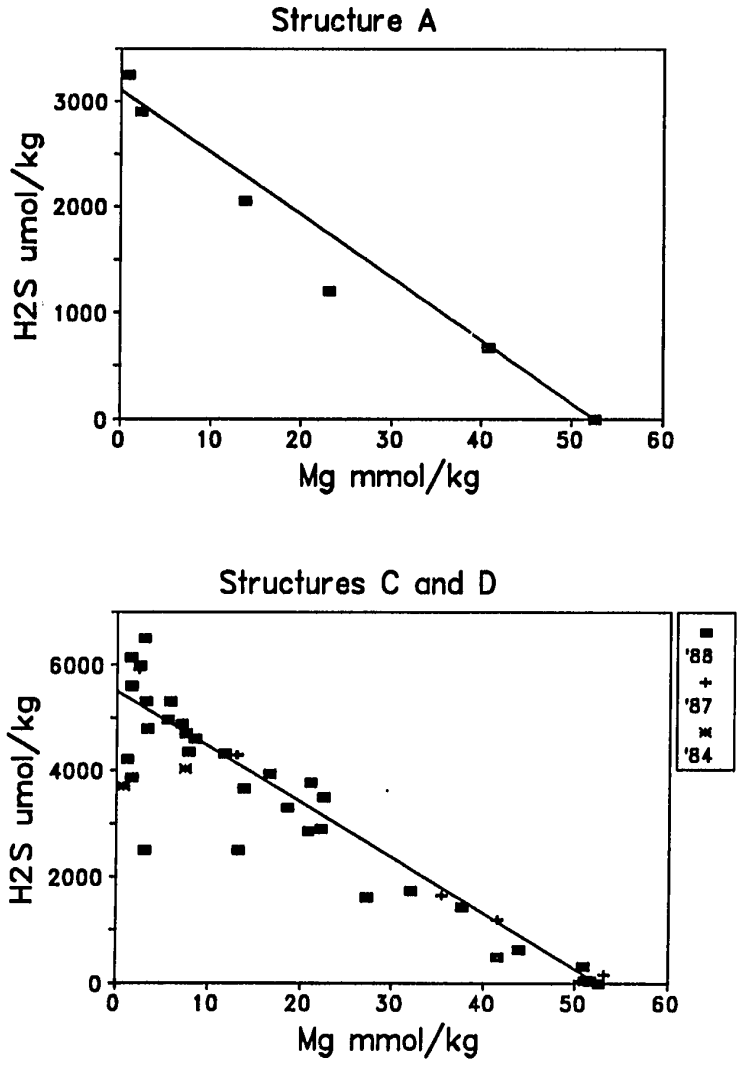

Figure 3.13. Hydrogen sulfide versus magnesium for structures A, C and D.

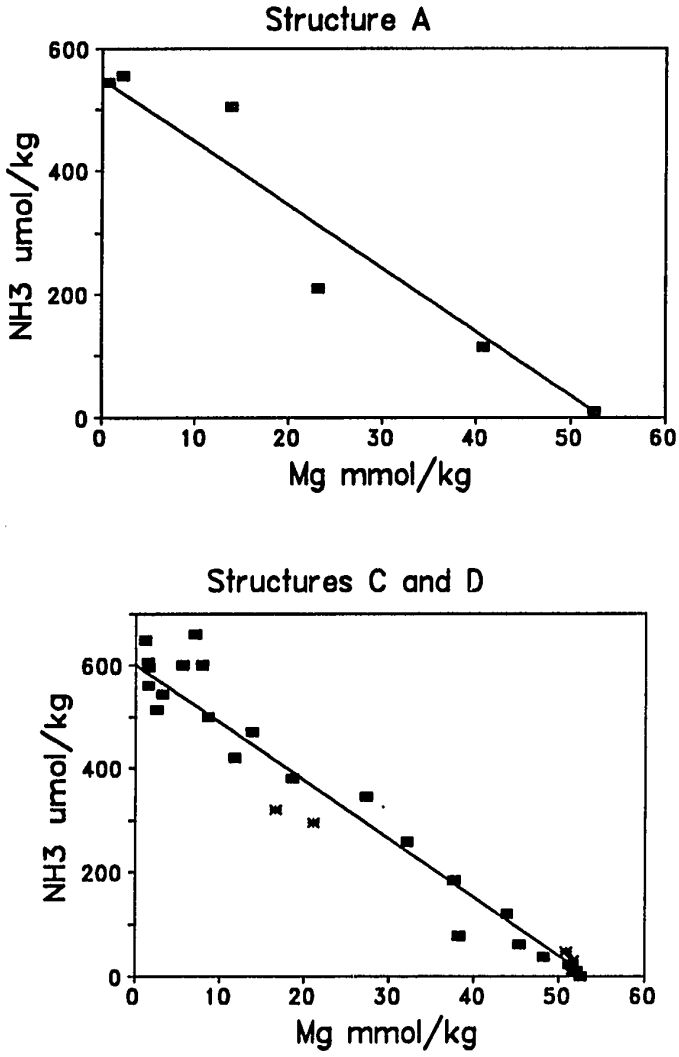

Figure 3.14. Ammonia versus magnesium for structures A, C, and D.

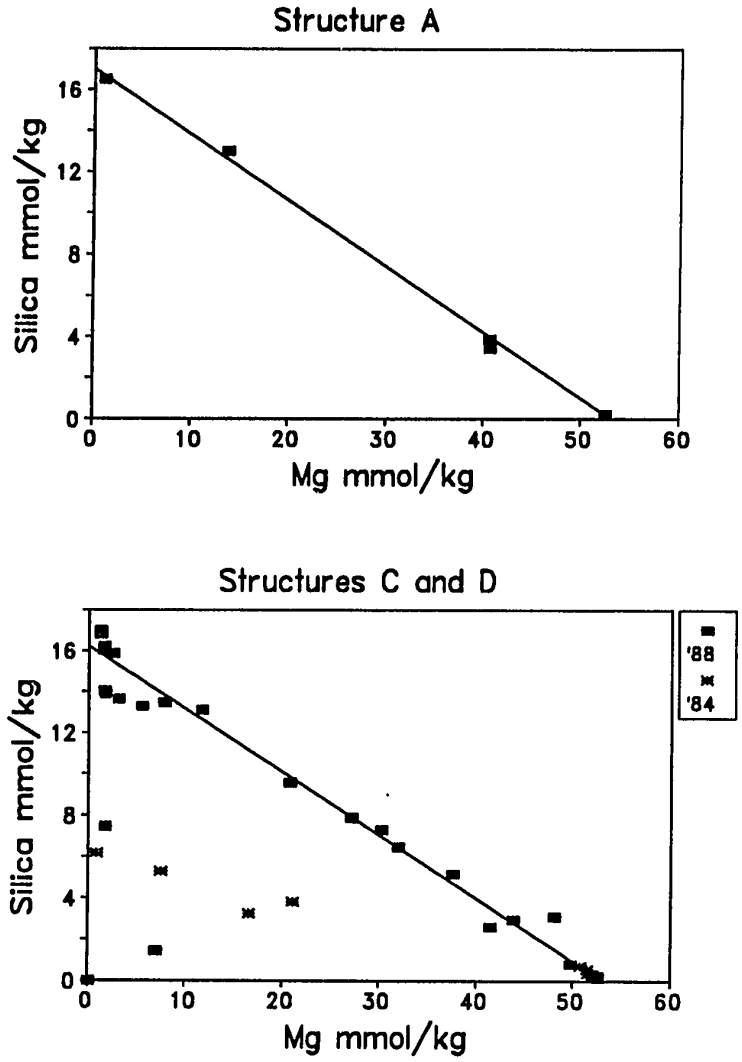

Figure 3.15. Silica versus magnesium for structures A, C, and D. Lines drawn between seawater and best estimate of high-temperature endmembers.

and D are consistent with a very shallow (0-1 km) depth of reaction, according to the quartz geobarometer of Fournier [1983]. the correlation of silica with chlorinity for these structures could be due to the effect of chlorinity on quartz solubility, to a gradient in the depth of reaction, or to mixing of high and low chlorinity fluids (brine and vapor phases) with different silica concentrations. The endmember for structure E is based on only one data point, so it is not as reliable as the other endmembers, but, even with the fairly large uncertainty, the endmember silica content is well below the quartz saturation level for seafloor pressure and the measured temperature.

Alkalinity and pH When all of the 1988 alkalinity data are plotted against magnesium, they show considerable scatter about a mixing line with a zero-magnesium endmember of ~-0.2 meq/l (Fig. 3.16). Although some individual vents are consistent and seem to fall close to a single mixing line, there is too much scatter in the data to estimate endmembers for individual structures. For example, vents 98, 102, and 16, which are all on or near structure D, plot high, low, and near the middle, respectively, on a plot of alkalinity vs. magnesium.

Similarly, a plot of pH vs. magnesium (Fig. 3.17) shows scatter about a single dilution curve with an approximate endmember pH of 4.2. The scatter is worst among the low-magnesium samples. The scatter in both pH and alkalinity is probably due to a combination of precipitation of metal sulfides and loss of CO_2 and H_2S by degassing.

Helium Helium was measured on gas-tight samples and on sub-samples of some titanium major samples by J. E. Lupton at UCSB. Results to date (Figure 3.18) indicate that there is a single trend on a plot of helium versus magnesium, extrapolating to an endmember of 35 μcc/g or 1.57 μmol/kg. The analyzed samples come from structures C and/or D, and range in temperature from 275°C to 400°C.

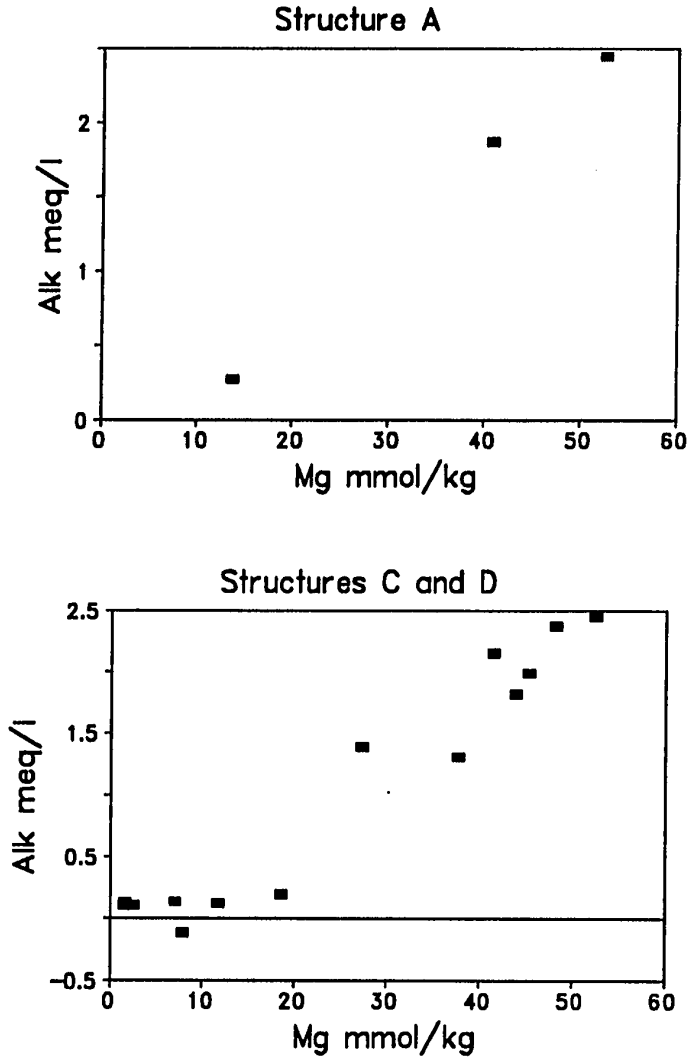

Figure 3.16. Alkalinity versus magnesium for structures A, C, and D.

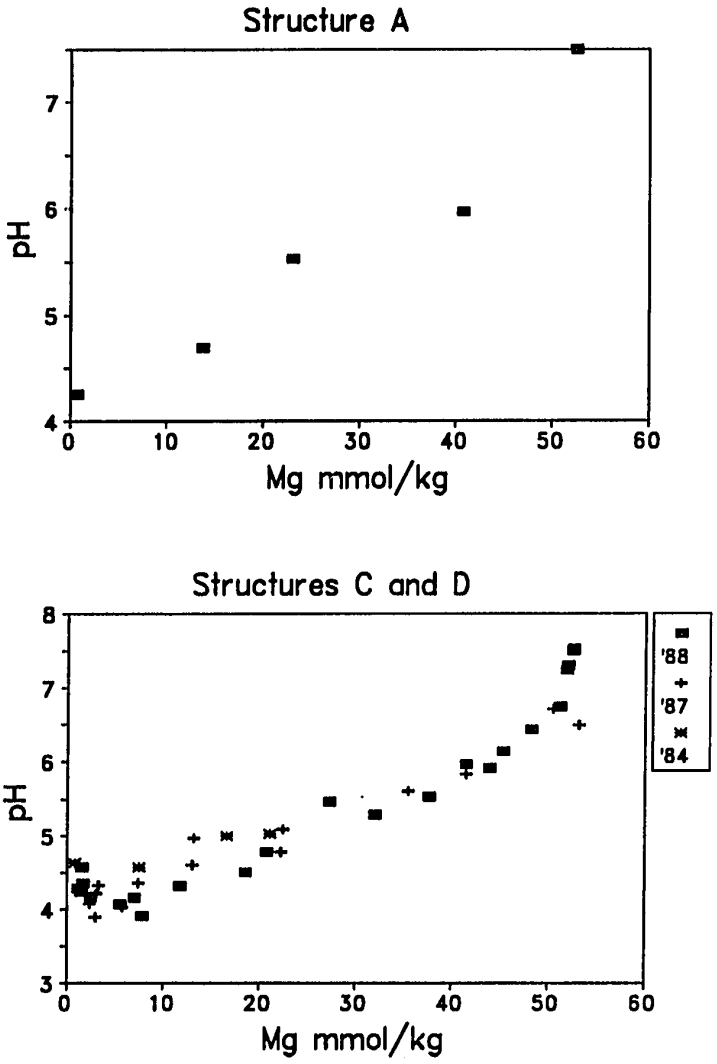

Figure 3.17. Measured shipboard pH versus magnesium for structures A, C, and D.

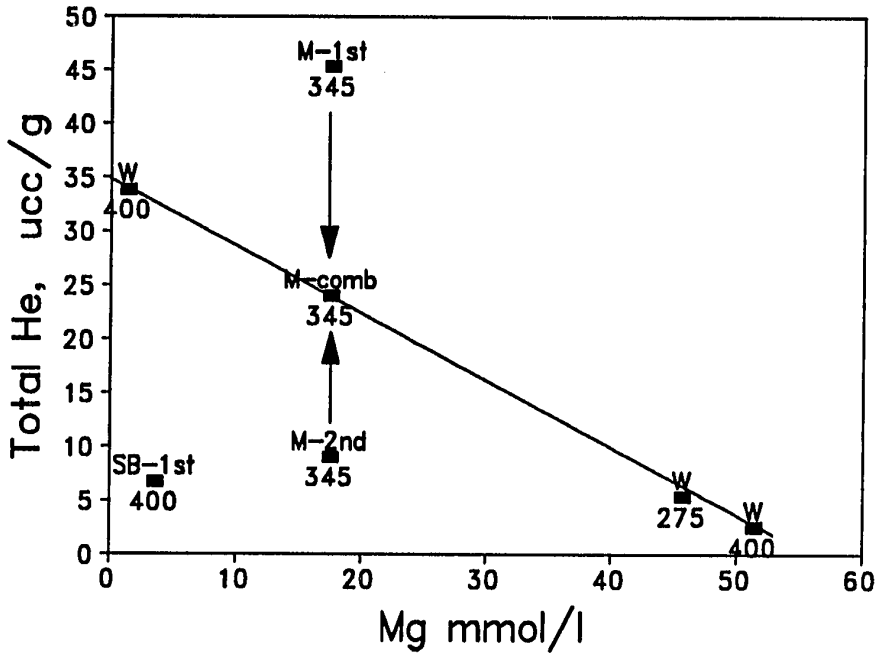

Figure 3.18. Total helium versus magnesium. Data points are labelled with temperature below and type of sampler above and cut number (1st or 2nd) above. W refers to Walden samplers, which were contained in a single flask. Helium in the first cut of the UCSB sampler appears to be low, but helium data on the second cut is not available. M refers to gas analysis from a major sampler, for which data from the two cuts have been combined. Based on the available data, the Endeavour helium endmember concentration is ~35 μcc/kg. Helium data provided by J. Lupton.

Carbon dioxide CO_2 was measured in three different ways: by manometric measurement (J. E. Lupton, UCSB) of the condensable gas fraction from 1984 gas-tight samples, by shipboard gas chromatography (M. D. Lilley) in 1987, and by calculation from shipboard pH and alkalinity measurements in 1988. The few data points from 1984 (Figure 3.19) give an endmember CO_2 concentration of 14 ± 1.5 mmol/kg. The 1987 shipboard CO_2 data (Figure 3.19) yield an endmember CO_2 concentration of 12 ± 1 mmol/kg for all samples.

The 1988 calculated CO_2 concentrations show significant scatter among the low-magnesium samples, which is expected because calculation of CO_2 from pH and alkalinity becomes increasingly uncertain as pH and alkalinity decrease. I excluded the least diluted samples from the endmember extrapolation. The 1988 CO_2 endmember is 14.5 ± 1.5 mmol/kg. Samples from the NE part of the vent field plot on the low side of the trend.

The uncertainty in the CO_2 endmembers due to scatter in the data is larger than any discernible variation from year to year, and there are no strong geographic trends in CO_2 concentration. The available data indicate that fluids from vent 8F are anomalously low in CO_2, Fe and Mn.

Time-series sampling results.

The Endeavour vent field was sampled on three different dive series over a period of 4 years. There is some overlap of vent structures sampled on all three expeditions and, in some cases, the same vent chimneys were sampled in successive years. Although a wider range of samples was collected in 1988, the data from all three dive series are very similar. There are no significant changes over the 4 year period of sampling, so that if there is a chemical evolution taking place in this vent

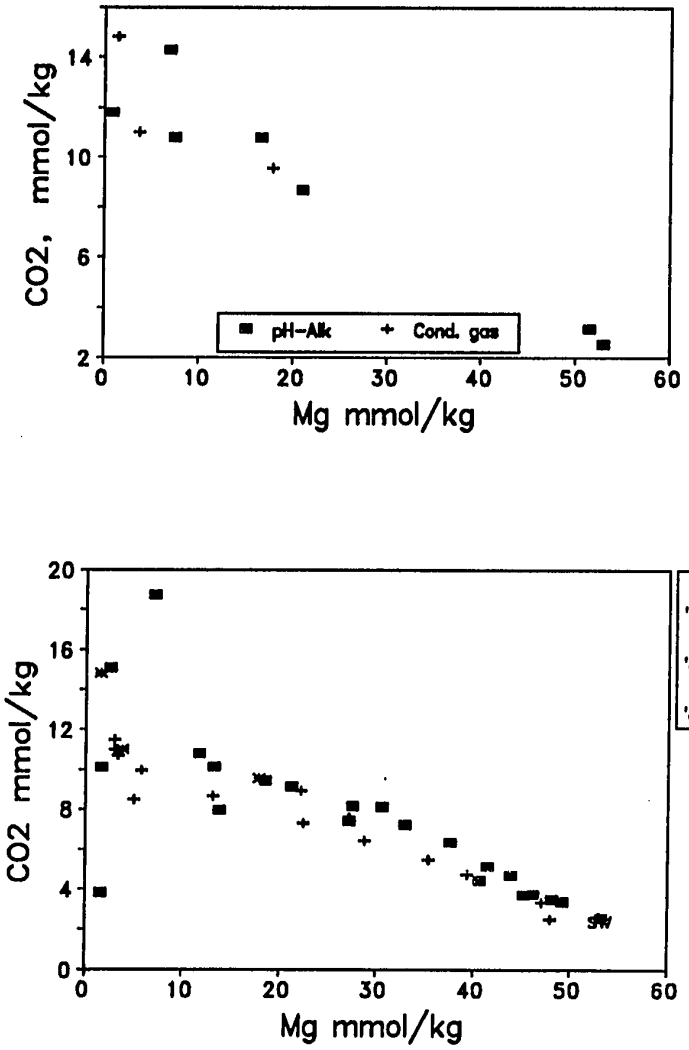

Figure 3.19. CO_2 versus magnesium for all structures. CO_2 concentrations were derived in different ways (see text). a) Comparison of 1984 CO_2 estimated from total condensable fraction of gas-tight samples and calculated from pH-Alkalinity data from major samples. b) All data from all years.

field, it is over a time scale of decades or more. This finding is in agreement with other time series studies of hydrothermal systems on the East Pacific Rise [Campbell *et al.*, 1988] and Axial Seamount [Massoth *et al.*, 1989; Butterfield *et al.*, 1990].

Time series for a single chimney.

In addition to the general observation that the fluid chemistry of large sulfide structures has been stable over the period of sampling (Figures 3.3-3.10), the data allow time series observations at a single vent orifice. Smoker 16, located on structure D, was sampled in 1987 and 1988, so we can compare the composition of a particular vent over a period of one year. The chemical data set for the 1987 samples is not complete, but it is apparent from Figure 3.20 that there have been no significant changes in major ion composition at this particular vent. This is consistent with the general observation that the major ion composition of fluids from the different sulfide structures at Endeavour did not change appreciably between 1984 and 1988.

Short-term fluctuations in temperature and composition.

There is some evidence, however, that short-term fluctuations in temperature and composition occur at individual vents. The most striking evidence comes from the transient temperature measurements of >400°C in 1988. The first 400°C+ temperature measurements [Delaney *et al.*, 1984] were made in 1984 somewhere on structure D [R. E. McDuff and M. K. Tivey, personal communication, 1990]. The search for this same vent in 1987 and 1988 proved unsuccessful. However, one of an array of 13 thermocouples in a corrosion experiment deployed in 1988 recorded a sharp increase in temperature to >400°C, while two other thermocouples rose to >375°C. These brief increases were followed by a gradual decline back to ~350°C [Spindel *et al*, 1988; Tivey *et al.*, 1990].

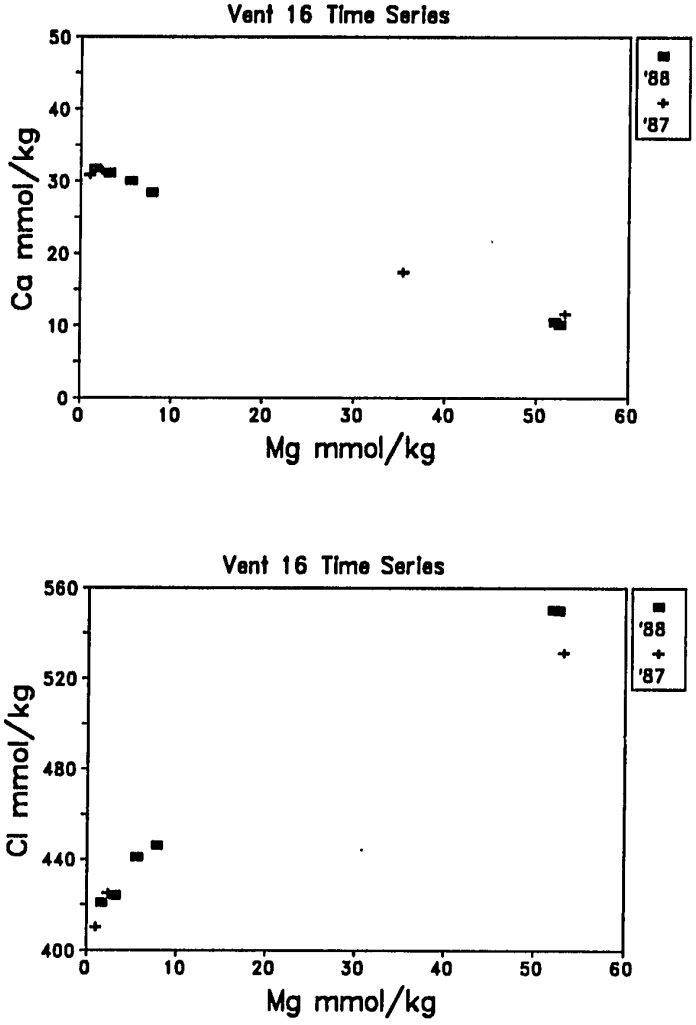

Figure 3.20. Calcium and chloride versus magnesium for samples taken at Vent 16 on structure D in 1987 and 1988. This time series at an individual smoker shows no significant difference between endmembers for 1987 and 1988.

The 400°C temperature measurements raise so many questions about the plumbing system beneath hydrothermal vents, the mechanisms controlling vent fluid temperature, the maximum fluid temperature at depth in the system, and the physical and chemical state of the fluids that one's first reaction may be to reject them as erroneous measurements. However, every effort has been taken to find fault with the measurement systems used, and there is no indication that any of the components malfunctioned in either 1984 or 1988. All of the thermocouples in the corrosion experiment were connected to the same electronics package which was placed in cold ambient water, and all of the thermocouples were calibrated and functioning properly when the instrument package was deployed. The temperature fluctuations appear to be real.

It is interesting that the temperature rose only in some parts of the flow path, apparently not in the region of strongest flow, raising questions about the flow regime. Is fluid flow in the conduit turbulent or laminar, and if the fluid is exiting in a turbulent flow regime, how could a temperature difference of nearly 50°C be maintained over a distance of a few centimeters? Do 400°C fluids travel along the same conduit as 350°C fluids beneath the vent orifice? Are the 400°C fluids injected into the 350°C fluid flow somewhere in the near sub-surface, and is mixing therefore still incomplete when the fluids exit the vent orifice, allowing the large temperature differences to exist over very small spatial scales? Are the 400°C fluids brine, vapor, or a mixture of both? Can two fluids travel through the same conduit in thermal disequilibrium due to their different physical properties? How can the chemical data help to distinguish between the different hypotheses put forward to explain the temperature measurements?

One would expect that a change in temperature from 350 to 400°C would be accompanied by changes in chemical composition. Disregarding for now the phase changes and the implications for the temperature at depth of a 400°C fluid at the seafloor, one may propose at least two distinct mechanisms for generating a transient 400°C fluid. The first requires conductively cooling a 400°C fluid to 350°C somewhere in the upflow zone: due to some perturbation (increase) in flow, there would be a decrease in cooling due to a shorter fluid residence time and 400°C fluids would reach the vent orifice. In this case the fluids come from the same source, so the 400°C fluid would be related to the 350°C fluid by conductive cooling, and only the elements which precipitate or dissolve rapidly would be affected. The second mechanism involves mixing fluids with different temperatures and compositions in the subsurface. The distinction between this mechanism and the first is that in this case the two fluids come from different sources or follow different flow paths and then mix before exiting at a vent. Again, some change in the sub-surface flow regime would result in a larger proportion of hotter fluid reaching the seafloor. This second mechanism should result in more of an overall correlation of fluid composition with temperature, since it involves mixing of two thermally (and therefore chemically) distinct fluids in the subsurface.

Unfortunately, while there are few 400°C temperature measurements, there are even fewer 400°C fluid samples, so it is difficult to test these two hypotheses with the available chemical data. We have no fluid samples to document whatever corresponding changes in composition may have taken place during the rise in temperature recorded by the corrosion experiment. Furthermore, only one fluid sample was taken from this vent (APL1) on structure B following recovery of the corrosion test collar from the vent, so we cannot determine whether the fluid composition changed over the course of the experiment. There are a total of 4

samples taken in 1984 on dive 1451 at a vent where the temperature measured between 372 and 426°C prior to sampling. After sampling was completed, the measured temperature was 375°C. Three of the samples were taken in gas-tight bottles (One UCSB bottle and two of the WHOI/Walden type) and one was a titanium major sample. One of the Walden gas-tight samples was less than 5% vent fluid, but the others were all >80% vent fluid. None of the presumed 400°C samples had in-line temperature measured during sampling, so we do not know the actual temperature of the samples. No samples were recovered from any vent with a measured temperature near 400°C in either 1987 or 1988.

The composition of the ~400°C titanium major sample is not measurably different from the other samples collected nearby from vents with temperatures of 350°C or less. End-member concentrations are the same for all elements measured, with the exception of copper. The apparent endmember copper concentration for samples with temperatures of 350°C or less is ~20 μmol/kg, while the measured concentration in major sample 1451-13 is 33 μmol/kg, which yields an endmember concentration of ~40 μmol/kg (Figure 3.21). The 400°C endmember is uncertain since it is based on a single data point, which could be affected by entrainment of sulfide particles during sampling. The 400°C gas-tight data for major elements plot on the same dilution lines as the other lower temperature gas-tight samples (Figures 3.18 and 3.19). (The gas-tight samples have not yet been analyzed for copper. Since they were not acidified, copper has probably precipitated from solution.) Since copper solubility is strongly dependent on temperature, the higher copper concentration in sample 1451-13 may be evidence that the recovered sample was indeed hotter than the other fluids. If we did succeed in sampling a 400°C fluid, then, since the major element chemistry is the same, the samples are probably related by conductive cooling rather than mixing of two chemically different fluids.

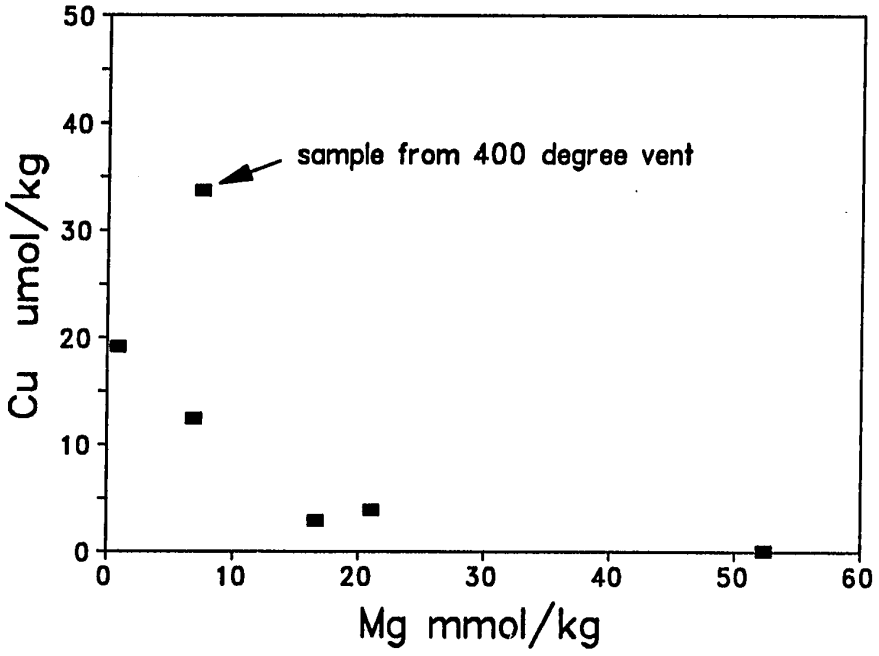

Figure 3.21. Copper versus magnesium from 1984 samples. The copper concentration from the single major sample taken at the 400°C vent gives an endmember approximately twice as high as the endmember for the other vents.

J.R. Delaney has proposed [personal communication, 1990] that there may be a pool or reservoir of ~400°C fluid trapped somehow beneath the large sulfide structures at Endeavour, and that this fluid cools to ~350°C by the time it reaches the vent orifice. The scant chemical data on the 400°C fluids is not inconsistent with this hypothesis. While there are very large differences in composition between vents from different structures in the Endeavour field, this variation does not seem to be associated with temperature: there is no clear vent fluid temperature gradient in the field. The nearly identical composition of the 400°C and 350°C fluids from the same structure, and the lack of chemical variability among different vents from a single structure implies that each structure is supplied by a single source fluid. M. Mottl [personal communication, 1990] recovered two fluid samples in September, 1988 from structure B, near marker 8D (site of the APL corrosion test), where the temperature was stable at ~375°C. These samples plot on exactly the same trend for chloride as the fluids sampled a month earlier when the temperature was 341°C. This is further evidence that changes in temperature at Endeavour do not result in significant changes in chemical composition of the major elements, and therefore that the changes in temperature are caused by conductive cooling and not sub-surface mixing of a 400°C fluid with a cooler fluid.

We can examine more closely the hypothesis that 400°C fluids are cooled conductively and not by mixing with seawater by looking at the fine-scale variability in the chemical data. Since ~350°C fluid samples with magnesium contents of less than 1 mmol/kg were collected from several vents we know that we have sampled nearly pure high-temperature fluids with no entrained seawater. However, it may be possible that seawater has mixed with hydrothermal fluids inside the sulfide structure, leaving magnesium behind in the form of a precipitated magnesium hydroxysulfate mineral. The presence of caminite in the black smoker chimney

recovered with the APL corrosion experiment [Tivey *et al.*, 1990] indicates that at least some magnesium can be quickly removed from a hydrothermal fluid mixing with seawater. This would result in a cooler fluid with a zero-magnesium endmember composition closer to seawater.

If one extrapolates the data from individual samples to obtain zero-magnesium endmembers, the plotted results will show a pattern of scatter due to the uncertainty or error in each measurement and due to the variation in endmember composition of the samples. If seawater is mixing with hydrothermal fluids at a shallow level in the crust with subsequent loss of magnesium from solution, one should see an ellipsoidal pattern on an endmember-endmember plot of the data from each structure, with the primary axis of the ellipse parallel to a line joining the seawater endmember with the "pure" hydrothermal fluid. One can see from the extrapolated data for Cl and Li (Figure 3.22) that there is some suggestion of mixing between a hydrothermal endmember and seawater, but the stretching of the data toward seawater composition is not much larger than the scatter perpendicular to a seawater-hydrothermal mixing line. A linear regression of these extrapolated endmembers gives a very poor correlation ($r^2 = 0.04$) and does not pass through seawater composition (Figure 3.22). The precision of this data set is not sufficient to allow a detailed interpretation of the pattern of extrapolated individual data points, but this does not affect the broader conclusions about intra-vent field chemical gradients.

If temperature fluctuations were modulated deep in the system, one would expect that they would be correlated with measurable changes in composition, since fluids differing in temperature by 50°C should move toward different equilibrium states (recall the conclusion drawn from the ASHES data of reaction in the upflow zone), and since a 400°C measurement at the seafloor implies a much higher temperature at depth and prevailing two-phase conditions along the upflow path

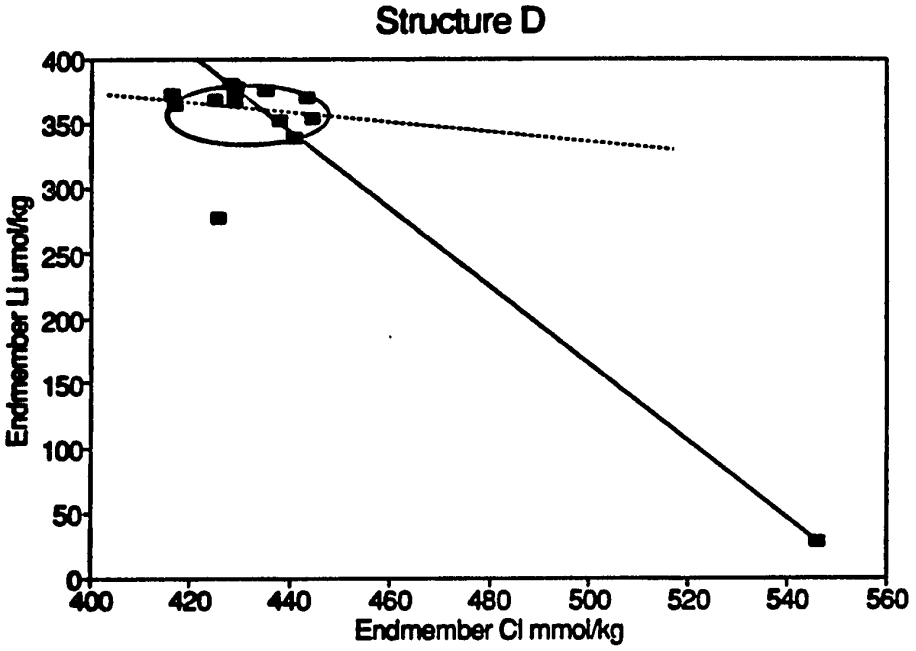

Figure 3.22. Scatter diagram of individually extrapolated zero-magnesium lithium and chloride endmembers from structure D. Dotted line is linear regression of the data. Solid line is is the trend expected if sub-seafloor mixing of seawater follwed by loss of magnesium were occurring.

[Bischoff and Pitzer, 1985], as opposed to single-phase conditions for 350°C. Furthermore, if the corrosion experiment results are correct, then it is difficult to envision how a pulse of hotter fluid from deep in the system could arrive at the seafloor and not be in thermal equilibrium with the fluid surrounding it. The available data are consistent with relatively shallow modulation of temperature fluctuations at vent orifices.

A fluid with a bulk chlorinity equivalent to seawater (3.2 wt % NaCl) at 400°C and 220 bars is in the two-phase region and would consist of a 29.3 wt % (NaCl equivalent) brine with a density of 0.91 and a 0.033 wt % vapor with a density of 0.12 [PVTx data from J. Bischoff, manuscript in prep., 1990]. In order to satisfy a mass balance of chloride, the fluid would consist of ~10% brine by weight and ~90% vapor, which yields a bulk density for a mechanical mixture of ~0.20. This is considerably less than the density of 0.67 for a hydrothermal fluid of seawater chlorinity at 350°C and 220 bars [Bischoff and Rosenbauer, 1985]. To account for the observation that most of the fluid exit temperatures are near 350°C, there would have to be some sort of physical barrier to impede the progress of the more buoyant 400°C fluid toward the seafloor long enough for the fluid to cool into the single phase region. Perhaps the large sulfide structures at Endeavour (and their sub-seafloor extensions of unknown dimensions) are caps to crustal conduits delivering 400°C fluids, as proposed by J. Delaney.

This model requires that the sulfide structure have a relatively low permeability in order to slow the flow of two-phase fluids and a high thermal conductivity to rapidly cool the fluids into the single phase region. The thermal diffusivity of pyrite (a proxy for the sulfide structure) is approximately 5 times higher than that of average basalt [Tivey, 1988; Lister, 1982; Strens and Cann, 1982], and a large decrease in permeability can be expected as precipitated sulfides clog the cracks and

conduits in the basalt near the seafloor. These circumstances make it plausible for the sulfide structures to function as radiators, and a significant portion of the total heat flux from the vent field could be in the form of conductive heat flow from the sulfide structures.

One can do a simple calculation to determine how long it would take to conductively cool a 400°C fluid to 350°C. Let us assume that hydrothermal fluids ascend through the sulfide structures in cylindrical conduits surrounded by a mixture of sulfide, anhydrite, and silica. We further assume that the inner conduit wall is at the same temperature as the hydrothermal fluid, and that the outside wall of the sulfide chimney, which we take to be a perfect cylinder, is maintained at 2°C by the ambient seawater. If the radius of the conduit is a and the radius of the chimney is b, then the heat flux per unit length of the pipe [Carslaw and Jaeger, 1959] is:

$$Q = 2\pi K \frac{(T_a - T_b)}{(\ln(b/a))} \tag{5.1}$$

where Q is the total heat flux out of the pipe in units of J m^{-1} s^{-1} and K is the thermal conductivity of the sulfide. It is simplest to calculate the cooling time with the enthalpy loss in going from a two-phase mixture at 400°C to a single phase fluid at 350°C, which is approximately 1225 kJ/g [Bischoff and Pitzer, 1985]. Dividing Q by the product of the cross sectional area and the fluid density gives the rate of heat lost from the fluid in J kg^{-1} s^{-1}. (For the calculation, I used 375°C for the temperature, fluid density of 500 kg m^{-3}, and a thermal conductivity of 4 W m^{-1} K^{-1}.) The cooling time depends strongly on the diameter of the conduit. Results indicate (Figure 3.23) that it would take tens to hundreds of seconds to cool a 400°C fluid to 350°C, which would correspond to conduit lengths of tens to hundreds of meters, assuming a flow velocity of approximately 1 m s^{-1}. Clearly the actual geometry of a sulfide structure is more complex than a cylindrical pipe, but this calculation

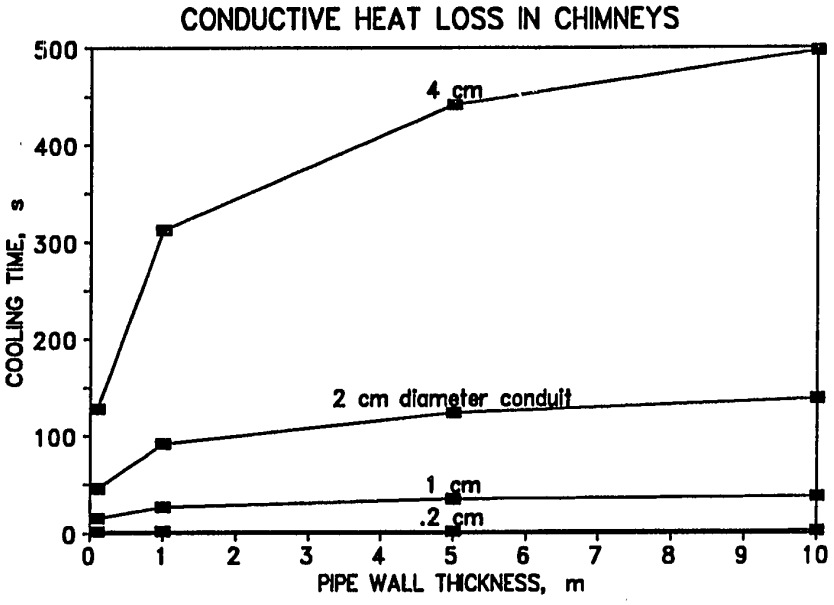

Figure 3.23. Calculation of the time required to conductively cool a two-phase 400°C hydrothermal fluid to 350°C by passage through an ideal cylindrical chimney surrounded by cold seawater. Plots show the effect of conduit diameter and wall thickness on cooling time. Calculation uses constant value of 4 W m^{-1} $°C^{-1}$ for the thermal conductivity of the sulfide chimney, average fluid temperature of 375°C, and fluid density of 500 kg m^{-3}. Conduit diameter is the most important parameter in determining cooling time in this model. Significant conductive cooling of fluids may take place within large sulfide structures and in near-seafloor conduits.

indicates that it is not out of the realm of possibility for substantial cooling to take place during passage through a 10 to 20 m high sulfide structure. Cooling would also occur during passage through the crust, which has a thermal conductivity of 2.5 $W\ m^{-1}\ K^{-1}$ [Strens and Cann, 1982], approximately half the value 4 $W\ m^{-1}\ K^{-1}$ used for sulfide [Tivey, 1988]. If this radiator model is correct, one would expect the hottest fluids to exit from the largest conduits, which have the shortest travel times through the sulfide structures and are least affected by cooling. There might also be a general decrease in temperature outward from the center of a structure.

It is difficult to propose a simple fluid history and crustal geometry consistent with all of the observations at Endeavour. The general requirements are: supercritical phase separation at depth in the system; subsequent partial physical segregation of the brine from the liquid, with variable loss of brine phase resulting in a chlorinity gradient beneath the vent field; delivery of ~400°C fluids to the base of the large sulfide structures; passage of 400°C fluids through the sulfide structure accompanied by cooling to single phase conditions, largely without physical segregation of vapor and brine (i.e. the 400°C fluid passes through the sulfide body as a mechanical mixture); occasional transient breakthrough of 400°C fluid due to changes in the flow regime in the sulfide bodies.

The combination of large short-term variations in temperature with overall long-term stability in the geographic compositional gradients implies that independent forces are at work. It may be that deep processes control the chemical composition of the vent fluids and are stable over long periods of time, while processes taking place in the upflow zone (e.g., microseismic activity, clogging of channels by mineral precipitation, submersible operations at a vent orifice) may cause short-term changes by altering the hydrothermal "plumbing" system. More detailed, high-precision temperature measurements and fluid sampling in the

Endeavour vent field could not help but improve our understanding of the processes controlling both short-term and long-term variability in temperature and composition.

Intra-field chemical variability.

Geographic trend of compositional variability.

The chlorinity of vent fluids from the Endeavour vent field increases from ~255 mmol/kg at vent 8E in the southwest to ~505 mmol/kg at vent 8F in the northeast. The chlorinity gradient is largely parallel to the dominant trend of the observed faults on the axial valley floor (~020°, see Figure 3.1). Based on our current sample coverage, vent fluid chlorinity increases in a roughly linear fashion along the trend of the faults, and there is no evidence of radial symmetry in the spatial pattern of chlorinity. A wider geographic range of sampling could determine whether there are other directional trends in chemistry, which may yield some insight into the sub-surface physical mechanisms involved in separating low-chlorinity fluids from high-chlorinity fluids.

While the similarity of composition between 400°C and 350°C fluids from the same structure suggests that temperature fluctuations are modulated by very shallow processes, the stability of the composition of individual structures over time and the persistence and pattern of the compositional gradients in the vent field argue that deeper processes are responsible for the intra-field variability. Intra-vent field compositional variability occurs on a scale larger than that of the large sulfide structures. The detailed mapping work of V. Robigou, J. Delaney and R. McDuff has shown that the location of sulfide structures in the Endeavour vent field, and even the location of smokers on these structures, is clearly related to visible faults. It

appears that the local geologic structure provides a pathway which focuses hydrothermal flow, but it is not clear whether or how the physical structure of the crust is related to the segregation of vapor and brine phases beneath the vent field.

Correlation of major ions with chlorinity.

All of the measured non-volatile ions except iron and manganese are strongly correlated with chloride (Figure 3.24). This implies that a single process is responsible for most of the compositional variation in the Endeavour vent field.

While the samples from 8E are at most 15% vent fluid, the extrapolation to zero magnesium still yields reasonably precise end-members for calcium, chloride, and lithium, so that we can compare the high-temperature endmember at 8E with the other vents, for which we have much less diluted samples.

Hypotheses for generating chlorinity variations at Endeavour.

Before proceeding with the mechanisms for generating high-temperature fluids of differing chlorinity at Endeavour, one should first consider the possibility that seawater is mixing with a single hydrothermal endmember.

The maximum measured temperature at 8F (high-Cl) is lower than at both 8E (lowest Cl) and structure C, and the iron, manganese, hydrogen sulfide, and carbon dioxide contents of vent 8F are lower than the vents on the central structures (Figure 3.24). (We do not have enough data to estimate the iron or manganese content of fluids from structure E.) These facts would suggest the possibility of dilution of a single high-temperature, low-chloride hydrothermal endmember fluid by ambient seawater in the subsurface, causing the trend of decreasing temperature and metal content with increasing chlorinity. However, except for iron and manganese, none of the trends in fluid composition are in agreement with this hypothesis. In particular, the fluids from vent 8F have significantly higher levels of Ca, Sr, K, and Li than the

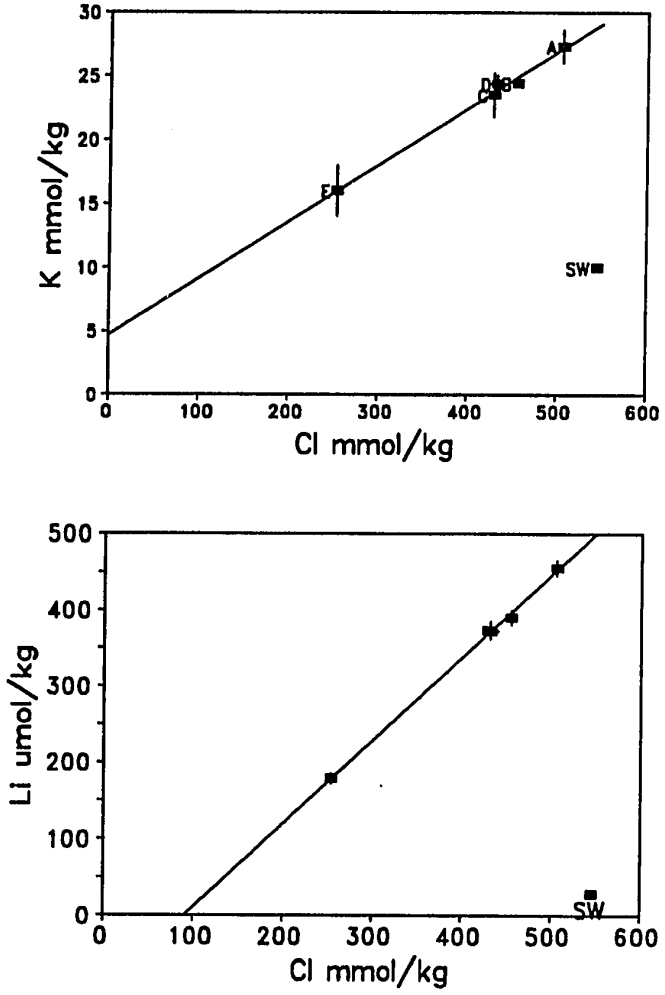

Figure 3.24. Endeavour vent field endmember element vs. chloride data. Linear regression lines drawn through points. a) Potassium versus chloride. b) Lithium versus chloride.

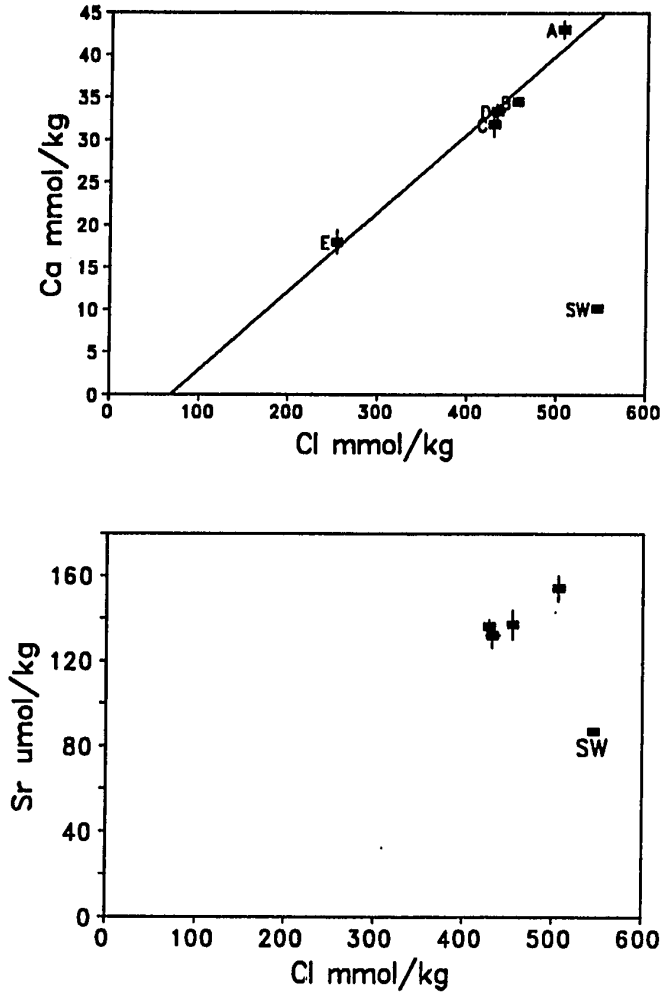

Figure 3.24 (continued) c) Calcium versus chloride. d) Strontium versus chloride.

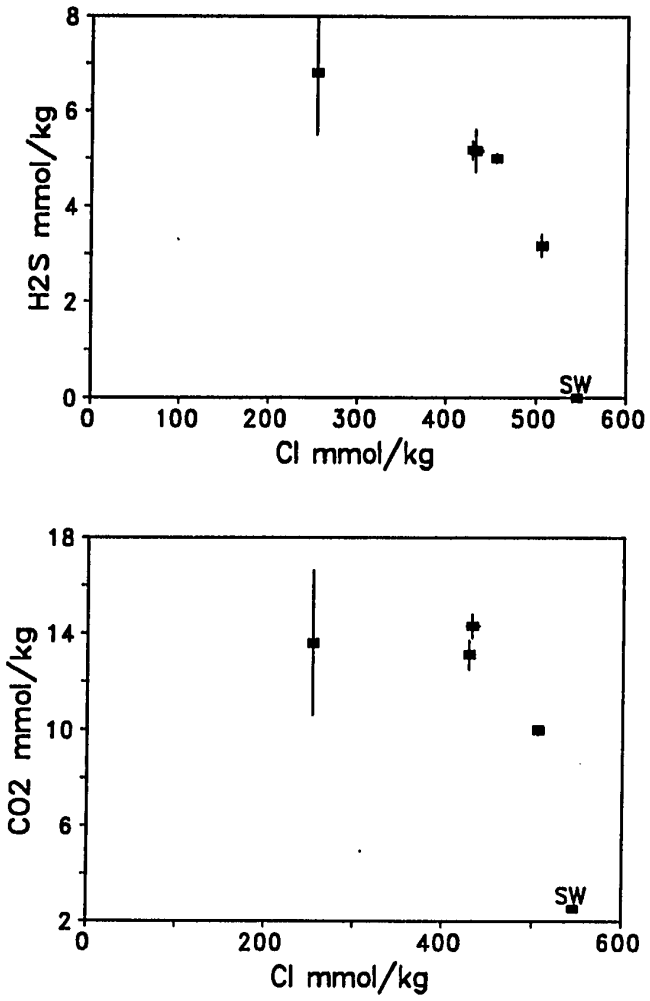

Figure 3.24 (continued) e) H_2S versus chloride. f) CO_2 versus chloride.

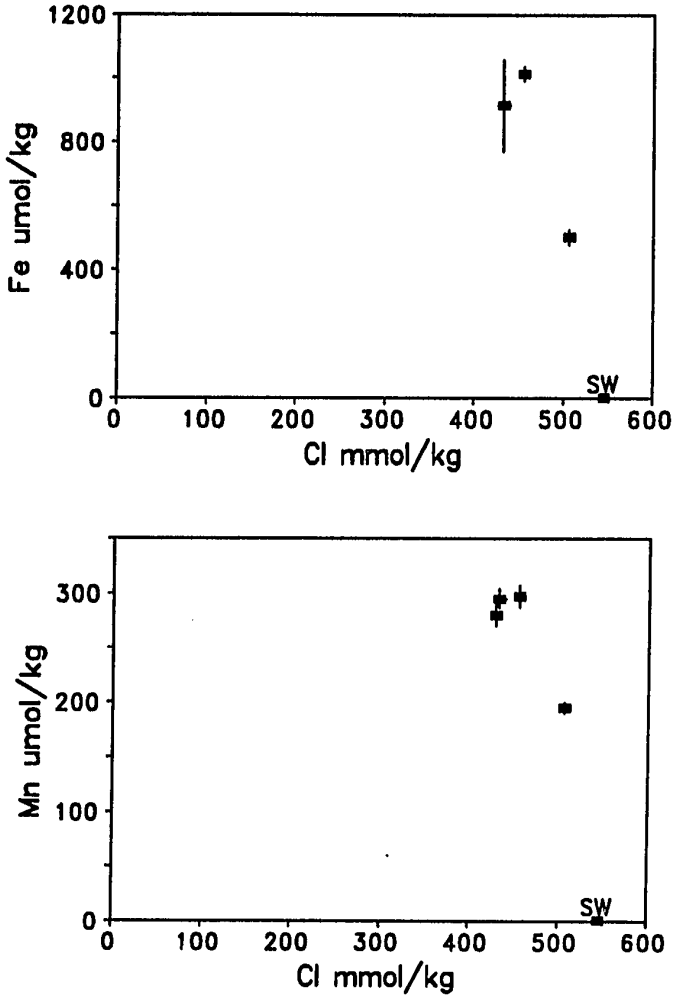

Figure 3.24 (continued) g) Iron versus chloride. h) Manganese versus chloride.

other vents, contrary to what one would expect from dilution of a high-temperature, low-chlorinity fluid with seawater. These observations require the existence of multiple high-temperature fluids at depth beneath the Endeavour vent field. The decreasing metal and sulfide contents are consistent with solubility control of iron and manganese. Manganese is not a common sulfide-forming metal in hydrothermal systems, though it can form a monosulfide, MnS, with crystal structures analogous to sphalerite or wurzite [Wuensch, 1974] and manganese-enriched mixed chlorite clays have been found in hydrothermally altered basalt in DSDP hole 504B [Alt *et al.*, 1984]. Measurement of strontium isotope ratios in the Endeavour fluids is currently underway, and should help to constrain sub-seafloor mixing processes. A wide range of fluid samples collected when the Endeavour vent field is revisited in 1991 should allow better definition of the compositional trends and controls on metal content.

By looking at the vectors of chemical difference between the endmember fluids, we may arrive at some conclusions regarding the processes giving rise to the chemical variability within the Endeavour vent field. Assuming that we have adequate sample coverage (i.e. that we have not missed a high-chlorinity fluid), then the Endeavour fluids have experienced either the loss of a chloride-enriched phase or addition of a chloride-depleted phase, relative to the initial seawater. It is clear from the endmember property-property plots that the chemical gradients at Endeavour are not caused by dilution of a single, low-chlorinity, high-temperature hydrothermal source with seawater beneath the seafloor. However, it is not immediately apparent what causes all the sampled fluids to be low in chlorinity, nor what process is causing the trend of increasing chlorinity from SW to NE in the vent field. There are clearly some very strong correlations of major element concentrations in the endmember fluids with the endmember chloride concentration, an observation which

may support phase separation and partial segregation of low- and high-chlorinity fluids as a cause of chloride variability. However, it is still possible, as others have suggested [Bowers *et al.*, 1988; Berndt and Seyfried, 1990], that some other process is responsible for or contributes to the chlorinity variations, and that the correlations of the other major ions is simply due to the dominance of chloride complexes in solution at high temperatures in fixing the solubility of most elements. Note, however, that it has not been shown that simply changing the chlorinity of a hydrothermal fluid by a fractionating mechanism (such as mineral precipitation) will result in a linear change in concentration of the other major ions in solution.

Arguments against phase separation are based primarily on the lack of correlation of gas content with chlorinity and on the confusing behavior of trace elements (e.g., boron and bromide) between vent fields. At supercritical temperatures and pressures, phase separation could cause large changes in chlorinity without significant fractionation of gases, by removal of a highly saline, gas-depleted brine from the original hydrothermal fluid. Arguments based on trace element correlations with chloride between different hydrothermal systems are subject to a myriad of interpretive complications: fluids emanating from different hydrothermal areas have certainly experienced a very wide range of subsurface conditions, including differences in residence time, rock composition, pressure and temperature, age of the system, etc. Boron chemistry in particular will depend very strongly on these factors. Bromide to chloride ratios in the fluids may be a better inter-vent field indicator of the causes of chloride variations. Regardless of what process initially generates the large changes in chloride concentration, the concomitant changes in elemental concentrations and in ionic strength can clearly change the saturation state of many minerals by changing the elemental concentraions, the activity coefficients,

and the level of complexing, so that re-equilibration may overprint the signature of the initial chloride-altering process, as has been specifically proposed for silica and boron in the ASHES vent field [Butterfield *et al,* 1990].

The task of modelling both phase separation and fluid-mineral equilibrium at temperatures well above 350°C and into the critical and supercritical region (which probably reflects conditions in the subsurface at Endeavour) is difficult due to the lack of thermodynamic data at these temperatures. In trying to evaluate whether the Endeavour data are consistent with supercritical phase separation, I am forced to rely on a few isolated experiments. Since I cannot construct a model based on reliable data (as was done for the Axial Seamount data), the strength of the arguments for supercritical phase separation at Endeavour will depend as much on the implausibility of other mechanisms for generating the observed chemical trends as on the consistency of the data with the general predictions of chemical changes caused by supercritical phase separation.

Input of low-chlorinity magmatic fluid.

That all observed chlorinities at Endeavour are below seawater chlorinity suggests that there may be significant input of a low-chlorinity magmatic fluid at depth. The major component of a low-chlorinity magmatic fluid would be carbon dioxide, accompanied by other magmatic gases. In order for addition of such a magmatic fluid to lower the chlorinity to the levels observed at Endeavour, the concentration of CO_2 would have to be several orders of magnitude higher than measured, and there would be a clear increase in gas content with decreasing chloride. Input of magmatic fluid cannot be responsible for the chemical gradients seen at the Endeavour vent field.

Precipitation of chloride-bearing mineral.

Experimental water-rock interaction studies have shown that it is possible to generate chloride variations of up to 100 mmol/kg without phase separation [Seyfried, Berndt and Jannecky, 1986], probably by precipitation (at T > 400°C) of an iron hydroxy chloride mineral with retrograde solubility. The exact composition of the mineral has not been determined, as it has not actually been recovered from any of the experiments. Subsequent experimental studies have shown [Bischoff and Rosenbauer, 1989] that in most cases no chloride depletions are seen in experiments conducted at temperatures in excess of 400°C, so that precipitation of the chloride-bearing phase may depend very specifically on rock texture and composition.

In order for significant chloride depletion (100 mmol/kg or more) to occur by the precipitation of an iron-hydroxy chloride phase, the large-scale co-transformation of some other iron mineral must take place, and some of the major cations (sodium, calcium, and potassium) must be removed from solution to maintain charge balance. To predict the observable effects of the loss of chloride by this mechanism requires knowledge of the whole chain of accompanying reactions which must take place to make it possible. The experimental results of Seyfried *et al.* [1986] show that the charge balance for chloride depletions was accomplished by different combinations of decreases and increases in concentration of the major cations. It is conceivable (though not likely) that some combination of chloride-bearing mineral precipitation and rock-fluid reaction would result in the removal of the major cations from solution in proportion to their initial concentration, so that a plot of endmember chloride versus endmember sodium (or calcium or potassium) for different vents would yield a line passing through the vent compositions and the origin (as in the ASHES figures). It is extremely unlikely, however, that the highly soluble trace

elements (such as Li and B) would be similarly affected. The observation that plots of endmember Cl versus endmember Na, Ca, K, Sr, and Li for the Endeavour vents lie very close to a line extending through the origin argues that it is a process (such as phase separation) which affects all of these elements equally that is causing the chloride depletions, and not a process which would leave many of the elements unaffected.

Fluid compositions and temperature measurements at Endeavour do not support the chloride-bearing mineral hypothesis. Since the proposed mineral has retrograde solubility, it has been suggested that chloride-enriched solutions should have lower temperatures than chloride-depleted fluids. While there is a significant chlorinity gradient in the Endeavour vent field, there is no discernible temperature gradient, and no correlation of chloride concentration with temperature. The correlations of chloride and many of the other major elements in the Endeavour hydrothermal fluids requires that a non-fractionating process has generated the chloride variations. This rules out mineral precipitation as a viable option.

Phase separation, loss of brine phase.

The repeated, extremely high (>400°C) measured temperatures at Endeavour represent sufficient evidence to seriously consider supercritical phase separation as the cause of the observed chemical variability. A venting fluid at 400°C is within the two-phase field at seafloor pressure and implies much higher temperatures at depth. If we assume that the fluid started with seawater chlorinity and has ascended under adiabatic conditions, then the temperature at the point of initial phase separation in the subsurface must have been 500 to 540°C [Bischoff and Pitzer, 1985; Tanger and Pitzer, 1990]. In this section I will consider to what extent the chemical data are in accord with general predictions for phase separation in the near-critical to super-critical P-T region.

Correlations of major ions with chlorinity. As established in chapter 4, sub-critical boiling results in the formation of a very low-chlorinity vapor phase, giving rise to a strong correlation between most major ions and chlorinity. Since the boiling point of seawater under seafloor pressure at Endeavour is ~380°C, subsurface boiling could occur under conditions approaching or exceeding the critical point, depending on the depth below the seafloor at which phase separation occurs. The vapor phase produced under near-critical or supercritical conditions would contain significant levels of dissolved salt. If phase separation occurs in the supercritical region, where a highly saline brine would condense from a vapor-like hydrothermal fluid, the appearance of a property-property plot (e.g., K vs. Cl) could be slightly different from the plots of the ASHES data because the affinities of the various elements for the vapor and condensed phases might differ by more than a few percent.

There are two recently published experimental data sets which are relevant to Endeavour fluids. The data of Bischoff and Rosenbauer [1987] may be a reasonable experimental analog to sub-seafloor conditions at Endeavour. In these experiments, phase separation is initiated above the critical point, then the system is decompressed and cooled to two-phase equilibrium near 390°C. The liquid phases in the two completed experiments are enriched in chlorinity 2 to 3 times over the initial seawater level. The experiments of Berndt and Seyfried [1990] were conducted at 425, 440, and 450°C with no rock present and were used to derive vapor-brine partition coefficients for several elements.

In graphical terms, removing a highly saline brine from a hydrothermal fluid of seawater salinity would move the residual vapor-like fluid toward the origin while the brine composition would lay roughly on a line directed from the origin through the original composition. The Endeavour data and the ASHES data appear very

similar to the experimental data on an element versus chloride plot in that lines connecting the high-chlorinity and low-chlorinity fluids pass very near the origin (Fig. 3.25), although the absolute concentrations of the different elements varies between the experiments and the vent fluids, and the vent fluids comprise a much smaller range of chlorinities than do the experimental fluids. Also note that the element/chloride ratio in supercritically condensed brines may be different from the element/chloride ratio of the original fluid and of the coexisting vapor, so that mixing lines between high- and low-chlorinity fluids may not pass through the origin. Endmember concentrations of Na, Ca, K, and Li are strongly correlated with endmember chloride concentration in the Endeavour fluids, as expected for loss of a brine phase. The overall correlation of the major elements with chlorinity at Endeavour is consistent with supercritical phase separation and partial unmixing of the two phases.

The phase separation experiments are an important step toward a more complete understanding of chemical variability in hydrothermal systems, since partition coefficients are needed to predict the compositional trends in high salinity brines. The work of Berndt and Seyfried [1990] and Bischoff and Rosenbauer [1987] shows (Figure 3.26) that the chloride-normalized partition coefficients for the alkali metals are close to unity (there is little fractionation relative to chloride), but that significant fractionation of the alkaline earth elements occurs. The partition coefficients vary with temperature. More experiments should be undertaken to demonstrate if and how the partition coefficients vary with overall composition.

I must note that the element to chloride ratios of the Endeavour vent fluids show some significant departures from the patterns expected for supercritical phase separation (Fig 3.26). For the low-chlorinity fluids at Endeavour, the endmember concentrations of chloride, calcium and lithium are known well enough to compare

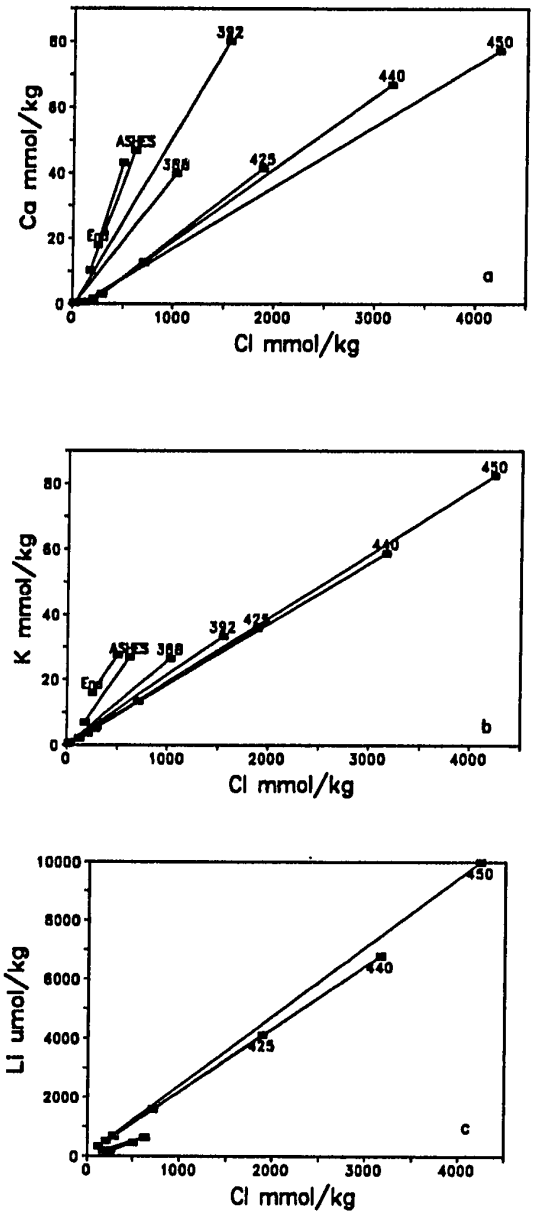

Figure 3.25. Element vs. chloride plots including experimental data from Bischoff and Rosenbauer (1987) and Berndt and Seyfried (1990). Also plotted are the extreme endmember data from ASHES and Endeavour.

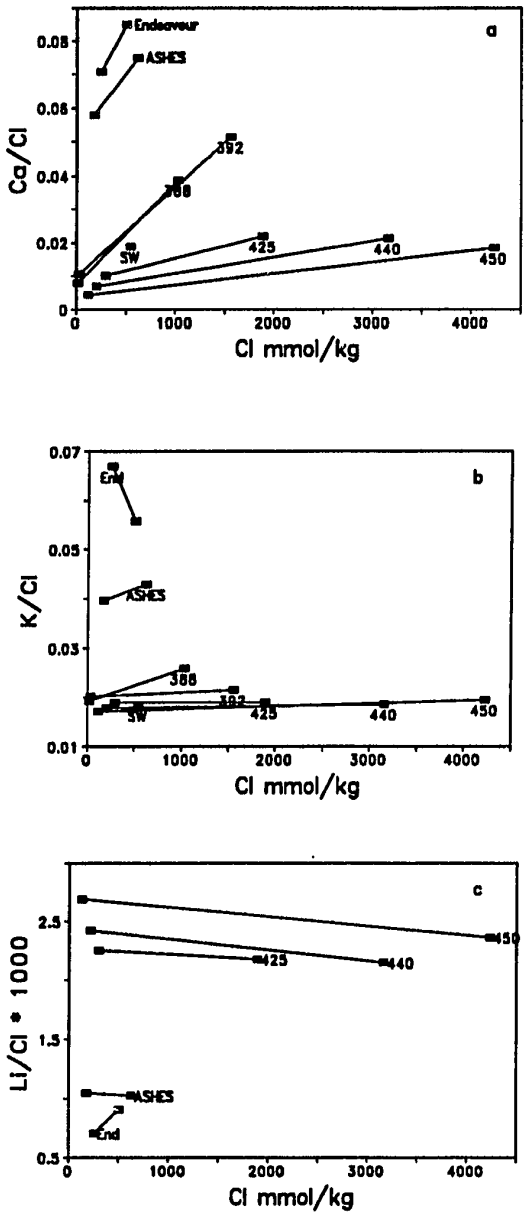

Figure 3.26. Plot of element to chloride ratio versus chloride concentration for the experimental data of Bischoff and Rosenbauer (1987) and Berndt and Seyfried (1990). Also plotted are the extreme endmembers from ASHES and Endeavour vent fields.

with the experimental data, while most of the other elements are not. Figure 3.24 shows that both lithium and calcium are depleted in the low-chlorinity fluids relative to the high-chlorinity fluids (i.e. both have negative y-intercepts on an element versus chloride plot). While this is expected for calcium, the experimental data show that lithium should actually have a slightly higher affinity than chloride for the low-chlorinity phase [Berndt and Seyfried, 1990]. Although there is no clear-cut explanation for this, it is possible that some seawater has mixed into the lower-chlorinity fluids at structure E in the subsurface, with subsequent removal of magnesium, lowering the ratio of lithium (and most other elements) to chloride in these fluids relative to the other vent fluids in the field. The quality of the samples at 8E makes it difficult to evaluate this hypothesis.

An additional factor which may cause the appearance of the vent fluid data on a property-property plot to differ from the ideal brine-vapor mixing pattern is the size of the Endeavour field. The distance between vents implies that the physical segregation of brine and vapor took place relatively deep in the system, so that the different fluids may have reacted and approached different equilibrium states. Furthermore, since venting occurs over a distance of ~400 m, one cannot assume that all vent fluids in the field emanate from a point source in the crust: there may be small heterogeneities in fluid composition at the level of the hydrothermal reaction zone. Indeed, a simple scenario for generating the compositional gradient at the seafloor requires only that a horizontal temperature gradient exist at the level of the deep hydrothermal source. The hottest fluids have the potential to generate and leave behind the most brine by supercritical phase separation, resulting in the lowest chlorinity fluid at the seafloor.

Gas chemistry. As the critical point is approached, the fluids generated by phase separation become more and more similar. There is a decreasing tendency to partition gases preferentially into the vapor phase, so the gas contents of vapor and liquid are similar [Drummond, 1981]. When phase separation occurs beyond the critical point, it has been assumed that the brine phase produced is totally depleted in gases [Von Damm, 1988; Kennedy, 1988], leaving the chloride-depleted phase enriched in gases, relative to its initial level, in proportion to the amount of brine produced. While this assumption about supercritical gas partitioning is not backed up by any experimental measurements of gas solubility, it does at least provide an upper limit to the amount of fractionation expected for loss of a brine phase.

Besides predicting small changes in gas content with chlorinity, this simple assumption about the behavior of gases during supercritical phase separation makes no predictions about changes in relative concentrations of the different gases with chlorinity. For example, two chemically different gases such as helium and carbon dioxide are considered to be equally insoluble in the brine phase, and would maintain their initial ratio in the low-chlorinity phase. More information regarding relative partitioning of gases between brine and vapor under supercritical conditions is needed to interpret the details of the gas chemistry. If the assumption that all gases are equally insoluble in supercritical brines is correct, then gas chemistry should be very insensitive to supercritical phase separation.

The lowest chlorinity fluid measured at Endeavour (~255 mmol/kg) can be produced by removal of only ~4-5 wt % of a highly saline brine (25-35 wt %, produced at temperatures between 410 and 425°C) from the highest chlorinity fluid (505 mmol/kg). Therefore, if supercritical phase separation is responsible for the variation in chlorinity observed at Endeavour, we would not expect to see large differences in gas content between endmembers of differing chlorinity. For H_2S, a

change of 5% due to gas partitioning could easily be obscured by precipitation of sulfide minerals in the upflow zone. For all of the gases, 5% is close to the uncertainty of the measurement, so with the observed range in chlorinity it will be very difficult to detect the small signal expected for supercritical phase separation.

The available CO_2 data (4 gas-tight samples from 1984, the 1987 shipboard data, and the 1988 calculated CO_2 data) do not show simple trends of decreasing gas content with chlorinity. Except for a few outlying data points, all of the 1988 endmember CO_2 concentrations lie in the range 10-16 mmol/kg, and there is no clear correlation with chlorinity, or with vent location (Figures 3.19 and 3.24). All of the '87 and '88 CO_2 data are from titanium major samplers (not gas-tight) and may be subject to errors due to loss of gas into the head space.

The gas-tight helium data show a single trend on a helium versus magnesium plot for all vents sampled, with no detectable difference between endmembers for vent temperatures of 275, 345, and 400°C. The endmember He content is ~35 μcc/g (STP) or ~1.56 μmol/kg [J. E. Lupton, personal communication 1990]. Using 15 mmol/kg for the CO_2 endmember, this gives a He/CO_2 ratio of 105×10^{-6}. Because these samples were treated with an unmeasured quantity of mercuric chloride, there is an error in the Cl measurement which makes it impossible to calculate exactly the endmember chloride content of these gas-tight samples, but, to within the uncertainty of the correction, they lie on the same trend as the major sampler chloride data for the central structures, where they were taken. The limited available data show no correlation of chlorinity with helium or carbon dioxide. This is not unexpected for phase separation under supercritical conditions.

If phase separation is the dominant process producing the observed chlorinity variations in hydrothermal systems in different mid-ocean ridge sites, one might expect to see a general trend of increasing gas content with decreasing chlorinity.

However, with the exception of noble gases of exclusively atmospheric origin [Kennedy, 1988], this is not necessarily true. There is a variety of evidence suggesting that mid-ocean ridge basaltic magmas are saturated with CO_2 at the time of their formation from the mantle [Bottinga and Javoy, 1989], which means that magma should actively degas as it rises. One would therefore expect an inverse correlation between ridge-crest depth and CO_2 concentration in hydrothermal fluids, and this trend would easily overprint the relatively small inter-field variations in gas content associated with supercritical phase separation. One should still be able to detect small differences in gas content among fluids of significantly different chlorinity taken from the same vent field, provided that high-precision measurements can be made. If the concentration of helium in the mantle and in mid-ocean ridge basalts is relatively constant, then one should also expect the ratio of helium to carbon dioxide to decrease with increasing CO_2 concentration, since releasing more CO_2 would progressively dilute the supply of helium. There are not enough gas data from seafloor hydrothermal systems to adequately demonstrate these trends of gas concentrations with depth, though the available data certainly suggest that ridge-crest depth is important (Table 3.2, Figure 3.27).

Changes in the Br/Cl ratio. The Endeavour bromide data measured by the iodometric titration method of J. Gieskes and C.-F. You [personal communication, 1990] show no trend of Br/Cl with chlorinity. All of the fluids have approximately the same Br/Cl ratio of ~0.001715 ± 0.00001, which is higher than the seawater ratio of 0.00155. Bromide data from the East Pacific Rise, the Mid-Atlantic Ridge and the Juan de Fuca Ridge all plot on the same trend against chlorinity, and give a slope which is slightly higher than the Br/Cl ratio in seawater.

TABLE 3.2 Comparison of Gas Concentrations From Several Hydrothermal Systems.

	Temp, °C Maximum Observed	CO_2, mmol/kg	He, µmol/kg	CH_4, µmol/kg	He/CO_2 x 10^6
Axial, Virgin Mound	299	285	11.2	NA	39
Axial, Inferno	328	50	2.45	25	49
Axial, Crack	218	179	8.44	NA	47
Loihi[a]	30	300	NA	7	
EPR, 21°N[b]	350	5.72	0.94	51-65	164
EPR, 13°N[c]	335	12-16	1.87-2.99		
SJdF[d]	285	3.92-4.46	0.89	82-118	200-227
Endeavour	400	15	1.56		105

Reported gas concentrations are zero-magnesium end-members, except Loihi data, which are values at 30°C.

[a] *Karl et al*, 1988.

[b] *Welhan and Craig* 1983 and *Kim et al*. 1984.

[c] *Merlivat et al.* 1987

[d] *Evans et al.* 1988 and *Von Damm and Bischoff* 1987.

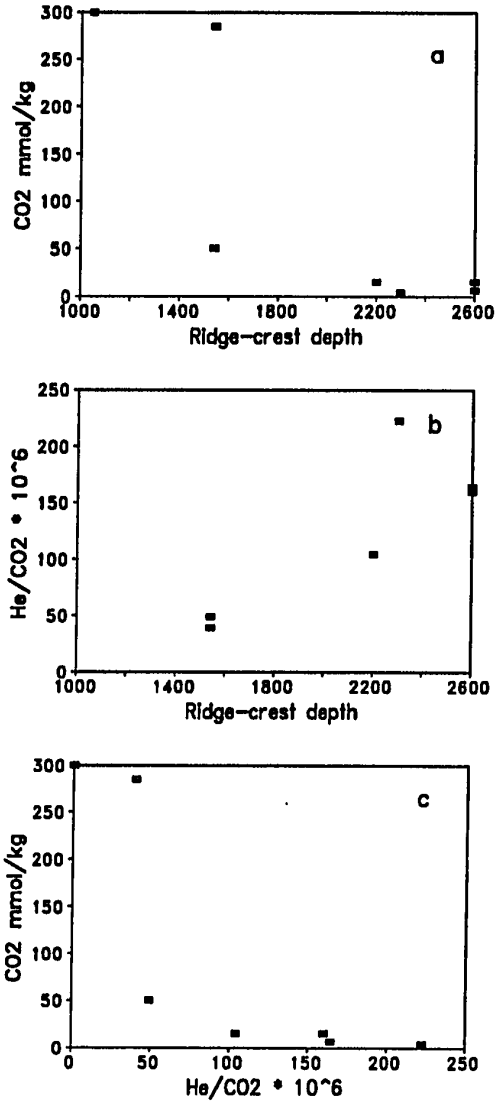

Figure 3.27. Relationship between gas content and ridge-crest depth. a) CO_2 versus ridge-crest depth. b) He/CO_2 ratio versus ridge-crest depth. c) CO_2 versus He/CO_2 ratio. Data and sources given in Table 3.2.

Recent experimental work [Berndt and Seyfried, 1990] indicates that there is a negative correlation between Br/Cl ratio and Cl concentration in fluids experimentally phase separated at 450°C or less. In other words, Br has a higher affinity for the "vapor-like" phase than does Cl. At 450°C the Br/Cl ratio in the vapor is 1.27 times the Br/Cl ratio of the brine. If removal of a high-chlorinity brine is causing the Cl variations at Endeavour, then we would expect a higher Br/Cl ratio in the lower chlorinity fluids, and all ratios should be elevated above the initial seawater value. We do see that all Endeavour fluids are elevated in Br/Cl over the seawater value, but there is no discernible trend of Br/Cl with chlorinity.

Given the systematics of the Br/Cl ratio in the phase separation experiments of Berndt and Seyfried, one must infer that, in addition to phase separation, there are one or more other processes that affect the Br/Cl ratio in hydrothermal fluids. Allowing this in no way excludes phase separation as the dominant process in generating deviations from seawater chlorinity in hydrothermal fluids. In fact, this change in Br/Cl ratio may be indirectly related to phase separation if halite saturation conditions are produced when a high-chlorinity brine is formed. If bromide is partly excluded from the halite phase, and if the halite remains in the crust, then the venting fluids would have an elevated Br/Cl ratio.

Phase separation, double diffusive convection.

Bischoff and Rosenbauer [1989] have proposed an alternative mechanism, which also invokes phase separation, to explain chlorinity variations in hydrothermal fluids. Their model involves a hot (~500-700°C), deeply circulating brine layer overlain by a seawater driven hydrothermal system. Heat and chemical exchange occurs by diffusion at the interface between the two convection cells. This model can cause chlorinity enrichment in hydrothermal fluids when brine is turbulently

entrained into the upper convection cell. Chlorinity depletions may result when hydrothermal seawater penetrates into the brine cell, lowering the salinity and causing the brine to boil off a low-salinity vapor.

The chloride enrichment and depletion mechanisms in this model are fundamentally different and should result in very different chemical signatures in the affected hydrothermal fluids. Chloride-enriched hydrothermal solutions at the seafloor would acquire a portion of the elemental ratios of the brine, which should not be the same as those of the upper hydrothermal cell because of the extremely different P-T conditions and chlorinities of the two cells and the differences in mineralogy between the lower plutonics near the heat source and the sheeted dikes and pillow basalts in the upper cell. On an endmember element versus chloride plot, a series of chloride enriched vent fluids would yield mixing lines with distinctively non-zero y-intercepts. These intercepts could be positive or negative depending on whether the deep brine is depleted or enriched in the element in question relative to the upper hydrothermal fluid. Prediction of the trends for individual elements depends on studies of elemental partitioning during supercritical phase separation (brine condensation), which would determine the initial composition of the brine before reaction with crustal rocks, and on fluid-mineral equilibrium calculations at high pressure, temperature, and salinity.

Chloride depletions in this model result from the addition of very low-chlorinity vapor boiled off from the brine cell and injected into the upper cell. Boiling results when the salinity of the brine (>20 wt % NaCl), which is maintained near its boiling point, is lowered by infiltration of hydrothermal seawater (~3.2 wt % NaCl) from the upper cell. Since the brine is already extremely depleted in gases, the vapor produced would not necessarily be gas-enriched. Low-chlorinity vent fluids generated by this mechanism would have near-zero y-intercepts on an

endmember element versus chloride plot, provided that the amount of brine entrained by the vapor phase is small and that fluid-rock reaction and mixing with seawater in the upflow zone are not important.

The predicted measurable chemical effects of this model in the case of low-chlorinity vent fluids is essentially the same as supercritical phase separation with partial loss of the brine phase. Both result in endmember mixing lines which pass near the origin for the non-volatile components, and have only a small effect on the gas-content. A difference would arise if both high- and low-chlorinity fluids were sampled from the same vent field. In the double diffusive case, there would be a break in slope on an endmember chloride versus element plot somewhere near seawater chlorinity, whereas for a single hydrothermal cell, both low- and high-chlorinity endmembers would lay on the same mixing line.

Summary and conclusions.

Hydrothermal fluids from the Endeavour vent field range from 47% to 94% of seawater chlorinity. Most of the major elements are strongly correlated with chlorinity, with the exception of gases, metals subject to solubility control, and ammonia. The limited available gas data do not show any strong correlation with chlorinity. Limited data indicates that 400°C fluid samples are not significantly different from 350°C fluids for any of the measured species, with the exception of copper, which (based on a single analysis) is approximately twice as concentrated in the 400°C fluids.

All vents sampled from a given sulfide structure have very similar compositions, but there is an increase in chlorinity from SW to NE in the vent field. There were no significant changes in fluid composition from structures revisited in 1984, 1987 and 1988.

These observations are consistent with a mechanism involving supercritical phase separation for generating the observed chlorinity variations within the Endeavour vent field. The low-chlorinity fluids are related to the higher-chlorinity fluids by loss of a brine phase somewhere in the subsurface. Based on the scale of the compositional gradients, the process controlling segregation of brine and vapor occurs fairly deep in the system. Temperature fluctuations at a given vent are probably modulated in the near sub-surface by perturbations to steady state flow. The large sulfide structures in the Endeavour vent field may be acting as radiators to cool 400°C mixtures of brine and vapor below the two-phase boundary.

Chapter 4
CONCLUSIONS

The focus of my work has been the chemical analysis of hydrothermal vent fluids from two sites on the Juan de Fuca Ridge and interpretation of the chemical data. Results indicate that phase separation is the primary cause of variations in fluid chemistry in both the ASHES and Endeavour vent fields. This conclusion was made possible in part by sampling as many vents as possible in both vent fields. It is not likely that we have missed any major vents in the small, well-studied ASHES vent field, but we have only sampled a small percentage of the vents at the Endeavour field. While temperature measurements at Endeavour suggested that phase separation was probably occurring there, we had no clear chemical evidence for phase separation until the 1988 samples had been analyzed and it was found that there was a significant chlorinity gradient in the field. It is extremely important that a wide range of vents was sampled at Endeavour, because without the 3 samples from vent 8E, the chlorinity range would have spanned only about 80 mmol/kg instead of 250 mmol/kg. The fluid chemistry at Endeavour is complicated enough that without the full range of compositions, the evidence for supercritical phase separation would have been equivocal.

The ASHES data fit a simple, closed system, vapor-liquid partitioning model remarkably well, and are consistent with sub-critical phase separation and physical segregation of the vapor and liquid phases.

The Endeavour data cannot be modelled so easily for a number of reasons. First of all, chemical partitioning between vapor and brine under supercritical conditions has not been thoroughly investigated. Secondly, supercritical phase separation may cause only subtle variations in gas content, which removes a key

difference between phase separation and other chlorinity-changing mechanisms. Finally, the Endeavour field is large enough that horizontal chemical and temperature gradients in the high-temperature reaction zone may exist prior to phase separation, and significant re-equilibration of partially segregated vapor-brine mixtures may overprint the chemical signature of phase separation.

Conclusions specific to the Axial Seamount and Endeavour sites are included in the preceding chapters. Here I present some of the important general conclusions of these studies.

Phase separation and implication for sub-seafloor temperature.

First and foremost, there can no longer be any doubt that phase separation occurs in submarine hydrothermal systems. The remarkably good agreement between a simple closed-system boiling model and the ASHES major element and gas data represents the first unequivocal evidence of active phase separation in a submarine hydrothermal system. The presence of low-chlorinity, gas-enriched fluids and high-chlorinity, gas-poor fluids in the same vent field implies that phase separation has taken place and that the vapor and liquid phases have become physically segregated. The data are consistent with a minimum sub-seafloor temperature of 370°C at the point of initial boiling.

The compositional gradients in the Endeavour vent field are consistent with removal of a brine phase generated by supercritical phase separation. The available gas data do not show significant trends of gas content with chlorinity, and this is also consistent with removal of a high-chlorinity brine depleted in gases. Measured temperatures of >400°C support the hypothesis of supercritical phase separation beneath the Endeavour vent field.

The data from Axial Seamount and Endeavour described in this study, and the data from the Southern Juan de Fuca Ridge [Von Damm and Bischoff, 1987] indicate that phase separation is occurring in at least three different hydrothermal systems along the Juan de Fuca Ridge. These three sites comprise a wide spectrum of venting regimes. At ASHES, phase separation is sub-critical and both liquid and vapor phases have been sampled. At the Endeavour site, phase separation is supercritical and the brine phase has not been sampled. At the Southern Juan de Fuca site, phase separation is also supercritical and nearly all of the fluids sampled are brine-enriched (there is some weak evidence for a diluted low-chlorinity fluid at SJFR). Further sampling at Endeavour and SJFR may reveal the presence of the co-existing brine and vapor phases, but for now the implication is that brine is accumulating beneath the Endeavour field, while brine is preferentially venting at SJFR. Taken as a whole, the chemical data from the Juan de Fuca Ridge hydrothermal fluids indicate that phase separation may be quite common in submarine hydrothermal systems.

While the chemical data strongly support the hypothesis of phase separation in hydrothermal fluids at temperatures above 375°C, most vent fluid temperature measurements are considerably below two-phase conditions at seafloor pressures. In addition, experimental fluid-rock studies best reproduce the observed hydrothermal compositions when temperatures are in the range 375-425°C [Seyfried, 1987]. The discrepancy between temperatures implied by the chemistry and typical maximum observed vent temperatures clearly implies that conductive heat loss, and possibly heat loss due to mixing with cold seawater, can significantly reduce vent temperatures. It is unreasonable to estimate maximum temperatures at depth by simple extrapolation of vent temperatures along an adiabat. Hydrothermal fluid temperatures in the crust are not limited to 350-370°C.

Phase separation does not require low-chlorinity fluids to be gas-rich.

It has been argued that phase separation is common in hydrothermal systems, then one should see the highest gas contents in the lowest chlorinity fluids, and vice versa [Bowers *et al.*, 1988; Campbell *et al.*, 1988; Von Damm, 1990]. The ASHES data illustrate this gas fractionation at sub-critical temperatures. However, one can generate low-chlorinity fluids under supercritical conditions by removing a very small amount of gas-depleted, high-chlorinity brine and the gas content of the reduced-chlorinity fluid will not change by more than a few percent from the original gas content. Gas contents in hydrothermal systems are variable and the inter-field differences are much larger than the expected change due to supercritical phase separation. For example, even the high-chlorinity fluids at ASHES have considerably higher gas content than reported for any other hydrothermal system. Ridge-crest depth is probably one of the most important parameters in determining gas concentration in hydrothermal fluids (see chapter 3).

It has also been argued that phase separation should result in low-chlorinity fluids with generally lighter stable isotope ratios than in high-chlorinity fluids [Bowers *et al.*, 1988; Von Damm, 1990]. Von Damm points out the complications introduced by chemical processes occurring in the upflow zone. There is an additional flaw in this argument, however, because vapor-liquid isotope fractionation decreases with increasing temperature. The predicted isotope fractionation for both oxygen and hydrogen isotopes becomes vanishingly small at temperatures above 300°C [Henley *et al.*, 1984], so one would not expect the vapor phase to be isotopically different from the liquid phase at the time of phase separation.

Fluid-rock reaction in the upflow zone.

One of the most interesting conclusions comes out of the disagreement between the ASHES boiling/mixing model and the measured chemistry. The large excess of

silica in the low-chlorinity fluids clearly shows that the fluids have continued to react with the crust in the upflow zone after phase separation took place. This is contrary to the idea that fluids ascend rapidly with little change in chemistry or temperature from a high-temperature reaction zone at depth [Bowers *et al.*, 1988], and implies that at least some hydrothermal fluids continue to react along the entire length of the flow path. Von Damm [1988] has also suggested that fluids may re-equilibrate after undergoing phase separation. The magnitude of chemical change in an ascending fluid will depend on the thermodynamic driving force for dissolution and precipitation reactions, or the degree of disequilibrium, which is likely to be increased by phase separation and physical segregation of liquid and vapor phases. Given the probability of conductive cooling and continued reaction in the upflow zone, one cannot use the measured composition and temperature of hydrothermal fluids to directly infer an equilibrium composition and temperature in a deep reaction zone.

Phase separation, global variability, and hydrothermal fluxes.

Nearly all elements are correlated with chlorinity in end-member hydrothermal fluids (Figure 4.1). Phase separation is the most likely mechanism for causing the large variations in chlorinity observed in hydrothermal fluids, and is therefore the cause of much of the global variability in composition. It is clear, of course, that there are still important differences in composition which cannot be attributed to phase separation, and these must be due to inter-field differences in age, pressure, temperature, mineralogy, fluid flow regime, etc. Much work remains to be done in descibing and quantifying how these geological parameters influence hydrothermal fluid chemistry.

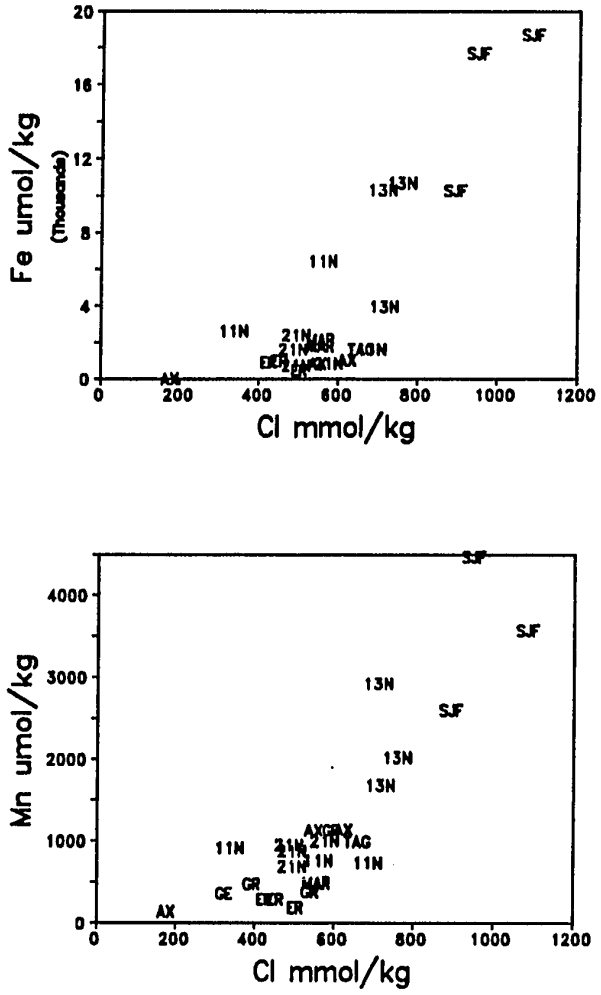

Figure 4.1. Global Variability in Hydrothermal Fluids. Endmember concentrations of nearly all major elements show strong correlation with chlorinity. The most likely mechanism for generating the chlorinity variations is phase separation. Data are from this study (Axial Seamount and Endeavour), and sources cited in Von Damm, 1990. a) Iron verus chloride. b) Manganese versus chloride.

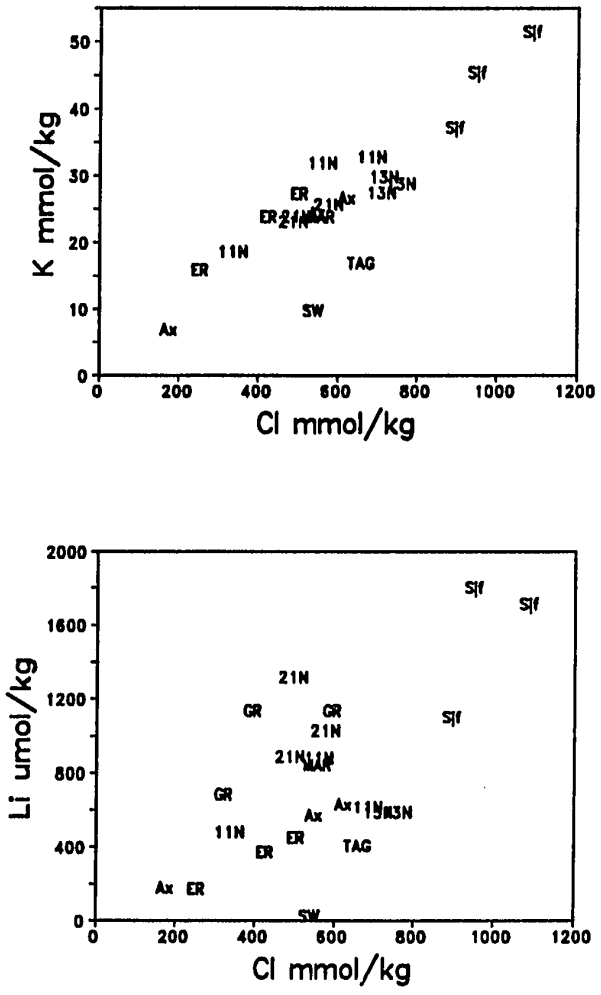

Figure 4.1. (continued) c) Potassium versus chloride. d) Lithium versus chloride.

Let us assume that all of the variation in chlorinity is caused by phase separation. How does this affect the hydrothermal flux of chloride and other elements to the oceans? Unless the pressure and temperature are such that halite solubility is exceeded, then phase separation is conservative with respect to chloride, i.e., each high-chlorinity fluid has a low chlorinity counterpart. Hydrothermal circulation will not be a source or sink for chloride unless there is a mechanism for trapping significant quantities of fluid in the crust. Since the low-chlorinity phase is much more buoyant, it is less likely to be trapped than the denser, metal-rich, high-chlorinity brines, so hydrothermal circulation is more likely to be a sink for chloride than a source. The common occurrence of high-salinity fluid inclusions (many with no co-existing vapor phase) in ophiolites [Vanko, 1986 and 1988] is evidence that brines remain in the ocean crust.

Until we can make a quantitative estimate of how much brine remains in the crust, the method of calculating fluxes by multiplying the average excess concentration of a particular element in hydrothermal fluid by the global mass flux of hydrothermal fluid should be modified to use chloride-normalized averages. This will at least remove any sampling bias toward high- or low-chlorinity fluids and considerably reduce the range of concentrations for most elements, although many other uncertainties [Von Damm, 1990] in hydrothermal flux calculations remain.

BIBLIOGRAPHY

Alt, J. C., C. Laverne, and K. Muehlenbachs, Alteration of the upper oceanic crust: mineralogy and processes in Deep Sea Drilling Project Hole 504B, Leg 83. In Initial Reports of the Deep Sea Drilling Project, 83, 217-247, Washington, D. C., U.S. Government Printing Office, 1984.

ASHES Expedition, Pisces submersible exploration of a high-temperature vent field in the caldera of Axial Volcano, Juan de Fuca Ridge (abstract), *Eos Trans. AGU 67*(44), 1027, 1986.

Baker, E. T., R. E. McDuff, and G. J. Massoth, Hydrothermal venting from the summit of a ridge axis seamount: Axial Volcano, Juan de Fuca Ridge, *J. Geophys. Res., 95,* 12843-12854, 1990.

Bischoff, J. L., and F. W. Dickson, Seawater-basalt interaction at 200°C and 500 bars: Implications for origin of seafloor heavy-metal deposits and regulation of seawater chemistry, *Earth Planet. Sci. Lett., 25,* 385-397, 1975.

Bischoff, J. L, and K. S. Pitzer, Phase relations and adiabats in boiling seafloor geothermal systems, *Earth Planet. Sci. Lett., 75,* 327-338, 1985.

Bischoff, J. L., and R. J. Rosenbauer, The critical point and two-phase boundary of seawater, 200-500°C, *Earth Planet. Sci. Lett., 68,* 172-180, 1984.

Bischoff, J. L., and R. J. Rosenbauer, An empirical equation of state for hydrothermal seawater (3.2 percent NaCl), *Am. J. Sci., 285,* 725-765, 1985.

Bischoff, J. L., and R. J. Rosenbauer, Phase separation in seafloor geothermal systems: An experimental study of the effects on metal transport, *Am. J. Sci., 287,* 953-978, 1987.

Bischoff, J. L., and R. J. Rosenbauer, Liquid-vapor relations in the critical region of the system NaCl-H_2O from 380 to 415°C: A refined determination of the critical point and two-phase boundary of seawater, *Geochim. Cosmochim. Acta, 52,* 2121-2126, 1988.

Bowers, T. S., A. C. Campbell, C. I. Measures, A. J. Spivack, M. Khadem and J. Edmond, Chemical controls on the composition of vent fluids at 13°-11°N and 21°N, East Pacific Rise, *J. Geophys. Res., 93,* 4522-4536, 1988.

Burnham, C. W., The importance of volatile constituents, in *The Evolution of the Igneous Rocks: Fiftieth Anniversary Perspectives*, edited by H. S. Yoder, Jr., pp. 439-482, Princeton University Press, Princeton, N. J., 1979.

Butterfield, D. A., G. J. Massoth, R. E. McDuff, J. E. Lupton and M. D. Lilley, Geochemistry of hydrothermal fluids from Axial Seamount Hydrothermal Emissions Study vent field, Juan de Fuca Ridge: subseafloor boiling and subsequent fluid-rock interaction, *J. Geophys. Res., 95*, 12895-12921, 1990.

Campbell, A. C., T. S. Bowers, C. I. Measures, K. Kennison Falkner, M. Khadem, and J. M. Edmond, A time series of vent fluid compositions from 21°N, East Pacific Rise, and the Guaymas Basin, Gulf of California, *J. Geophys. Res., 93*, 4537-4549, 1988.

Campbell, A. C., M. R. Palmer, G. P. Klinkhammer, T. S. Bowers, J. M. Edmond, J. R. Lawrence, J. F. Casey, G. Thompson, S. Humphris, P. Rona, and J. A. Karson, Chemistry of hot springs on the Mid-Atlantic Ridge, *Nature, 335*, 514-519, 1988.

Carslaw, H. S. and J. C. Jaeger, *Conduction of Heat in Solids, 2nd edition*, 510 pp, Oxford Science Publications, Oxford, 1959.

Cline, J. D., Spectrophotometric determination of hydrogen sulfide in natural waters, *Limnol. Oceanogr., 14*, 454-458, 1969.

Cowan, J., and J. Cann, Supercritical two-phase separation of hydrothermal fluids in the Troodos ophiolite, *Nature, 333*, 259-261, 1988.

Delaney, J. R., and B. A. Cosens, Boiling and metal deposition in submarine hydrothermal systems, *Mar. Technol. Soc. J., 16*, 62-66, 1982.

Delaney, J. R., R. E. McDuff, and J. E. Lupton, Hydrothermal fluid temperatures of 400°C on the Endeavour segment, northern Juan de Fuca (abstract), *Eos Trans. AGU, 61*, 992, 1984.

Delaney, J. R., D. W Mogk and M. J. Mottl, Quartz cemented breccias from the Mid-Atlantic Ridge: Samples of a high-salinity hydrothermal upflow zone, *J. Geophys. Res, 92*, 9175-9192, 1987.

Dixon, J. E., E. Stolper and J. R. Delaney, Infrared spectroscopic measurements of CO_2 and H_2O in Juan de Fuca Ridge basaltic glasses, *Earth Planet. Sci. Lett., 90,* 87-104, 1988.

Drummond, S.E., Jr., Boiling and mixing of hydrothermal fluids: Chemical effects on mineral precipitation, Ph.D. dissertation, 380 pp., Penn State Univ., University Park, 1981.

Drummond, S. E., and H. Ohmoto, Chemical evolution and mineral deposition in boiling hydrothermal systems, *Econ. Geol., 80,* 126-147, 1985.

Dyrssen, D., A Gran titration of seawater on board *Sagitta, Acta Chem. Scand., 19,* 1265, 1965.

Edmond, J. M., C. I. Measures, R. E. McDuff, L. H. Chan, R. Collier, B. Grant, L. I. Gordon, and J. B. Corliss, Ridge crest hydrothermal activity and the balance of the major and minor elements in the ocean: The Galapagos data, *Earth Planet. Sci. Lett., 46,* 1-18, 1979.

Edmond, J. M., K. L. Von Damm, R. E. McDuff and C. I. Measures, Chemistry of hot springs on the East Pacific Rise and their effluent dispersal, *Nature, 297,* 187-191, 1982.

Ellis, A. J., and R. M. Golding, The solubility of carbon dioxide above 100°C in water and in sodium chloride solutions, *Am. J. Sci., 261,* 47-60, 1963.

Embley, R. W., K. M. Murphy, and C. G. Fox, High resolution mapping of the summit of Axial Volcano: Volcanological and tectonic implications, *Eos Trans. AGU, 69,* 1467, 1988.

Evans, W. C., L. D. White, and J. B. Rapp, Geochemistry of some gases in hydrothermal fluids from the Southern Juan de Fuca Ridge, *J. Geophys. Res., 93,* 15,305-15,313, 1988.

Fox, C. G., The consequences of phase separation on the distribution of hydrothermal fluids at ASHES vent field, Axial Volcano, Juan de Fuca Ridge, *J. Geophys. Res.*, this issue.

Fournier, R. O., A method of calculating quartz solubilities in aqueous sodium chloride solutions, *Geochim. Cosmochim. Acta, 47,* 579-586, 1983.

Fournier, R. O., Conceptual models of brine evolution in magmatic-hydrothermal systems, *U.S. Geol. Surv. Prof. Pap. 1350*, 487-506, 1987.

Gehrig, M., H. Lentz and E. U. Franck, Thermodynamic properties of water-carbon dioxide-sodium chloride mixtures at high temperatures and pressures, in *High-Pressure Science and Technology, Vol. 1, Physical Properties and Material Synthesis*, edited by K. D. Timmerhaus and M. S. Barber, pp 539-542, Plenum, New York, 1979.

Gieskes, J. M., Interstitial water studies, Leg 15. Alkalinity, pH, Mg, Ca, Si, PO4, and NH4, in Heezen, B. C., *et al.*, Initial Reports of the Deep Sea Drilling Project, Vol. XX: Washington, D. C., U.S. Government Printing Office, pp. 813-829, 1973.

Giggenbach, W.F., Geothermal solute equilibria. Derivation of Na-K-Mg-Ca geoindicators, *Geochim. Cosmochim. Acta, 52*, 2749-2765, 1988.

Glover. R. B., Boron distribution between liquid and vapour in geothermal fluids, in *Proceedings of the 10th New Zealand Geothermal Workshop 1988*, pp. 223-227, University of Auckland Press, Auckland, New Zealand, 1988.

Goldfarb, M. S., and J. R. Delaney, Response of two-phase fluids to fracture configurations within submarine hydrothermal systems, *J. Geophys. Res., 93*, 4585-4594, 1988.

Grant, M. A., I. G. Donaldson and P. F. Bixley, *Geothermal Reservoir Engineering*, 369 pp., Academic, San Diego, Calif., 1982.

Grasty, R. L., C. W. Smith, J. M. Franklin and I. R. Jonasson, Radioactive orphans in barite-rich chimneys, Axial Caldera, Juan de Fuca Ridge, *Can. Mineral., 26*, 627-636, 1988.

Harvey-Kelly, F. E. L., I. R. Jonasson, J. M. Franklin and R. W. Embley, Sulfide deposits on Axial Seamount: Mineralogy and chemistry, *Eos Trans. AGU, 69*, 1499, 1988.

Henley, R. W., A. H. Truesdell, P. B. Barton, Jr., and J. A. Whitney, Fluid-Mineral Equilibria in Hydrothermal Systems, Reviews in Economic Geology, Vol. 1, 1984.

Himmelblau, D. M., Solubilities of inert gases in water: 0°C to near the critical point of water, *J. Chem. Eng. Data, 5,* 10-15, 1960.

Janecky, D. R., and W. E. Seyfried, Jr., Formation of massive sulfide deposits on oceanic ridge crests: Incremental reaction models for mixing between hydrothermal solutions and seawater, *Geochim. Cosmochim. Acta, 48,* 2723-2738, 1984.

Kadko, D., and W. Moore, Radiochemical constraints on the crustal residence time of submarine hydrothermal fluids: Endeavour Ridge, *Geochim. Cosmochim. Acta, 52,* 650-668, 1988.

Karl, D. M., G. M. McMurtry, A. Malahoff, and M. O. Garcia, Loihi Seamount, Hawaii: A mid-plate volcano with a distinctive hydrothermal system, *Nature, 335,* 532-535, 1988.

Kelley, D. S., and J. R. Delaney, Two-phase separation and fracturing in mid-ocean ridge gabbros at temperatures greater than 700°C, *Earth Planet. Sci. Lett., 83,* 53-66, 1987.

Kennedy, B. M., Noble gases in vent water from the Juan de Fuca Ridge, *Geochim. Cosmochim. Acta, 52,* 1929-35, 1988.

Khaibullin, I. Kh., and N. M. Borisov, Experimental investigation of the thermal properties of aqueous and vapor solutions of sodium and potassium chlorides at phase equilibrium, *Teplofiz. Vys. Temp., 4,* 518-523, 1966.

Kim, K. -R., J. A. Welhan, and H. Craig, The hydrothermal vent fields at 13°N and 11°N on the East Pacific Rise: *Alvin* 1984 results (abstract), *Eos Trans. AGU, 65,* 973, 1984.

Lupton, J. E., Water column hydrothermal plumes on the Juan de Fuca Ridge, *J. Geophys. Res., 95,* 12829-12842, 1990.

Lupton, J. E., G. P. Klinkhammer, W. R. Normark, R. Haymon, K. C. McDonald, R. F. Weiss, and H. Craig, Helium-3 and manganese at the 21°N East Pacific Rise hydrothermal site, *Earth Planet. Sci. Lett., 50,* 115-124, 1980.

Malahoff, A., G. McMurtry, S. Hammond, and R. Embley, High-temperature hydrothermal fields - Juan de Fuca Ridge, Axial Volcano (abstract), *Eos Trans. AGU, 65,* 1112, 1984.

Massoth, G. J., H. B. Milburn, S. R. Hammond, D. A. Butterfield, R. E. McDuff, and J. E. Lupton, The geochemistry of submarine venting fluids at Axial Volcano, Juan de Fuca Ridge: New sampling methods and a VENTS program rationale, in *National Undersea Research Program Res. Rep. 88-4*, pp. 29-59, National Oceanic and Atmospheric Administration, Washington, D.C., 1989*a*.

Massoth, G. J., D. A. Butterfield, J. E. Lupton, R. E. McDuff, M. D. Lilley, and I. R. Jonasson, Submarine venting of phase-separated hydrothermal fluids at Axial Volcano, Juan de Fuca Ridge, *Nature, 340*, 702-705, 1989b.

Michard, G., F. Albarede, A. Michard, J.-F. Minster, J.-L. Charlou, and N. Tan, Chemistry of solutions from the 13°N East Pacific Rise hydrothermal site, *Earth Planet. Sci. Lett., 67,* 297-307, 1984.

Mottl, M. J. and W. E. Seyfried, Sub-seafloor hydrothermal systems - rock- vs. seawater-dominated, in *Seafloor Spreading Centers: Hydrothermal Systems,* edited by P. A. Rona and R. P. Lowell, Dowden, Hutchinson and Ross, Stroudsberg, Pa., 1980.

Potter, R. W., II, and D. L. Brown, The volumetric properties of aqueous sodium chloride solutions from 0°C to 500°C at pressures up to 2000 bars based on a regression of the available data in the literature, *Geol. Surv. Bull., 1421-C*, pp. 1-36, 1977.

Potter, R. W., II, and M. A. Clynne, The solubility of the noble gases He, Ne, Ar, Kr, and Xe in water up to the critical point, *J. Solution Chem., 7*(11), 837-844, 1978.

Presley, B. J., J. Culp, C. Petrowski, and I. R. Kaplan, Interstitial water studies, Leg 15. Major ions, Br, Mn, NH_3, Li, B, Si, and $\delta^{13}C$. In Heezen, B. C., I. G. MacGregor, et al., Initial Reports of the Deep Sea Drilling Project, *20,* 805-809, Washington, D. C., U.S. Government Printing Office, 1973.

Pruess, K., SHAFT, MULKOM, TOUGH: A set of numerical simulators for multiphase fluid and heat flow, *Rep. LBL-24430*, 25 pp., Lawrence Berkeley Lab., Univ. of Calif., Berkeley, 1988.

Ramboz, C., E. Oudin, and Y. Thisse, Geyser-type discharge in Atlantis II Deep, Red Sea: Evidence of boiling from fluid inclusions in epigenetic anhydrite, *Can. Mineral., 26,* 765-786, 1988.

Rosenbauer, R. J., and J. L. Bischoff, Uptake and transport of heavy metals by heated seawater: A summary of the experimental results, in *Hydrothermal Processes at Seafloor Spreading Centers*, edited by P. A. Rona et al., pp. 177-197, Plenum, New York, 1983.

Seyfried, W. E., Jr., Experimental and theoretical constraints on hydrothermal alteration processes at mid-ocean ridges, *Annu. Rev. Earth Planet. Sci., 15,* 317-335, 1987.

Seyfried, W. E., Jr., D. R. Janecky, and M. J. Mottl, Alteration of the oceanic crust: Implications for geochemical cycles of lithium and boron, *Geochim. Cosmochim. Acta, 48,* 557-569, 1984.

Seyfried, W. E., Jr., M. E. Berndt, and D. R. Janecky, Chloride depletions and enrichments in seafloor hydrothermal fluids: Constraints from experimental basalt alteration studies, *Geochim. Cosmochim. Acta, 50,* 469-475, 1986.

Sourirajan, S., and G. C. Kennedy, The system H_2S-NaCl at elevated temperatures and pressures, *Am. J. Sci., 260,* 115-141, 1962.

Spindel, R. C., L. O. Olson, V.W. Miller, M. K. Tivey, and R. K. Light, Hydrothermal vent experiment on the Juan de Fuca Ridge, Summer 1988: Final report, *Tech. Rep. APL-UW TR 8824,* Appl. Phys. Lab., Univ. of Wash., Seattle, 1988.

Spivack, A. J., and J. M. Edmond, Boron isotope exchange between seawater and the oceanic crust, *Geochim. Cosmochim. Acta, 51,* 1033-1043, 1987.

Strens, M.R. and J. R. Cann, A model of hydrothermal circulation in fault zones at mid-ocean ridge crests, *Geophys. J. R. astr. Soc., 71,* 225-240, 1982.

Stumm, W., and J.J. Morgan, *Aquatic Chemistry*, 2nd ed., 780 pp., John Wiley, New York, 1981.

Takenouchi, S., and G. C. Kennedy, The binary system H_2O-CO_2 at high temperatures and pressures, *Am. J. Sci., 262,* 1055-1074, 1964.

Takenouchi, S., and G. C. Kennedy, The solubility of carbon dioxide in NaCl solutions at high temperatures and pressures, *Am. J. Sci., 263,* 445-454, 1965.

Tanger, J. C., IV, and K. S. Pitzer, Thermodynamics of NaCl-H_2O: A new equation of state for the near-critical region and comparisons with other equations for adjoining regions, *Geochim. Cosmochim. Acta, 53,* 973-987, 1989.

Tivey, M. K., Physical and chemical controls on the growth of hydrothermal vent structures: A model of transport and chemical reaction, Ph.D. dissertation, 169 pp., Univ. of Wash., Seattle, 1988.

Turekian, K. K., and J. K. Cochran, Flow rates and reaction rates in the Galapagos Rise spreading center hydrothermal system as inferred from $^{228}Ra/^{226}Ra$ in vesicomyid clam shells, *Proc. Nat. Acad. Sci. U. S. A., 83,* 6241-6244, 1986.

Von Damm, K.L., Chemistry of submarine hydrothermal solutions at 21°N, East Pacific Rise and Guaymas basin, Gulf of California, Ph.D. thesis, 240 pp., Mass. Inst. of Technol.-Woods Hole Oceanogr. Inst. Joint Program in Oceanogr., Cambridge, 1983.

Von Damm, K.L., Systematics of and postulated controls on submarine hydrothermal solution chemistry, *J. Geophys. Res., 93,* 4551-4561, 1988.

Von Damm, K. L., Seafloor hydrothermal activity: black smoker chemistry and chimneys, *Annu. Rev. Earth Planet. Sci., 18,* 173-204, 1990.

Von Damm, K. L., B. Grant, and J. M. Edmond, Preliminary report on the chemistry of hydrothermal solutions at 21°N, East Pacific Rise, in *Hydrothermal Processes at Seafloor Spreading Centers*, edited by P. A. Rona et al., pp. 369-390, Plenum, New York, 1983.

Von Damm, K. L., J. M. Edmond, B. Grant, C. I. Measures, B. Walden, and R. F. Weiss, Chemistry of submarine hydrothermal solutions at 21°N, East Pacific Rise, *Geochim. Cosmochim. Acta, 49,* 2197-2220, 1985.

Von Damm, K. L., and J. L. Bischoff, Chemistry of hydrothermal solutions from the Southern Juan de Fuca Ridge, *J. Geophys. Res., 92,* 11,334-11,346 , 1987.

Walker, G. P. L., Three Hawaiian calderas: An origin through loading by shallow intrusions?, *J. Geophys. Res., 93,* 14,773-14,784, 1988.

Welhan, J. A., and H. Craig, Methane and hydrogen in East Pacific Rise hydrothermal fluids, *Geophys. Res. Lett., 6,* 829-831, 1979.

Welhan, J. A., and H. Craig, Methane, hydrogen and helium in hydrothermal fluids at 21°N on the East Pacific Rise, in *Hydrothermal Processes at Seafloor Spreading Centers,* edited by P. A. Rona et al., pp. 391-409, Plenum, New York, 1983.

Wells, J. T., and M. S. Ghiorso, The influence of reaction kinetics and fluid flow on the concentration of silica in hydrothermal fluids, *Geol. Soc. Am. Abstr. Programs, 20,* A96, 1988.

Westall, J. C., J. L. Zachary, and F. M. Morel, MINEQL, a computer program for the calculation of chemical equilibrium composition of aqueous systems, *Tech. Note 18,* 91 pp., Dep. Civ. Eng., Mass. Inst. of Technol., Cambridge, 1976.

Wolery, T. J., Calculation of chemical equilibrium between aqueous solution and minerals: The EQ3/6 software package, *Rep. UCRL-52658,* Lawrence Livermore Nat. Lab., Livermore, Calif., 1979.

Wuensch, B. J., Sulfide crystal chemistry, in *Mineralogical Society of America Short Course Notes, Sulfide Mineralogy,* edited by P. H. Ribbe, Southern Printing Co., Blacksburg, Virginia, 1974.

Appendix A

SAMPLING AND ANALYTICAL METHODS

Sampling and sample storage.

Samples analyzed in this study were collected by submersible on several cruises to the Juan de Fuca Ridge between 1984 and 1988 (Table A-1)

Samples were collected in several different sampling devices. Most of the samples were collected in 755-mL titanium syringes (major samplers) [Von Damm *et al.*, 1985] which were deployed either as single bottles or in pairs. In 1984 and 1986 all major samplers were actuated by the mechanical submersible arm after positioning the snorkel tip in the fluid to be sampled. In 1987 and 1988, major samplers were also deployed as part of the submersible-coupled in situ sensing and sampling system (SIS^3) [Massoth *et al.*, 1989], a flow-through manifold sampling device with in-line temperature probes at the sample inlet tip and at the entrance to the manifold chamber. The chamber had 5 sample ports which connected to 3 major samplers and 2 150-mL titanium gas-tight bottles (all metal, vacuum-tight to 350 bars). Each gas-tight bottle was hydraulically actuated simultaneously with a major-sampler. Use of the SIS^3 allowed us to monitor the sample temperature during sampling to insure that entrainment of ambient seawater was minimized. Some major samplers and gas-tight samplers were also deployed in the discrete mode by the submersible arm during the time that the SIS^3 was installed.

Analytical methods.

Samples were processed as quickly as possible after submersible recovery. A clean piece of Tygon tubing, fitted with a three-way Teflon valve, was slipped over the outlet to the major samplers and rinsed with approximately 20-30 mL of the sample. Aliquots for shipboard gas analysis were drawn into a gas-tight syringe

Table A-1 Sample Collection Information

Dates	Location	Vessel
Aug/Sept 1984	Endeavour Segment	Atlantis II/Alvin
Aug/Sept 1986	Axial Seamount	Pandora II/Pisces
Sept/Oct 1987	Axial Seamount	Atlantis II/Alvin
Oct 1987	Endeavour Segment	Atlantis II/Alvin
Aug 1988	Axial Seamount	Atlantis II/Alvin
Aug/Sept 1988	Endeavour Segment	Atlantis II/Alvin

through a piece of surgical tubing attached to the three-way valve and clamped at one end. Aliquots for alkalinity, *p*H, and total sulfide were drawn in the same manner and measured within 8 hours of arrival at the surface, except in 1986, when aliquots for sulfide were sealed in glass with zinc acetate and analyzed colorimetrically on shore. Samples for trace metals and major ions were expressed directly into acid-cleaned polyethylene bottles. Trace metal samples were acidified to *p*H <1.8 with ultrapure HCl. In 1988, aliquots for silica determination were immediately diluted 100- to 200-fold and analyzed shipboard by flow injection analysis (FIA) colorimetry. Some subsamples were filtered, while others were purged with nitrogen to remove H_2S. Gas-tight samples were transferred shipboard to evacuated glass flasks containing solid mercuric chloride to stop bacterial action.

Shore-based determinations of the major ions were carried out at the University of Washington, with the exception of iron and manganese, which were determined at NOAA/PMEL. Shore-based gas analysis was carried out at UCSB. ICP analysis was done in the laboratory of A. Irving, Department of Geology, University of Washington.

Anions

Chloride. Chloride was measured by an automated potentiometric titration with silver nitrate, using silver wire electrodes inserted into the silver nitrate titrant reservoir and into the sample beaker. Approximately 0.5 mL of sample was weighed on an analytical balance, diluted with a few mL of distilled deionized water (DDW) and placed on a magnetic stirrer. The silver wire electrode was placed in the beaker and the titration was started. Titrant was delivered from a Gilmont micrometer buret driven by a stepper motor and controlled by an HP85 computer. The potential difference between the two silver electrodes depends on the difference in silver ion concentration in the beaker and the titrant reservoir. The potential was measured

with a Keithley 614 electrometer fed into an HP data logger. Titrant was delivered increasingly slowly as the rate of change of potential increased and the endpoint was defined as the volume where the maximum rate of change was reached (the inflection point in a plot of potential against volume of titrant added). IAPSO standard seawater was used to standardize the silver nitrate. Precision of the method, as determined by replicate analyses, is ±0.5 mmol/kg or approximately 0.1% (1σ) for a sample of seawater chlorinity.

Some samples were titrated manually with silver nitrate using a potassium chromate/potassium dichromate indicator (Mohr titration). Precision of this method is ± 2 mmol/kg or approximately 0.5%.

Bromide. Bromide was determined colorimetrically by the method of Presley [1971]. Standards were prepared by dissolving dry potassium bromide in artificial seawater (sodium chloride, magnesium sulfate, and sodium bicarbonate). Precision of the method based on replicate analyses of standard seawater is 3%. This method worked satisfactorily for the Axial Seamount samples, but results for the Endeavour samples were variable and difficult to reproduce. A subset of samples was sent to J. Gieskes at SIO for analysis by a titration method under development in his laboratory. It was found that the colorimetric method gave systematically low results, probably due to interference by dissolved organic carbon some other component of the samples. Unfortunately, the ASHES colorimetric bromide results were already published when this systematic error was discovered. None of the conclusions are altered significantly by the slight change in bromide endmembers.

Sulfate. Two methods were used to analyze sulfate. For the ASHES samples, sulfate was measured by polarographic measurement of excess lead on a PAR/EGG Model 174A Polarographic Analyzer and a Model 303 static mercury drop electrode in the sampled DC mode. Samples were measured in glass sample cups which were

cleaned first in detergent, then soaked in 10% HCl and rinsed in DDW. Procedure is to pipet 0.800 mL of 10.00 mM $PbNO_3$ into the sample cup, followed by 0.500 mL of sample or standard, 2.0 mL of 95% ethanol, 100 µL of Triton-X 100, and 7.0 mL of 0.100 M KCl. Samples were purged for 2 minutes with purified nitrogen and scanned at 10 mV/sec from 0 to -0.75 V vs. a Ag/AgCl reference electrode. Standards were prepared by mixing varying proportions of surface seawater collected from the NE Pacific and sulfate-free artificial seawater (29.22 g NaCl and 10.169 g $MgCl_2 \cdot 6H_2O$ in 1 liter DDW). IAPSO standard seawater was used to check the accuracy of the method. Precision of this method is 4% based on replicate analyses of standard seawater.

Endeavour Ridge samples were analyzed for sulfate approximately two years after the time of sample collection by ion chromatography in the laboratory of Dr. T. Bates, NOAA/PMEL. This method is much simpler and faster than the polarographic method. Samples are simply diluted 1:1000 with DDW and injected into the ion chromatograph, which utilized Dionex strong anion column, guard column and suppressor coupled with a Shimadzu conductivity detector. IAPSO standard seawater and a potassium bromide solution were used as standards. Precision of the analysis is 3% based on replicate analysis of samples and standards.

Cations

Magnesium and calcium. Magnesium and calcium were determined by EDTA/EGTA titration with colorimetric (visual) endpoint [Gieskes, 1973]. IAPSO standard seawater was used to standardize the titrants. Precision of this method is 0.5%.

Potassium. Potassium was determined by Flame Atomic Emission analysis. Samples were diluted ~800-fold in 0.1% La/0.1% Na solution. Standards were

prepared by dissolving KCl in DDW. NaCl solution was added to standard dilutions to match the ionic strength of the samples. IAPSO standard seawater was used as an additional standard. Precision of the method is 2%.

Lithium and Strontium. Li and Sr were determined by flame atomic absorption. Samples were diluted 1:3 in 0.1% Lanthanum. Standards were prepared by dissolving LiCl or $Sr(NO_3)_2$ in DDW. NaCl was added to standard dilutions to match ionic strength. IAPSO standard seawater and an artificial hydrothermal vent fluid were used to check the accuracy of the method. Precisions are 1% for Li and 3% for Sr.

Iron and Manganese. Fe was measured shipboard by Flow Injection Analysis using the ferrozine method. Shore-based Flame or Graphite Furnace (for low concentrations) Atomic Absorption analysis for Fe and Mn was performed in the laboratory of G. J. Massoth at NOAA/PMEL using standard techniques.

Trace metals. Cu, Zn and Pb were measured by Graphite Furnace Atomic Absorption at PMEL. Precisions are 2%, 5%, and 5%, respectively.

Barium. Barium was measured on a subset of 9 samples from ASHES by Inductively Coupled Plasma Atomic Emission Analysis in the laboratory of Tony Irving in the Department of Geological Sciences at UW. Precision of the method is 8%.

Gases

Carbon dioxide. In 1987 CO_2 in the 755-mL major samples was measured shipboard by M. D. Lilley using gas chromatography. Precision of the method is 5%. Shore-based manometric measurement of total condensible gases (equivalent to CO_2 after quantitative precipitation of hydrogen sulfide) from gas-tight samples was

performed at UCSB by J. E. Lupton. Precision of the manometric method is 3%. In addition, CO_2 was calculated from the pH and alkalinity data for some samples (see below).

Hydrogen sulfide. Prior to the 1987 field season, H_2S was measured by the molybdenum blue method [Cline, 1969] on subsamples preserved in sealed glass vials with zinc acetate added to precipitate and stabilize the sulfide. The acidic reagent was added directly to the vials to dissolve the precipitated sulfide, then quantitatively transferred to volumetric flasks for dilution and spectrophotometric measurement. The precision of the Cline method is 5%. In 1987 and 1988 H_2S was measured shipboard using a Flow Injection Analysis adaptation of the molybdenum blue method. Samples were taken from the major samplers in gas-tight syringes and immediately diluted up to 250-fold in DDW, then injected into the FIA system. Sulfide standards were made by dissolving reagent grade sodium sulfide in deoxygenated DDW and stored in glass bottles fitted with a septum for removing aliquots by syringe. The bottles were back-filled with prepurified nitrogen to maintain pressure inside the bottle and covered with black tape to protect from light. Sulfide standards were periodically standardized by iodometric titration against a primary iodate solution. These standards were stable for months if kept in the dark.

Helium. Total helium and ^3He were measured at UCSB as described by Lupton *et al.* [1980]. Precision of the total helium measurement is 3%.

Other constituents

pH pH was measured shipboard in a constant temperature, closed atmosphere glass bulb fitted with a Corning semi-micro combination electrode. The pH vessel was first rinsed with about 15 mL of sample, then filled. The precision of the pH measurement is $\pm$ 0.005 pH units.

Alkalinity. Alkalinity was measured by titrating a precise volume of the sample with a standardized HCl solution [Dyrssen, 1965].

Boron. Boron was also measured by ICPAES at a precision of 8%.

Calculation of CO_2 from measured pH and alkalinity.

It is possible to estimate the CO_2 content in vent fluids taken in the major samplers using the pH and alkalinity data, when both were measured. We start with the definition of carbonate alkalinity [Stumm and Morgan, 1981]:

$$C_T = \frac{(Alk - OH^- + H^+)}{(\alpha_1 + 2\alpha_2)} \tag{4.1}$$

For pH values less than 6, α_2 is negligible and $OH^- << H^+$, so α_2 and OH^- drop out of equation 4.1, as does the last term inside the brackets involving K_2 in the following expression for α_1:

$$\alpha_1 = 1 + \left(\frac{H^+}{K_1}\right) + \left(\frac{K_2}{H^+}\right)^{(-1)} \tag{4.2}$$

One can solve for C_T by taking the measured pH and alkalinity and iterating until

$$1 + \frac{H^+}{K_1} = \frac{C_T}{(Alk + H^+)} \tag{4.3}$$

The value used for pK_1 is 6.13 [Stumm and Morgan, 1981]. To account for the contribution of H_2S to the titration alkalinity, I subtracted $\alpha_1 H_2S$ prior to solving for C_T, using 7 and 13.9 for pK_1 and pK_2 of H_2S. The H_2S correction generally lowers the estimated total CO_2 by 1-5%. The calculation works best for samples which contain ~25% or more entrained seawater. Errors become very large when pH < 5, and the calculation does not work for negative alkalinities.

Analysis of major ions in gas-tight samples.

After the gases had been stripped from the gas-tight samples at UCSB, the remaining water was sent to U.W. for analysis of the Mg content, needed to calculate endmember gas concentrations. The samples had all been treated with ~3 ml of saturated $HgCl_2$ in order to stop bacterial action and precipitate sulfide prior to gas extraction. Hg interferes with the Mg and Ca titration method, masking the color change of the endpoint, so these samples were analyzed by flame atomic absorption. In addition to magnesium, I measured Ca, Sr, Li, and K by AA following methods outlined in the Perkin Elmer 5000 Operations Manual. I conducted a comparison of standards prepared with and without mercuric chloride added and found no detectable difference, so that interference by mercury is not a problem in these analyses.

In addition to the cations, I measured chloride by manual titration of 0.25 g of sample with $AgNO_3$ using a chromate/dicrhomate indicator. Results of this analysis had to be corrected for the chloride introduced into solution by the $HgCl_2$. This was done by assuming that exactly 3 ml of saturated $HgCl_2$ containing 6g/100ml (CRC Handbook of Chemistry and Physics) was added to each flask (the quantities were not precisely measured since it was not foreseen that the samples would be analyzed for their chloride content) and then evaporated. The magnitude of this correction depends on the mass of sample in the glass flask, but for most samples amounts to about 3% of the actual concentration.

The addition of $HgCl_2$ to the samples made it possible to estimate the H_2S content. I assumed that all H_2S was precipitated as HgS, which is extremely insoluble, and weighed the precipitate obtained from each flask by filtration. The filtered precipitate was washed with DDW to remove soluble salts and dried before weighing. In all cases, the amount of Hg in the flask was sufficient to precipitate all

of the sulfide. (The precipitation of H_2S releases protons into solution and lowers the pH of the samples. The pH of most of the samples, as measured after gas extraction, was close to 2.0 and is not representative of the pH at the time of sample collection.)

An additional correction was needed to account for the mass of water distilled off of the sample into the gas extraction lines. The samples were accurately weighed before and after gas extraction, so this is a simple correction to make.

Appendix B

VENT FLUID CHEMICAL DATA

This appendix presents all of the vent fluid data used to determine endmembers reported in this study. Sample numbers consist of the Alvin dive number and the titanium sampler number as a suffix. A superscript i on the sample number refers to data from ICP analysis. At Endeavour, the area denotes the sulfide structure from which the samples were taken, and the vent refers to the nearest marker, when there is one. Flange fluids are denoted by FL in the vent column, and if the flange was near a marker, the marker is included. In the ASHES vent field, vent refers to the structure from which the sample was taken. Suffixes -t, -b, and -s on a vent name refer to samples taken from the top, base, or side of the sulfide structure, respectively.

The reported temperatures are the maximum temperatures measured during or prior to sampling for each vent.

Concentrations are reported in mmol per kg of fluid (m) or μmol per kg of fluid (μ). Titration alkalinity is reported in milequivalents per liter.

Table B-1 1988 Endeavour Anions, Gases, and Silica

SAMPLE #	AREA	VENT	TEMP	Mg	Cl	SO_4	SO_4 purged	Br	ALK	pH	CO_2	H_2S	SiO_2
				m	m	m	m	µ	meq/l		m	m	m
1988	seawater			53.20	547	28.2	28.2	849	2.45	7.60	2.5	0	.178
2095-10	C	8A	346	20.78	473	11.9				4.78		2.86	9.58
2096-10	D	16		3.13	424	4.9		sio 740				5.31	13.7
2096-11	E	8E		45.12	505	26.5		sio 796				0.96	0.86
2096-13	D	16		5.54	441	3.7				4.07		4.96	13.3
2096-16	D	16		1.63	421	3.8	1.0	sio 750	0.13	4.35	10.1	3.87	14.0
2096-9	D	16		7.84	446	5.4			-0.12	3.92		4.35	13.5
2097-12	D			51.84	546								
2098-12	C	12	330	18.55	465	8.9	8.7		0.20	4.50	9.4	3.30	
2098-13	C	12	330	13.79	462	8.0	7.7					3.66	
2098-9	C	14		8.52	450	5.8						4.60	
2099-10	D	9		1.16	428	2.3				4.29		4.21	16.8
2099-12	D	FL,9		21.28	463	11.0			0.24	4.75	9.1	3.01	9.44
2099-13	D	FL		41.58	523	23.1				5.60		0.76	3.57
2099-16	D	9		1.70	432								7.47
2099-9	D	9		7.02	445	3.4			0.14	4.16	18.7	4.88	1.43
2100-10	D	FL	345	2.51	431	4.6	0.5		0.11	4.17	15.1	5.98	15.9
2100-12	D	FL,9	345	11.70	431	7.9			0.13	4.32	10.8	4.33	13.1
2100-13	D	FL	345	38.17	513								
2100-16	D	FL	345	1.50	427	5.0	0.7			4.24		6.13	16.0
2101-12	D	FL		51.93	546			816		7.50			
2101-13	D	FL		45.29	530				2.00	6.14	3.7		
2102-10			280	30.96									
2102-13	A	8F	322	2.27	507		0.9	sio 874				2.90	
2102-16	A	near 8F	290	23.09	524		16.6	sio 835		5.53		1.20	
2102-9	A	8F	319	0.81	507	1.6		sio 869		4.25		3.25	
2103-11	D	16		52.54	550	28.3		837		7.52			0.16
2103-13	D	98	221	30.22		16.7							7.30
2103-15	D	16		52.00	550	29.2				7.31			0.30
2103-16	B	APL1	341	2.79	460	4.6		sio 764		4.36		4.89	15.7
2103-9	D	98	221	27.21	492	16.3			1.39	5.47	7.4	1.61	7.87
2104-11	D	98	174	41.45	519	22.1	24.3		2.15	5.97	5.2	0.49	2.63
2104-16	D	98	174	48.17					2.37	6.43	3.5		3.10
2104-9	?	#86	175	46.23	532				2.21	6.26	3.8	0.27	2.01
2105-10	A	disc 36	281	40.67		22.5							3.87
2105-15		FL	330	13.23	428	7.5	5.7		0.34	4.67	10.1	4.33	13.0
2105-16	A	disc 36	281	40.72	534	23.1			1.87	5.97	4.4	0.67	3.45
2105-9	A	near 8F	293	13.74	516	8.4	7.2	777	0.28	4.70	8.0	2.05	13.0
2106-10	D	102		51.82	548					7.25			
2106-11	C	8A	330	51.20	543					6.74		0.068	
2106-12	D	102		32.03	506	17.1	16.4			5.28		1.73	6.49
2106-13	D	102		37.63	516	20.1	19.4		1.30	5.52	6.3	1.43	5.18
2106-15	C	8A		49.80		27.3							0.79
2106-9	D	102		43.86	527	23.1	22.9		1.82	5.91	4.7	0.64	2.99
2108-10	E	8E	27	49.18	527	26.9		774	2.41	6.51	3.4		
2108-12	D	FL,8L	210	32.88	500	16.2			1.20	5.41	7.2		
2108-13	D	FL,8L	210	27.48	501	15.8	13.8		0.87	5.19	8.2		
2108-16	E	8E	27	49.78	531	28.0				6.60			
2108-9	D	FL,8L	170	30.56	506	17.2	16.6		1.31	5.39	8.1		
2109-11	D	9		1.58	444	3.7	1.8		0.10	4.57	3.8	5.60	16.2
2109-12	?	FL	330	50.32	559					6.79			
2109-13	?	FL	330	50.74	557					6.68			
2109-15	D	9		1.20		3.8		sio 753					17.0
2109-9	?	FL	330	52.23	537					7.31			

Units are in mmol/kg (m) or µmol/kg (µ). Reported pH values are shipboard measurements at ~25°C. Bromide data preceeded by sio were analyzed by J. Gieskes.

Table B-1 (continued) Endeavour Anions, Gases, and Silica

SAMPLE #	AREA	VENT	TEMP °C	Mg m	Cl m	SO_4 m	SO_4 purged m	Br µ	ALK meq/l	pH	CO_2 m	H_2S µ	SiO_2 m
1987													
1929-12	D	16		2.38	425	3.66		535		4.08		5.91	
1929-14	D	16		3.0	410	2.97				4.26	11.0	4.80	
1930-3F	C	12		13.17	454	5.7				4.97	8.67	2.50	
1930-10	C	12		22.48	479	14.9				5.09		3.50	
1930-13	D	16c		35.42		16.5				5.60	5.49	1.65	
1930-14	C	12		39.42	502					5.72	4.72		
1930-15	C			2.98						3.89	11.6	6.50	
1931-9	C	14		3.07	431	6.1		585		4.22	10.9	2.50	
1931-10	C	25		5.74	473	3.9				4.03	9.94	5.30	
1931-12	C	14		3.31	434					4.33	10.6	4.80	
1931-13	C	14		7.45	438	4.6				4.36	-	4.70	
1931-15	C	14		22.2	469	11.8				4.78	8.92	2.90	
1932-9F	?			5.0	477	5.2				4.46	8.49	4.20	
1932-10	?			47.14	524	22.9				6.30	3.36	0.24	
1932-12F	?			28.81	505	15.9				5.37	6.42	1.60	
1932-13	?			27.18	501	14.0				5.14	7.59	2.10	
1932-15	D	16		52.8	531	27.2				6.49	2.61	0.16	
1933-9	D	16b		41.48	513	19.5				5.83		1.20	
1933-13	D	16b		13.0	449	5.5				4.61		4.30	
1933-15	D	16b		50.48	533	24.1				6.71		0.050	
1984													
1438-9	near A	Ltobo	270	6.91	486	3.9		669	0.366	4.57	14.3	2.86	3.94
1445-13			345	21.07	471	12.3			0.684	5.03	8.68	3.77	3.81
1447-8			220	16.62	459	9.5			0.737	5	10.8	3.94	3.24
1451-13	D		380	7.49	443	5.2			0.316	4.58	10.8	4.03	5.30
1453-4			340	0.84	432	2.5		581	0.395	4.64	11.8	3.70	6.18
1436-9	near A		1.7	52.34	541	28.0						0	0.15
1439-1	near A		113	51.62	538	27.8						0.031	0.34
1444-9				52.1	540	27.9							0.18
1446-8	C	tlc	56	51.5	534	27.8			2.789	7	3.16	0.036	0.56
1447-9	C	lotobo	15	50.81	539	27.4						0.32	0.70

TABLE B-2 Endeavour Cations

SAMPLE #	Mg m	Li µ	Na m	K m	Ca m	Sr µ	Fe µ	Mn µ	NH3 µ
1988									
2095-10	20.78		392		24.59		367	167	
2096-10	3.13	353	333	23.0	31.19	131			543
2096-11	45.12	50	405	10.8	11.26	87			82
2096-13	5.54	332	346	23.3	30.01	119	780	247	600
2096-16	1.63	354	329	23.2	31.70	125	891	283	560
2096-9	7.84	321	351	23.6	28.39	116	666	249	600
2097-12	51.84	28	439	10.5	10.28				
2098-12	18.55	255	367	19.8	24.50	115	325	186	380
2098-13	13.79	275	375	17.1	23.78	123	417	174	470
2098-9	8.52	320	354	22.8	29.70	130			500
2099-10	1.16	361	329	24.5	34.19	143	992	290	648
2099-12	21.28	223	367	18.3	22.89	102			335
2099-13	41.58	91	419	13.2	14.32	94			128
2099-16	1.70	370	340	23.5	32.86	125			
2099-9	7.02	332	349	23.1	29.52	131	795	249	660
2100-10	2.51	376	334	24.2	32.71	137	920	276	513
2100-12	11.70	380	340	24.9	22.93	137	620	234	420
2100-13	38.17	130	409	14.1	16.99	104			77
2100-16	1.50	375	333	24.1	33.37	137			605
2100-16[1]	0.76		335	24.1	32.30	127	1019		
2101-12	51.93	24	436	11.1	11.29	82			
2101-13	45.29	67	425	12.1	13.03	84			62
2102-10	30.96				22.96				
2102-13	2.27	443	393	27.5	40.74	158			555
2102-16	23.09	195	410	16.8	31.28	115			209
2102-9	0.81	443	390	27.9	42.76	155	498	195	545
2102-9[1]	1.06			27.9	41.84	151	488		
2103-11	52.54	28	442	10.4	10.16	92			
2103-13	30.22	186		16.9	20.86	104			
2103-15	52.01	30	443	10.2	10.41	87			11
2103-16	2.79	371	362	23.7	33.50	139	942	282	552
2103-16[1]	2.84			23.7	32.87	129	976		
2103-9	27.21	198	391	16.8	21.40	111	19	123	345
2104-11	41.45	83	416	12.7	14.97	102			
2104-16	48.17	39			11.60	95			37
2104-9	46.23	61	424	12.0	13.74	96			55
2105-10	40.67	133		14.3	17.71	113			
2105-15	13.23	333	330	22.0	26.68	132	776	241	590
2105-16	40.72	118	426	13.9	16.79	105			115
2105-9	13.74	332	404	20.8	34.48	133	137	139	505
2106-10	51.82	32	440	10.2	10.77	81			9
2106-11	51.20	37	435	10.2	11.34	82			22
2106-12	32.03	158	406	14.8	18.25	107			259
2106-13	37.63	128	445	14.2		108	235	89	183
2106-15	49.80	43		8.6		105			
2106-9	43.86	85	421	12.6	14.15	95	158	37	120
2108-10	49.18	36	423	10.7	10.41	94			
2108-12	32.88	213	397	14.6	19.68	117	371	128	
2108-13	27.48	220	397	14.8	23.45	104	382	134	
2108-16	49.78	35	426	10.6	10.35	84			
2108-9	30.56	184	401	17.2	20.72	108	366	110	
2109-11	1.58	330	354	22.8	32.00	130			596
2109-11[1]	1.72		354	22.7	32.16	127			
2109-12	50.32		485						
2109-13	50.74		482						
2109-15	1.20	351		22.6	31.45	135			
2109-9	52.23	28	430	9.6	10.30	94			

Table B-2 (continued) Endeavour Cations

SAMPLE#	Mg m	Li µ	Na m	K m	Ca m	Sr µ	Fe µ	Mn µ	NH3 µ
1987									
1929SF	2.30		336	23.5	31.66				120
1929-12	2.38		335	23.3	31.47		230		135
1929-14	3.00				30.90		921		
1930-3F	13.17		356	20.9	28.27		608		
1930-10	22.48				23.66		340		
1930-13	35.42				17.30		4		
1930-14	39.42				13.63				
1930-15	2.98			19.7	25.27				
1931-9	3.07				32.85		584		
1931-10	5.74		334	23.0	32.97		877		
1931-12	3.31		338	23.5	32.87		583		123
1931-13	7.45		338	22.4	32.78		549		
1931-15	22.20				24.55		85		
1932-9F	5.00				28.60		740		
1932-10	47.14				13.08		17		
1932-12F	28.81				23.40				64
1932-13	27.18				23.11		132		
1932-15	53.00				11.55				
1933-9	41.48				14.37				
1933-13	13.00		359	19.3	25.60		323		121
1933-15	50.48				11.14				
1984									
1438-9	6.91	375	380	24.6	34.30	132	551	210	445
1445-13	21.07	228	374	19.1	22.60	110	204	140	296
1447-8	16.62	265	361	21.0	25.60	113	277	159	320
1451-13	7.49	349	342	24.7	31.70	127	593	207	
1453-4	0.84	394	332	27.2	34.60	135	915	256	
1436-9	52.34	27.4	433	10.0	10.41	87	0	0	
1439-1	51.62	31.9	441		10.31			3	30
1444-9	52.10	27.5	443		10.31			0	
1446-8	51.50	38	436		11.05			6	12
1447-9	50.81	40.4	442		10.95			8	47

Table B-3 Gas-tight Sample Data

Sample #	Vent temp, °C	Mass of sample,g	Mg, corr mmol/kg	Cond. Gas mmol/kg	He, total µcc/g	H2S mmol/kg	Cl, corr mmol/kg	Li, corr mmol/kg
Endeavour							0	
1438-SB2-2		47.5	8.2				508	360
1438-W2		24.1	9.5					332
1439-W2	100	43.6	44.8			1.96	569	105
1445-M1-1	345	209.2	17.6	11.4	8.98			
1445-M1-2	345	147.5	17.5	6.9	45.22			
1445-M1-pair	345	356.7	17.6	9.6	23.96	4.05	456	0
1445-W2	275	11.8	45.7		5.33		347	38
1446-M1	low	98.0	49.9			0.69	535	55
1446-SB2-1	57.6	102.8	38.7			3.06	516	140
1447-M13-2		204.8	50.8			4.07	532	35
1447-M4-2		70.5	28.4			5.98	535	209
1451-SB3-1	400	122.9	3.7	11.9	6.64			366
1451-SB3-2	400	31.9	4.0					367
1451-SB-pair	400	154.8	3.8			7.26	433	157
1451-W2	400	74.9	1.4	14.8	33.74	7.68	420	368
1451-W5	400	26.0	51.5		2.50		474	41
1453-SB3-1	350	108.7	18.1					270
1453-SB3-2	350	52.2	18.2					266
1453-SB-pair	350	160.9	18.1			4.94	463	0
1929-SB-2	356	149.2	0.8			4.88	453	394
1933-SB-2	351	147.7	25.7			5.69	499	243
ASHES								
1729SB	326		30.3	24	1.0			
1733-M3	298		35.5	58	.48			
1918-SB3	326		23	28	1.4	4.24		
1920-SB2	198		29.3	79	3.7	4.65		
1920-SB3	298		31.7	122	4.4			
1923-SB2	298		36.8	71	3.4	5.78		

Sample suffixes refer to the type of sampler: SB = Titanium gold-sealed UCSB bottles designed by J. Lupton; W = small volume WHOI sampers designed by B. Walden; M = split from titanium major sampler (not gas-tight). The final suffix number is the cut number (many samples were split in two, as the volume was too great to expand into a single glass flask). In cases where both cuts of a single sample have been analyzed, the results are recombined to reflect the actual sample composition. Concentrations are corrected for water loss and chloride addition (see Appendix A). Condensable gas (equivalent to CO_2) and helium data provided by John Lupton, UCSB.

Table B-4 ASHES Anions, Gases, and Silica

SAMPLE #	VENT	Temp °C	Mg m	Cl m	SO_4 m	Br µ	ALK meq/l	pH	CO_2 m	H_2S m	SiO_2 m
seawater		2.4	52.9	539	27.78	839	2.354	7.47	2.393	0	0.169
1986											
1721-3	INF-s	330	41.04	540	25.0	870	1.64	5.40		1.2	3.18
1721-4	INF-s	330	42.86	541	24.7		1.63	5.50		1.2	2.75
1722-3	MM	283	50.76	531	27.7		2.24	6.12		0.19	0.49
1722-4	MM	283	51.06	533	27.5	864	2.28	6.09		0.17	0.50
1727-3	INF-s	145	45.20	537	25.8			5.45			2.25
1727-4	INF-s	145	45.78	543	25.0		1.95				2.34
1733-3	VM	250	35.13	423	20.1	654	1.67	4.80		2.0	1.37
1733-4	VM	250	35.88	428	20.7	687		3.90		3.7	1.40
1987											
1917-12	INF-t	149	46.14	550	24.8	873		5.60	6.42		
1917-16	INF-t	326	7.40	597	3.3	925	-0.18	3.70	37.2	7.3	3.36
1917-16[1]	INF										13.2
1918-14	INF-t	325	16.95	584	7.4	907	0.0	5.89	33.2	6.2	
1918-16	INF-t	306	42.61	551	23.6	879	1.76	4.45	9.3		3.07
1919-16	CRACK	75	40.24	476	21.5	767	1.90	4.87	34.1	0.74	3.41
1920-10	ISCA	21	51.43	526	27.9	853					
1920-13	ISCA	21	44.38	491	26.2	785	2.03	4.96		2.3	2.42
1920-14	VM	288	2.31	189	1.5	279	0.41		372	6.9	7.70
1920-14[1]	VM										13.3
1920-15	ISCA	21	43.16	493	24.2	788	2.04	4.93	20.5	2.4	2.36
1920-16	ISCA	21	50.72	536	26.2	848	2.57	6.29	3.68	0.002	0.36
1920-S1	CRACK		44.47	483	23.7	774					
1921-12	ISCA	22	50.80	529	25.7	902	2.58	6.30	3.5	0.036	0.42
1921-13	MM	240	37.72	529	19.7	831	1.32	4.81	110	2.6	2.94
1921-14	MM	240	5.94	520	3.7	779	-0.22	3.62		8.4	7.20
1921-16	HILL	180	11.28	484	5.9	730	0.03		90.6	7.5	3.47
1921-3	MM	240	31.65	536	18.6	841	1.0	4.63	125.5	3.8	5.13
1922-12	MM	90	39.95	534	22.7	852	1.61	4.91	102		2.52
1922-13	WARM	9	51.52	538	27.5	863	2.29	6.31	6		
1922-14	HELL	301	18.25	547	8.8	859	0.49	4.58	65.8	3.8	3.01
1922-3	HELL	301	48.35	537	27.0	857	2.13	5.88	28.4		1.22
1923-10	HILL	161	44.27	530	24.5		1.73		9		
1923-12	VM	293	20.85	323	12.0	512	1.04	4.58	61.2	5.9	
1923-14	HELL	261	36.34	540	19.5	850	1.58	5.31	8.8		
1923-15	CRACK	198	32.20	437	17.1	676	1.34	4.72	33.2		
1923-9	HELL	261	26.15	541	14.1		0.52	4.74	14.3		
1924-12	INF-s	150	36.80	561	19.2	880	1.27	4.98	16.3		
1927-15	INF-s		21.86	590	12.6		0.25	4.28			
1988											
2083-10	INF-t	317	4.15	624	2.0	938		3.58		6.0	13.0
2083-10[1]	INF										14.0
2083-12	INF-t	319	5.73	618	2.0	968	-0.12	3.54		5.4	13.8
2083-12[1]	INF										14.4
2083-13	INF-t	317	34.32	574	18.2	887	1.29	5.0		2.1	5.0
2083-16	VM	299	10.50	246	6.9	384		4.45		5.9	9.9
2083-9	VM	299	9.62	248	6.2	291	0.57	4.43		4.6	10.0
2083-9[1]	VM										11.0
2089-12	HILL	323	5.17	496	3.4	749	-0.64	3.48		7.0	14.4
2089-12[1]	HILL										14.0
2089-13	ISCA	6	52.87	544	27.2	846	2.28	6.85		0.001	0.28
2089-16	CRACK	158	12.74	322	6.4	496	0.89	4.61		5.3	12.0
2089-16[1]	CRACK										11.9
2089-9	HELL	289	25.30	546	12.6	835	0.56	4.87		2.3	8.88
2089-9[1]	HELL										8.36
2090-9	INF-t	317	7.35	617	3.4	943	0.20	3.60		5.7	13.8
2091-12	VM	26	48.0	479	22.8	715	2.14	5.09		1.1	1.43
2091-13	ISCA	28	51.21	534	27.0		2.78	6.14		0.065	0.92
2091-9	VM	298	4.59	197	2.1	305	0.51	4.36		5.4	12.9
2091-9[1]	VM										12.9

Table B-5 ASHES Cations

SAMPLE #	Mg m	Li µ	Na m	K m	Ca m	Sr µ	Fe µ	Mn µ	Cu µ	Zn µ	Pb µ	B m
seawater	52.9	28	458	9.9	10.27	87	0.0034	0.0023	0.004	0.012		0.416
1986												
1721-3	41.04		457	13.56	18.01		247	278	3.7	35	0.07	
1721-4	42.86		456	13.05	16.85		218	255	7.1	46	0.56	
1722-3	50.76		453	10.26	10.78		28.3	23	0.03		0.03	
1722-4	51.06		454	10.24	10.67		26.2	21.3	0.23	10	<.03	
1727-3	45.2		455	12.41	15.05		169	194	1.13	35	0.08	
1727-4	45.78		459	12.46	14.56		127	191	1.09	23	0.05	
1733-3	35.13		363	9.34	10.45		4.55	39.5	0.12		0.20	
1733-4	35.88		367	9.34	10.58		6.33	41.2	0.10	117	0.40	
1987												
1917-12	46.14	95.6	466	12.3	14.54		139	152				
1917-16	7.4	548	478	23.95	40.89		990	987	12			
1917-16[1]	6.59	406.3	493	24.75	40.22	175.7	955	1150				0.575
1918-14	16.95	441	471	22.15	33.97		581	943				
1918-16	42.61	137	466	13.29	16.72		247	245				
1919-16	40.24	84.5	404	10.45	12.01		4.7	66				
1920-10	51.43	31.7	447	10.2	11.01							
1920-13	44.38	67.9	418	10.4	12.72		7.2	46.5				
1920-14	2.31	183	158	7.55	10.27		12.3	130				
1920-14[1]	1.86	94.5	158	7.46	10.59	49.5	5	142				0.429
1920-15	43.16	64.7	419	10	12.75		7.9	22.1				
1920-16	50.72		455	10.41	11.09		2.75					
1920-S1	44.47	48.7	411	9.51	10.66							
1921-12	50.8	41.7	447	10.1	10.96		4.1	21.1				
1921-13	37.72	172	441	13.2	18.49		283	320				
1921-14	5.94	484	418	20.7	36.09		943	970	89			
1921-16	11.28	392	393	18	29.23		623	704				
1921-3	31.65	230	447	16.2	21.92		388	454				
1922-12	39.95	151	451	12.93	16.95		252	271				
1922-13	51.52	33.2	459	10.4	10.54		8.9	13.5				
1922-14	18.25	380	447	19.35	29.49		599	765				
1922-3	48.35		458	11.35	12.31		77.9	75.9				
1923-10	44.27	94.6	451	11.8	13.47		101	133				
1923-12	20.85	122	275	8.84	10.38		9.8	83				
1923-14	36.34	189	452	14.55	19.01		226	401				
1923-15	32.2	130	368	10.83	13.85		4.6	18.4				
1923-9	26.15	323	449	17.55	23.82		348	619				
1924-12	36.8	222	465	16	21.4		315	394				
1927-15	21.86	369	483	18.87	33.31		519	707				
1988												
2083-10	4.149	584	502	25.65	43.833		943	983		83		0.601
2083-10[1]	3.49	415.5	502	25.96	43.59	187	921	1203				0.586
2083-12	5.725	581	494	26.05	43.049	173	909	991		101		
2083-12[1]	3.02	444.2	493	25.94	43.62	185.2	890	1205				0.577
2083-13	34.317	249	483	10.3	22.942	118	353	432		46		0.536
2083-16	10.5	153	210	7.36	10.426		8	102				0.527
2083-9	9.623	150	214	7.06	10.05	63.5	7.9	140				
2083-9[1]	10.4	83.4	213	7.84	10.25	53.1	4	117				0.427
2089-12	5.173	447	404	19.93	32.155	132	726	837				
2089-12[1]	3.71	279	404	20.31	32.1	140.2	735	951				0.516
2089-13	52.869	28.3	461	10.06	10.279	84.1	5	6.8				
2089-16	12.743	222	265	10.98	16.689	101						
2089-16[1]	10.32	172.0	264	11.43	16.60	81.8	4	238				0.509
2089-9	25.298		451	17.65	25.037		442	625		74		0.592
2089-9[1]	25.16	111.5	452	17.35	24.56	123.3	438	630				0.462
2090-9	7.346	552	495	24.53	42.16	164	817	1002		108		0.657
2091-12	48	52.6	399	9.21	10.259	69.1	1.8	13				
2091-13	51.209	46.7	450	11.4	11.737	86.9	2.9	28.8				
2091-9	4.593	171	165	6.75	10.179	62	7.1	129				
2091-9[1]	3.34	110.4	164	7.36	10.34	49.6	0	136				0.447

Curriculum Vitae

David A. Butterfield
Born August 10, 1957, Vancouver, Washington
Current address:
4747 Latona NE
Seattle, WA 98105
206-634-2986

Education

9/75-6/76	Attended Reed College, Portland, Oregon.
1980	B.A. with honors in Chemistry and German from Portland State University, Portland, Oregon.
6/84 to 12/90	Graduate study in Chemical Oceanography at the University of Washington. Ph.D. Dissertation title: Phase Separation in Submarine Hydrothermal Systems: Evidence from the Juan de Fuca Ridge.

Awards/Fellowships

1980 Sherman-Shaefer Award for outstanding undergraduate chemistry students.

1990 National Research Council Postdoctoral Research Associateship.

Employment

1981-1983	Secondary physics and chemistry teacher in the Peace Corps, Togo, West Africa.
1983	Technical coordinator for Peace Corps science teacher training, Togo, West Africa.
1984-1990	Graduate Research Assistant, University of Washington.
1986 and 1990	Graduate Teaching Assistant, University of Washington.

Professional Affiliations

Member of the American Geophysical Union and The Geochemical Society.

Research Experience

August 1984- R/V Wecoma, analyzed nutrients and sulfur species from hydrothermal fluids collected by ALVIN from the Endeavour Ridge.

August/September 1986- R/V Pandora/Pisces submersible, shipboard chemical analysis of hydrothermal fluids from Axial Seamount.

September 1987- R/V Atlantis II/DSV ALVIN, shipboard chemical analysis and development of *in situ* chemical analyzer (ISCA), Axial Seamount and Southern Juan de Fuca Cleft Segment.

October 1987- R/V Atlantis II/DSV ALVIN, shipboard chemical analysis of hydrothermal fluids from Endeavour Ridge.

August 1988- R/V Atlantis II/DSV ALVIN, shipboard chemical analysis and testing of second generation ISCA, Southern Juan de Fuca Cleft Segment and Axial Seamount.

September 1988- RV Atlantis II/DSV ALVIN, shipboard chemical analysis of hydrothermal fluids from Endeavour Ridge.

August 1990- RV Atlantis II/DSV ALVIN, continued development and deployment of in situ chemical analyzer for hydrothermal plume experiment.

Publications

Refereed journal articles:

G.J. Massoth, D.A. Butterfield, J.E. Lupton, R.E. McDuff, M.D. Lilley, and I.R. Jonasson, Submarine venting of phase-separated hydrothermal fluids at Axial Volcano, Juan de Fuca Ridge, Nature, 340, pp. 702-705, 1989.

D.A. Butterfield, G.J. Massoth, R.E. McDuff, J.E. Lupton, and M.D. Lilley, The geochemistry of hydrothermal fluids from ASHES vent field, Axial Seamount, Juan de Fuca Ridge: sub-seafloor boiling and subsequent fluid-rock interaction, J. Geophys. Res., Vol 95, pp. 12,895-12,922, 1990.

Nonrefereed articles:

G.J. Massoth, H.B. Milburn, S.R. Hammond, D.A. Butterfield, R.E. McDuff, and J.E. Lupton, The geochemistry of submarine venting fluids at Axial Volcano, Juan de Fuca Ridge: New sampling methods and a Vents Program rationale, in Global Venting, Midwater, and Benthic Ecological Processes, National Undersea Research Program report #88-4, 1988.

Abstracts of meeting presentations:

D.A. Butterfield, R.E. McDuff, M.D. Lilley, G.J. Massoth and J.E. Lupton, Evidence for phase separation of hydrothermal fluids from Axial Volcano, Juan de Fuca Ridge, *EOS Trans. Am. Geophys. U., 69*, p. 303, 1988.

D.A. Butterfield, R.E. McDuff, M.D. Lilley, G.J. Massoth, and J.E. Lupton, Chemistry of hydrothermal fluids from the ASHES vent field: Evidence for phase separation, *EOS Trans. Am. Geophys. U., 69*, p. 1468, 1988.

D.A. Butterfield, R.E. McDuff, M.D. Lilley, and G.J. Massoth, Chemical heterogeneity in vent fluids from the Endeavour Ridge, *EOS Trans. Am. Geophys. U., 70*, p. 1163, 1989.

J.E. Lupton, M.D. Lilley, D.A. Butterfield, R.E. McDuff and G.J. Massoth, Gas chemistry of submarine hydrothermal systems on the Juan de Fuca Ridge, *EOS Trans. Am. Geophys. U., 69*, p. 1468, 1988.

M.D. Lilley, J.A. Baross, D.A. Butterfield, E.J. Olson, R.E. McDuff, S.A. Macko, J.A. Welhan, and C.N. Dahm, Volatiles in Endeavour vent fluids, *EOS Trans. Am. Geophys. U., 70*, p. 1163, 1989.

G.J. Massoth, E.T. Baker, R.A. Feely, J.E. Lupton, D.A. Butterfield and R.E. McDuff, Hydrothermal fluids and plumes of Cleft Segment, Juan de Fuca Ridge, *EOS Trans. Am. Geophys. U., 69*, p. 1497, 1988.

D. A. Butterfield, R. E. McDuff, M. D. Lilley, and G. J. Massoth, Geochemistry of hydrothermal fluids from the Endeavour Segment, Juan de Fuca Ridge, *EOS Trans. Am. Geophys. Un., 71*, p. 1680, 1990.

In preparation:

D. A. Butterfield, R. E. McDuff, M. Mottl, M. D. Lilley, G. J. Massoth, and J. E. Lupton, Geochemistry of hydrothermal fluids from Endeavour Segment Juan de Fuca Ridge: supercritical phase separation, to be submitted in 1991.